Alma Mater Studiorum – Università di Bologna

DOTTORATO DI RICERCA IN

Scienze di biotecnologiche e farmaceutiche

Ciclo 31

Settore Concorsuale: BIO10

Settore Scientifico Disciplinare:05E1

Defective Oxidative Phosphorylation Induced by CoQ10 Depletion Reshaped Cancer Metabolism: Implications for Cancer Targeting

Presentata da: Wang Wenping

Coordinatore Dottorato **Supervisore**

Prof. Santi Mario Spampinato **Prof. Romana Fato**

Esame finale anno 2019

TABLE OF CONTENTS

Acknowledgments

My first and most profound appreciation goes to my fantastic supervisor, Professor Romana Fato, the most dedicated and supportive supervisor I've ever seen since I came here. She is so amiable to me and persistently bear with my dullness and stubbornness. She has been instilling knowledge in me and inspiring me with her meticulous attitude toward scientific research. She has modeled to me in both life and science. And I am so grateful for your guidance, criticism, and encouragement that I think is the most precious things that I am given. I consider myself extremely fortunate to have had a supervisor who has cared so deeply not just about my project, but also about my professional and personal development. Thank you for always making an effort to give me helpful feedback, to communicate clearly and often, and to be generous in offering me opportunities to put my work forward. Without her guidance and help, this dissertation would not have been possibly completed.
Also, I would submit my enormous gratitude to my co-supervisor Christian Bergamini, whose constant hard work and overwhelming expertise have been a powerful example to me. Thank you for teaching me from ABCs of biochemistry and almost all scientific techniques that I know. You have been endlessly patient with my mistakes, have been so generous with your time, and have been giving me so many opportunities to be involved in your projects. And I'm genuinely thankful for the insightful viewpoints and constructive suggestions you selflessly shared on my study. Those suggestions are treasures to me, the value of them can never be overstated. Thank you for pulling back from the wrong track. all the fantastic things you have done to me, enabling me to come till the end.
To guys in the lab, Marco Accorsi, Irene Liparulo, Luca Masin, Nicola Rizzardi and all excellent members with great passions and enthusiasm, you have been helpful every time I turn to you. I do not underestimate how much I owe to all of you. Most of all, a special mention for my working pal, MarcoAccorssi, who made the long hours in the lab and brought a lot of fun, and who was extremely keen to help. It is you that make Bologna a home-like place. Thanks for putting up with my many mistakes in the lab, and for bearing patiently with my youthful idealism, for teaching me how to be a good colleague… too many things to name them all. I can't believe that it was three years ago that I first walked into the University of Bologna. The time we have spent together over these years has been such a unique and significant part of my life.
Thank you to all who have contributed their time and expertise to the work included in this thesis, particularly the many hours of help and explanation from professor Natalia Calonghi and her Ph.D. student Julia for the SDS-PAGE and immunostaining of GLUTs, and technical expertise of flow cytometry from Manuela. Many others have contributed data or technical knowledge and are gratefully acknowledged for their contributions to those who have provided invaluable advice and criticism of my experimental procedures, data, and writing.
To all my friends outside the lab, new and old, who have stood with me through these years, I would cherish the joys and fooling around that had together during the stay in Bologna. I am so grateful for your encouragement, understanding, and kindness towards me, and the many and numerous ways that you have all shown that your care. I hope you all know your support has meant a great deal to me.
Finally, to my parents, thank you for your love and support throughout my whole life. I'm very grateful for all that you have done and continue to do for me. Thank you for always encouraging

me to try my best, providing so many opportunities for me to learn, and being so supportive of my study and my life in general. I would not have gotten here without a lifetime of you both telling me that I could.

Abstract

Cancer cells usually featured with variable oxidative phosphorylation (OXPHOS) during its progression, leading to metabolic reprogramming. We aimed to study different metabolic propensity of cancer cells with different oxidative phosphorylation (OXPHOS) activity. In particular, we focused on study how glycolysis was remodeled to meet bioenergetic, biosynthetic and redox requirements. Also, we aimed to investigate the dependence of cancer cells on a specific metabolic pathway or metabolic enzymes. This study can provide an insightful understanding of metabolic reprogramming in cancer cells with different oxidative phosphorylation (OXPHOS) activity. And it can offer potential selective targets for cancer therapy.

Impaired oxidative phosphorylation was induced by cellular CoQ10 depletion. It was achieved by inhibiting CoQ10 biosynthesis. 4 mM 4-nitrobenzoate (4NB) was effective to deprive approximately 60-70% of cellular CoQ10 from the cancer cells. As a result, the biosynthesis of cholesterol was elevated since the biosynthesis of CoQ10 shares a common precursor with cholesterol biosynthesis. CoQ10 is involved in electron transport chain and antioxidative defense. Thus, we accessed the effect of CoQ10 depletion on oxidative phosphorylation (OXPHOS) using oxygen consumption rate, NADH autofluorescence as well as the evaluation of mitochondrial respiratory complexes. We found that the depletion of CoQ10 resulted in compromised oxidative phosphorylation (OXPHOS). Specifically, the oxidation of NADH and the conversion of succinate to fumarate would be diminished due mainly to reduced CoQ10 pool and decreased activity of respiratory complexes. Besides, the CoQ10 depletion perturbed oxidative homeostasis since we demonstrated that the elevated level of ROS and diminished level of glutathione (GSH).

In addition to oxidative phosphorylation (OXHPOS), CoQ10 depletion also had a significant impact on other mitochondrial network morphology and other functions. We accessed the mitochondria by using molecular probes such as MitoTraker Green and JC-1. We found that the mitochondrial network was slightly fragmented when CoQ10 was depleted by 4NB treatment while the mitochondrial membrane potential was increased in the presence of 4 mM 4NB.

Furthermore, we discovered the effect of 4NB on an energetic charge; we found that cells with 4NB treatment were mildly stressed. It presumably resulted from the reduced energetic demand and compensation of ATP production from upregulated glycolysis in cancer cells. Finally, we found that 4NB treatment affected endogenous oxygen availability. The decrease of endogenous oxygen would have a profound impact on the metabolism since the hypoxic state regulates a broad variety of metabolic pathways. In a word, the CoQ10 depletion induced by 4NB treatment altered the oxidative phosphorylation (OXPHOS), oxidative hemostasis, bioenergetics, and endogenous oxygen.

The cancer cells with 4NB treatment were metabolically different from cancer cells without 4NB. Driven by the alterations induced by CoQ10 depletion, metabolic pathways such as glycolysis, TCA cycle, and glutaminolysis have been inevitably reshaped. To gain a better understanding of the metabolic alterations in response to CoQ10 depletion, we studied metabolic pathways involved in cancer progression. Concerning glycolysis, we determined glucose uptake using fluorescent glucose analog 2-NBDG as a tracer. By using flow cytometry, we found that glucose uptake was increased in cancer cells treated with 4NB. To verify this finding, we measured glucose consumption of cells with and without 4NB treatment by glucose oxidase (GO) catalyzed assay. In consistent with glucose uptake data, glucose consumption was elevated by 4NB treatment as well. Furthermore, we

investigated the expression of GLUT1 and GLUT3 which are predominant transporters involved in glucose uptake in MCF7 cells employing immunostaining. The confocal microscopic images have shown that both GLUT1 and GLUT3 were slightly overexpressed in MCF7 cells treated with 4NB. Furthermore, we discovered the activity of pyruvate kinase (PK) which is a primary regulatory site of glycolysis, was activated by 4NB treatment. Although the Vmax of pyruvate kinase (PK) was unaffected, the affinity of pyruvate kinase (PK) for phosphoenolpyruvate (PEP) was increased. The reduced Km indicated that phosphoenolpyruvate (PEP) flux through pyruvate kinase (PK) might be increased due to upregulated glycolytic flux and increased pyruvate kinase (PK) activity. Moreover, we measured lactate secretion rate, 4NB treated cells exhibited reduced basal lactate secretion although glycolysis was upregulated. However, we also found that glycolytic reserve decreased in cancer cells with 4NB treatment. Given the fact that the basal lactate secretion rate was reduced regardless of enhanced glycolysis, pyruvate flux is very like to be redirected to amino acids formation.

On the other hand, we also measured the activity of glutaminase (GLS) and glutamate dehydrogenase (GDH) which are closely involved in glutaminolysis. And we found that the glutaminase (GLS) was upregulated while glutamate dehydrogenase (GDH) was unaffected. We can speculate the activity of glutamate dehydrogenase was reduced due to the elevated NADH levels. However, alanine transaminase (ALT) and aspartate transaminase (AST) can alternatively convert glutamate to α-ketoglutarate regardless of elevated NADH. Besides, oxidative glutamine metabolism depends on the mitochondrial respiratory chain. Given the reduced succinate dehydrogenase activity (SDH), we estimated that the flux of α-ketoglutarate (α-KG) would be rewired to isocitrate via reductive carboxylation, which contributed to *de novo* lipogenesis ultimately.

We studied how the altered metabolism affected the cancer cell survival to prooxidant TBH, glucose deprivation and glutamine deprivation, as well as cytotoxic drugs doxorubicin and cisplatin. Firstly, we studied the antiproliferative effect of 4NB and its effect on cell cycle progression. 4NB inhibited the cancer cell proliferation in a dose-dependent manner and delayed cell cycle progression. It might be attributable to the compromised mitochondrial energy generation and oxidative stress. Moreover, we evaluated the cancer cells survival to prooxidant TBH. Unsurprisingly, cancer cells with 4 mM 4NB treatment have shown more considerable sensitivity to 100 μM TBH. We deprived the glucose of cancer cells through galactose replacement and hexokinase (HK) inhibition. Although 4 mM 4NB did not affect energetic stress, we found that 4NB treatment remarkably sensitized cancer cells to glycolytic inhibition due to smaller spare OXPHOS capacity in cells with 4NB treatment. In respect to glutamine deprivation, glutamine-free culture medium and dialyzed FBS was used to culture cancer cells. 4NB treated cancer cells, either MCF7 cells or HepG2 cells, have shown insensitivity to glutamine deprivation in comparison to the control. Other than that, we found that cancer cells with 4NB treatment were selectively resistant to cytotoxic drug doxorubicin. However, 4NB treatment sensitizes cancer cells to cytotoxic drug cisplatin. This ROS generation and apoptotic effectors might be associated with this resistance or susceptibility. The underlying mechanism remains to be elucidated.

In conclusion, 4NB treatment induced CoQ10 depletion in cancer cells consequently led to increased cholesterol level. Besides, CoQ10 depletion impaired mitochondrial respiratory complex II and complex IV, thereby led to compromised oxidative phosphorylation. Moreover, CoQ10 depletion resulted in mitochondrial fragmentation, an elevated level of NADH, perturbed oxidative

homeostasis and hypoxic state. As a result, cancer cell metabolism was reshaped, in particular in glycolysis. The glucose uptake was upregulated. GLUT1 and GLUT3 were overexpressed in 4NB treated cells. Moreover, pyruvate kinase (PK) was activated, and lactate secretion rate was decreased. Pyruvate flux might be redirected to amino acids formation. Besides, glutaminolysis and TCA cycle were deregulated by CoQ10 depletion in many ways. Finally, we found that cancer cells with compromised oxidative phosphorylation were more sensitive to glycolytic inhibition. However, cancer cells with compromised OXPHOS were more resistant to glutamine deprivation. Besides, we also found cancer cells with 4NB treatment were more sensitive to HIF-1α inhibition.

Key words：

CoQ10 depletion; Defective oxidative phosphorylation; Hypoxia; Glycolysis; Tricarboxylic acids cycle; Glutaminolysis; Cancer cell survival

Abbreviations

CoQ10	**Coenzyme Q10**
4NB	**4-nitrobenzoate**
HPLC	**High-Performance Liquid Chromatography**
2-DG	**2-deoxy-D-glucose**
OXPHOS	**Oxidative phosphorylation**
PPP	**Pentose phosphate pathway**
FCCP	**Carbonyl cyanide-4-(trifluoromethoxy)phenylhydrazone**
AA	**Antimycin A**
TCA	**Tricarboxylic acid cycle**
LDH	**Lactate dehydrogenase**
HK	**Hexokinase**
PDC	**Pyruvate dehydrogenase complex**
PK	**Pyruvate kinase**
IDH	**Isocitrate dehydrogenase**
KGDC	**Ketoglutarate dehydrogenase complex**
MDH	**Malate dehydrogenase**
ME	**Malic enzyme**
GDH	**Glutamate dehydrogenase**
GLS	**Glutaminase**
ALT	**Alanine transaminase**
AST	**Aspartate transaminase**
PDHs	**Prolyl domain hydrogenases**
ATP	**Adenosine triphosphate**
ADP	**Adenosine diphosphate**
AMP	**Adenosine monophosphate**
NAD^+	**Nicotinamide adenine dinucleotides**
NADH	**Nicotinamide adenine dinucleotides reduced from**

$NADP^+$	**Nicotinamide adenine dinucleotides phosphate**
NADPH	**Nicotinamide adenine dinucleotides phosphate reduced from**
GLUTs	**Glucose transporters**
PEP	**Phosphoenolpyruvate**
OAA	**Oxaloacetate**
α-KG	**α-ketoglutarate**
GO	**Glucose oxidase**
HIF-1α	**Hypoxia-inducible factor 1α**
MTT	**3-(4,5-dimethylthiazol-2-yl)-2,5-diphenyltetrazolium bromide**
2-NBDG	**2-(N-(7-Nitrobenz-2-oxa-1,3-diazol-4-yl)-Amino)-2-Deoxyglucose**
BTP	**Bis(2-(2′-benzothienyl)- pyridinato-N,C3′)iridium(acetylacetonate)**
ROS	**Reactive oxygen species**
OCR	**Oxygen consumption rate**
GSH	**Glutathione**
NEM	**N-ethylmaleimide**

Part I Introduction

Chapter 1 CoQ10 deficiency and mitochondrial dysfunction

1. 1 CoQ10 and its biological functions

Coenzyme Q is usually referred to as CoQ or ubiquinone, which is ubiquitously present in both prokaryotes and eukaryote. It consists of benzoquinone and poly-isoprenoid tail that is of variable length in various species and organisms (As shown in Figure 1.1.1.A). Coenzyme Q10 or CoQ10, which is the predominant form of ubiquinone in human, a member of the ubiquinone family, consists of 1,4-benzoquinone and ten units of the isoprenoid side chain. As one of the very significant electron carriers, CoQ10 primarily resides in the mitochondrial membrane given its high hydrophobicity. It can diffuse freely in the mitochondrial membrane, and it plays a very critical role in oxidative phosphorylation (as shown in Figure 1.1.1.B). Notably, oxidized CoQ10 plays as a single electron receptor or double electrons from iron-sulfur clusters, which produces reduced from semi-ubiquinone and hydroquinone respectively.

NAD(P)H + a quinone → $NAD(P)^+$ + a hydroquinone

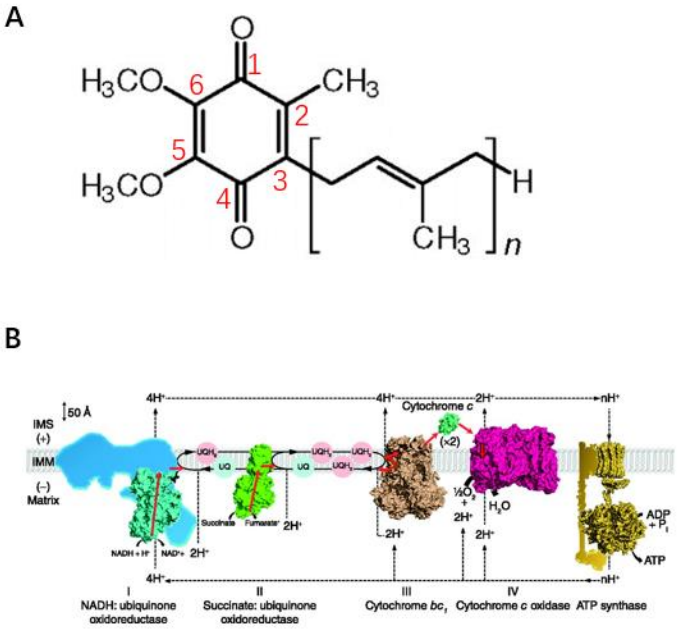

Figure 1.1.1 General chemical structure of ubiquinone (A) and diagram of the mitochondrial respiratory chain (B)

Besides, quinone is also an endogenous antioxidant which plays a critical role of scavenging radical species. Together with other endogenous antioxidants, reduced CoQ10 can protect cells from oxidative damage. It can be reduced to hydroquinone by NAD(P)H quinone oxidoreductase 1 (NQO1)[1, 2]. This protein's enzymatic activity prevents the one electron reduction of quinones that results in the production of radical species. And many studies have shown NQO1 is critical in protecting cells from oxidative damage.

NADPH oxidase: NADPH + 2 O^2 ↔ NADP+ + $2O^{2-}$ + H^+

In its reduced form, CoQH2, ubiquinol, inhibits protein and DNA oxidation. And it is the effect on lipid peroxidation that has been most deeply studied. Coenzyme Q is the only lipid-soluble antioxidant synthesized endogenously. Ubiquinol inhibits the peroxidation of cell membrane lipids and also that of lipoprotein lipids present in the circulation[3].

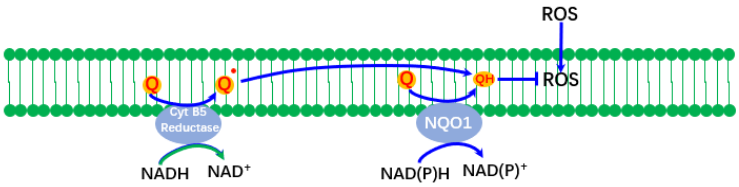

Figure 1.1.2 Role of CoQ10 in plasma membrane redox system

As part of the mitochondrial electron transport chain, CoQ10 is thought to be freely diffusing in the mitochondrial membrane, enabling electron transportation effectively.

Therefore, CoQ10 deficiency has been implicated in many diseases. CoQ10 deficiency elicits mitochondrial-associated diseases such as myopathy[4-7], cardiovascular disease[8], diabetes[9-11], neurodegenerative disease[12-16] et al.

CoQ10 deficiency usually results from the failure of CoQ10 biosynthesis or poor uptake from diets. CoQ10 has a high catabolic rate which is indicated by the relatively short half-life, T1/2. The half-life varies among tissues, and it ranges between 49 and 125 h. To maintain CoQ10 level, CoQ10 could be supplemented from dietary intake, and it could be from CoQ10 synthesized *de novo*. There are many metabolic pathways involved in CoQ10 *de novo* biosynthesis[17, 18]. Although they remain unclear, it has been well characterized in the yeast model. And many enzymes in the yeast model are conserved in human cells. The speculative process of CoQ10 biosynthesis could be broken down into four steps: the synthesis of decaprenyl group, the synthesis of 1,4-hydroxybenzoate, the attachment of 1,4-hydroxybenzoate with isoprenoid side chain and modifications.

1.2 CoQ10 biosynthesis and inhibition

As mentioned above, the CoQ10 side chain is composed of 10 units of isoprenoids. In mammalian cells, the biosynthesis of CoQ10 is perceived to be initiated from isoprenoid side chain synthesis, which takes place in the cytosol. Mevalonate pathway is involved in the biosynthesis of these essential intermediate precursors (As shown in Fig.3) which share with cholesterol, steroids, and bile biosynthesis. Intermediate precursors contain single units of isoprenoids such as isopentenyl pyrophosphate (IPP), and the mevalonate pathway synthesizes dimethylallyl pyrophosphate (DPP) in the cytosol. Specifically, the isoprenoid is converted from cytosolic acetyl-CoA, which catalyzed by HMG-CoA synthase and HMG-CoA reductase using NADPH as a cofactor. Afterward, elongation of the isoprenoid chain is achieved by a series of sequential condensation reactions which are catalyzed by various prenyltransferases. To synthesize the side chain contains ten units of isoprenoid, geranyl pyrophosphate (two units of isoprenoid, GPP) and a molecule of isopentenyl pyrophosphate (IPP) are condensed to be farnesyl pyrophosphate (FPP) in the cytosol, which is catalyzed by farnesyl diphosphate synthase enzyme encoded by FDPS gene. Then, FPP would be converted into decaprenyl pyrophosphate in mitochondria. Furthermore, it is also hypothesized that the isoprenoid chain could be assembled alternatively in mitochondria from a molecule of isopentenyl pyrophosphate (IPP) and dimethylallyl pyrophosphate (DPP)[18]. The entire process could be described briefly as follow.

1. Acetyl-CoA are converted to 3-hydroxy-3-methylglutaryl-CoA (HMG-CoA);

2. HMG-CoA is converted to mevalonate;

3. Mevalonate is converted to the isoprene-based molecule, isopentenyl pyrophosphate (IPP);

4. elongation of isoprenoids in the cytosol, IPP + DPP → GPP + IPP → FPP, which is catalyzed by farnesyl synthase (1);

5. Further elongation of isoprenoids in mitochondria, FPP + 7 IPP → DPP, which is catalyzed by decaprenyl synthase (2).

Table 1 Isoprenoid intermediate precursors of CoQ10

Precursors of CoQ10	Molecular formula	Number of Isoprenoid unit
Isopentenyl pyrophosphate	$C_5H_{12}O_7P_2$	1
Dimethylallyl pyrophosphate	$C_5H_{12}O_7P_2$	1
Geranyl pyrophosphate	$C_{10}H_{20}O_7P_2$	2
Farnesyl pyrophosphate	$C_{15}H_{28}O_7P_2$	3
Decaprenyl pyrophosphate	$C_{50}H_{84}O_7P_2$	10

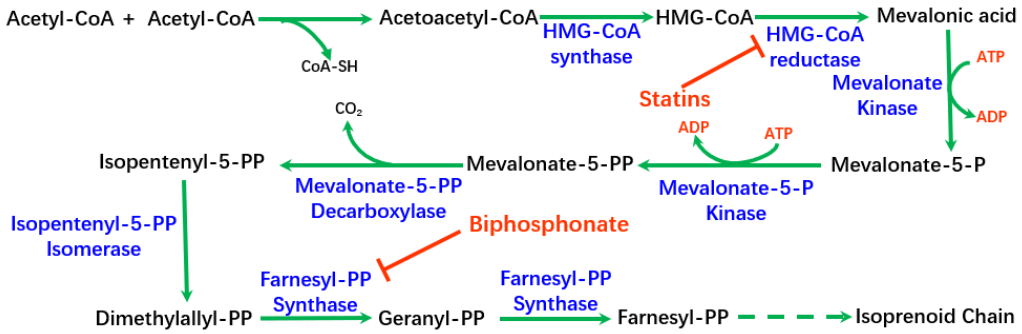

Figure 1.2.1 Proposed biosynthetic pathway of Coenzyme Q in eukaryotes

On the other hand, the precursor of CoQ10 aromatic ring is thought to be from 4-hydroxybenzoate (4-HB) derived from aromatic amino acids such as tyrosine or phenylalanine[19]. The attachment takes place in the mitochondria, which forms a covalent linkage of decaprenyl group with 4-hydroxybenzoic acid (4-HB). And it is subsequently modified by a putative mitochondrial multiple enzymes complex (COQ1-COQ10). Even though many enzymes have been characterized, the sequence of those modifications remains to be unknown. Various modifications include hydroxylation, O-methylation, decarboxylation, and methylation are occurred in mitochondria to form the reduced ubiquinone.

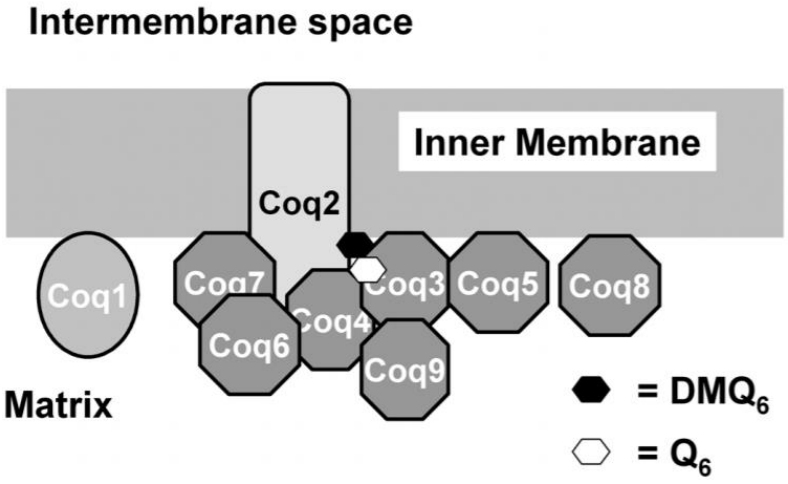

Figure 1.2.2 Putative mitochondrial complex enzyme（COQ1-COQ10） responsible for mitochondrial ubiquinone biosynthesis

1.3 CoQ10 deficiency and its implication

CoQ10 deficiency could be classified into primary CoQ10 deficiency and secondary CoQ10 deficiency. Coenzyme Q10 deficiency can be due either to mutations in genes involved in CoQ10 biosynthesis pathway which is primary CoQ10 deficiency or to mutations in genes unrelated to CoQ10 biosynthesis which is secondary CoQ10 deficiency[20].

Recently, *in vitro* and *in vivo* CoQ10 deficiency has been created to study related diseases. 4-nitrobenzoic acid is used to inhibit the biosynthesis of precursor 4-hydroxybenzoquinone, which ultimately inhibit CoQ10 biosynthesis[21-23]. Besides, HMG-CoA inhibitors such as statins are also frequently used to inhibit CoQ10 biosynthesis by blocking isoprenoid side chain biosynthesis. It conceivable that inhibition of the mevalonate pathway can block CoQ10 biosynthesis, either stain, a class of inhibitor of HMG-CoA reductase that is commonly used to treat hyperlipemia. As reportedly, statins are found to inhibit biosynthesis of CoQ10, which causes undesirable side effect such as myopathy, cognitive dysfunction and diabetes et al.[24].

Moreover, deficient genetics models are commonly used to study CoQ10 deficiency. Modifications of enzymes that involved biosynthetic pathway also are used to in establishment of CoQ10 deficiency model. COQ4 mutation and COQ2 mutation are validated in many models. It has been demonstrated that mutations can reduce cellular CoQ10 and induce respiratory chain defects. (As shown in Figure. 2).

Owing to its essential role in the respiratory chain and keeping oxidative homeostasis, it is conceivable that CoQ10 deficiency would have a profound impact on health and many cellular processes. It has been demonstrated that CoQ10 deficiency affects mitochondrial functions, mitochondrial membrane potential[25] and mitochondrial permeability, as well as oxidative stress. From the biological point of view, they are putative pathogenic mechanisms of CoQ10 deficiency. CoQ10 deficiency leads to the impaired respiratory chain due to it is a substrate of several mitochondrial complexes. But it does not necessarily mean the CoQ10 deficiency could lead to reduced oxidative phosphorylation[19]. It depends on the severity of CoQ10 deficiency.

Not surprisingly, depletion of CoQ10 pool (including reduced from and oxidized form) has a profound implication to mitochondria. It is widely reported that CoQ10 can impair respiratory chain. It has shown that CoQ10 deficient patients present decreased quinone-dependent activities (segments I + III or G3P + III and II + III) while mitochondrial complex activities of complexes I, II, III, IV, and V are normal. It has been suggested CoQ10 depletion leads to compromising oxidative phosphorylation (OXPHOS), it has been proven by measurement of oxygen consumption rate (OCR). Besides, a recent study has suggested that CoQ10 defect may be associated with a deficiency of CoQ10-independent MRC complexes[26].

It has been found that reactive oxygen species (ROS) such peroxide, as well as reactive nitrogen species such as NO level, are all elevated in a CoQ10 depleted cell model. It may be attributable to species formation or the unbalanced homeostasis of pro-oxidant and antioxidant. Although dietary CoQ10 supplementation has been proven to suppress proton leak[27], no evidence has been found that CoQ10 depletion has an effect on electron leak which is mainly attributable to mitochondrial ROS formation.

The dietary supplement of CoQ10 is considered to treat CoQ10 deficiency associated diseases. Because of its high hydrophobicity and large molecule, it is hard to be absorbed into the circulation

and taken up by tissue passively. Despite its poor availability, it has been shown that it can be taken up by tissue in a rat model[28]. Recently, the researcher has made water-soluble CoQ10 preparation, and it has shown enhanced availability in the study.

Chapter 2 Cancer Metabolic Reprogramming and Targeting Opportunities

2.1 General introduction of cancer metabolic reprogramming

Cancer is featured with uncontrollable proliferation, and it is primarily attributed to various protooncogene mutations such as RAS, PIK3CA, RAF, HER2, EGFR, and Myc, as well as mutations of tumor suppressors such as p53, PTEN, pVHL, and LKB1[29]. Thanks to the oncogenic transformation, the cellular metabolism is fundamentally reprogramed to meet biosynthetic, bioenergetic and redox demand[30]. In response to the proliferative signal, cancer depends on glycolytic intermediates and TCA intermediates for supplying enough nucleotides, proteins, and lipids for a cell to double its total biomass and then divide to produce two daughter cells. In respect of bioenergetics, cancer cells depend on glycolysis and concomitant variable OXPHOS for ATP production. Additionally, mutations of metabolic enzymes such as isocitrate dehydrogenase 1/2 (IDH1/2), succinate dehydrogenase (SDH) and mitochondrial complexes also contribute to metabolic abnormalities, which leads to tumorigenesis in return. Besides, cancer metabolism is highly plastic during the cancer progression in response to variable availability of nutrients (glucose, glutamine, and O_2 *et, al.*) and tumor microenvironment.

During the cancerogenesis, emerging metabolic hallmarks such as have been extensively noted:

(1) Deregulated uptake of glucose and amino acids;

(2) Use of opportunistic modes of nutrient acquisition;

(3) Use of glycolytic intermediates and TCA cycle intermediates for biosynthesis and NADPH production;

(4) Increased demand for nitrogen;

(5) Alterations in metabolite-driven gene regulation;

(6) Metabolic interactions with the microenvironment.

While few tumors display all six hallmarks, most display several[31].

Together, these observations have raised interest in targeting metabolic enzymes for cancer therapy, but they have also raised concerns that these therapies would have unacceptable effects on normal cells[32]. Some antimetabolites such as antifolates, purine analogs, and pyrimidine analogs are developed interfere nucleotide synthesis. Antimetabolites such as antifolates methotrexate and pemetrexed are used to inhibit nucleotide synthesis; pyrimidine analogs 5-fluorouracil, floxuridine, cytarabine, and 6-azauracil, as well as purine analogs azathioprine, mercaptopurine have been widely used for cancer therapeutic intervention. However, those antimetabolites are like most cytotoxic anticancer agents, are toxic to normal cells, especially to those normal proliferating cells such as immunocytes, enterocytes, hair follicle.

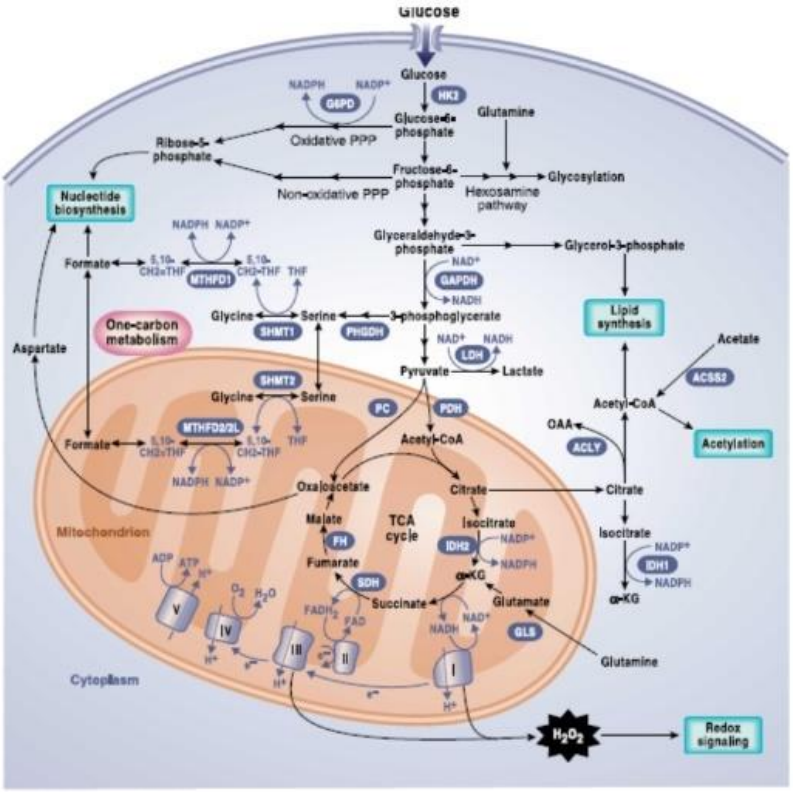

Figure 2.1.1 Schematic illustration of cancer energy metabolism. HK, hexokinase; GAPDH, Glyceraldehyde 3-phosphate dehydrogenase; LDH, lactate dehydrogenase; PDH, pyruvate dehydrogenase; PC, pyruvate carboxylase; IDH, isocitrate dehydrogenase. SDH, succinate dehydrogenase; FH, fumarate hydratase; GLS, glutaminase; ACLY, ATP citrate lyase; G6PDH, glucose-6-phosphate dehydrogenase; MTHFD, Methylenetetrahydrofolate dehydrogenase; SHMT, Serine hydroxymethyltransferase;

Targeting cancer cell metabolism has emerged as a novel anti-cancer strategy in the past decades. Particularly, glucose metabolism, glutamine metabolism and mitochondrial metabolism which contribute to generation energy, biosynthetic precursors, and redox homeostasis to a vast large extent. Advances in cancer metabolism research over the last decade have enhanced our understanding of how aerobic glycolysis and other metabolic alterations observed in cancer cells support the anabolic requirements associated with cell growth and proliferation. Understanding the metabolic propensity of cancer has the potential to provide the foundation for the development of novel approaches targeting tumor metabolism. Tumors characterized by aerobic glycolysis and glucose-dependence could be more sensitive than other tumors to agents targeting the tumor vasculature and glucose transport. Tumors characterized by impaired TCA cycle function and respiration that is glutamine-dependent could be sensitive to agents targeting glutamine metabolism (such as glutaminase). Tumors which have impaired mitochondrial/electron transport function could be susceptible to agents which target the reductive carboxylation and fatty acid synthesis pathways. This distinction of normal cells and cancers cells energy metabolism established a biochemical basis for novel anti-cancer strategy and anti-cancer agents.

Some currently successful cancer therapies have been shown to target metabolism, which demonstrates that it is possible to target tumor metabolism in patients safely[32]. Despite rapid technological advances in studying cell metabolism, we remain unable to reliably distinguish

cytosolic metabolites from those in the mitochondria and other compartments. Current fractionation methods often lead to metabolite leakage. Even within one subcellular compartment, there may be distinct pools of metabolites resulting from channeling between metabolic enzymes. A related challenge lies in the quantitative measurement of metabolic flux; For example, measuring the movement of carbon, nitrogen, and other atoms through metabolic pathways rather than merely measuring the steady-state levels of individual metabolites. While critical fluxes have been quantified in cultured cancer cells and methods for these analyses, continue to improve many obstacles remain such as cellular compartmentalization and the reliance of most cell culture on complex, incompletely defined media. Although some quantitative methods such as mass spectrometry, NMR have been used for metabolic flux analysis, a metabolomic way that can be used for studies of compartmental metabolites remains to be solved[33, 34].

2.2 Glucose metabolism

2.2.1 Glucose transporters and glucose uptake

Glucose transporters are a broad group of membrane proteins that facilitate the transport of glucose across the plasma membrane. They can be classified into an ATP independent GLUTs family and ATP and sodium-dependent SLGTs family. 14 GLUTs encoded by *SLC2A* genes have been identified so far, and they differ from each other depending on substrate selectivity, affinity, and tissue distribution. GLUT1 is responsible for basal glucose uptake due to its ubiquitous expression and relatively high affinity to glucose. GLUT2 is primarily expressed in pancreatic β-cells, responsible for insulin synthesis, where it participates in glucose sensing mechanism and, therefore, it is involved in the regulation of glucose-stimulated insulin secretion. GLUT3 is primarily located in tissues with high glucose demand such as the brain. GLUT4 can rapidly be translocated to the plasma membrane in response to insulin signaling, increasing glucose uptake in cells. GLUT5 exclusively use fructose as a substrate, which is frequently found overexpressed in breast cancer[35, 36].

The affinity and Km of different glucose transporters are varying. Recently, many studies have revealed that the Km for glucose of GLUT1-4 is approximately 1-2 mmol/L, 17mM, 1.8 mmol/L and 5-6 mmol/L respectively[37].

The release of glucose carried out by a conformational change of GLUTs. Many biochemical studies have suggested that GLUTs functions by alternately exposing a binding site for glucose, first on one side of the membrane and then on the other side of the membrane. Thus, the binding site of glucose cytoplasmic side can export glucose. Although it is remained to be elucidated, the internal conformational change of the protein is very likely involved in the changes the exposure of the glucose binding site from one side of the membrane to the other.

Except for passive facilitated diffusion, active transport of glucose can be done by SGLTs family. Until now, three members of SGLTs have been identified, and the distribution of SGLTs are usually tissued specific. SGLT1 (high affinity but low capacity) and SGLT2 (high capacity but low affinity) are mainly found in the gastrointestinal tract and proximal renal tubule respectively. They are involved in gastrointestinal glucose absorption and renal retention. Inhibitors of SGLT2 are used for an anti-diabetic drug.

Table 1 GLUTs family (*SLC2A*) and its properties

Transporters	Km	Tissue distribution	Expression in cancers
GLUT1	1-2 mM	Ubiquitous distribution	Various tumors
GLUT2	17 mM	Liver, pancreas, small intestine	Liver, breast, pancreatic, colon and gastric carcinoma

GLUT3	1.8 mM	Brain, neuron, sperm, placenta	Lung, brain, breast, bladder, laryngeal, prostate, gastric, head and neck;
GLUT4	5-6 mM	Skeletal muscle, adipose tissue, heart	Colon, lymphoid, breast, thyroid, pancreatic and gastric carcinoma
GTUT5	NA	NA	Breast, renal, colon, liver, testicular and lymphoid carcinoma
GTUT6	NA	NA	Breast, pancreatic and endometrial carcinoma, uterine leiomyoma
GLUT7	0.3 mM	NA	NA
GLUT8	2 mM	NA	Endometrial and lymphoid carcinoma, multiple myeloma
GLUT9	0.6 mM	NA	Liver, lung, skin, thyroid, kidney, adrenal, testicular and prostate carcinoma
GLUT10	NA	NA	NA
GLUT11	0.16 mM	NA	myeloma, prostate carcinoma
GLUT12	NA	NA	Breast, prostate, lung, colorectal cancer, oligodendroglioma, astrocytoma
HMIT	NA	NA	NA
GLUT14	NA	NA	NA

Overexpression of glucose transporters is ubiquitously present in various types of tumor, and this overexpression could be attributable to the deregulation of proliferative and pro-survival signals such as p53, c-Myc, HIF-1α, PI3K/AKT pathways[38]. Each glucose transporter isoform plays a specific role in glucose metabolism determined by its pattern of tissue expression, substrate specificity, transport kinetics, and regulated expression in different physiological conditions (as shown in Table 1).

Glycolytic flux could be measured by the measurement of lactate secretion rate or extracellular acidification rate (ECAR) which could be measured by HPLC-UV or Seahorse metabolic analyzer. In addition, glucose absorption kinetics can be detected by radiometry and fluorometry. Most commonly used methods are isotope labeling and fluorescent tracing. In some studies, H^3-2-deoxy-glucose has been used for the measurement of glucose uptake[39, 40]. Furthermore, fluorescent glucose analog such as 2-[N-(7-nitrobenz-2-oxa-1,3-diazol-4-yl) amino]-2-deoxy-d-glucose (2-NBDG) is also used to estimate glucose uptake[41].

2.2.2 Glycolysis

2.2.2.1 General introduction of glycolysis

As one of the fundamental carbon sources of many organisms, glucose metabolism is very critical in cancer bioenergetics, synthesis of biomass and redox homeostasis. There are many metabolic pathways involved in glucose metabolism, such as glycolysis, glycogenesis and glycogenolysis, gluconeogenesis, as well as pentose phosphate pathway (PPP) *et al*. There processes are interconnected by glycolysis.

In eukaryotic cells, glycolysis mostly takes place in the cytosol, and many enzymes are engaged in these ten steps reaction. The free energy released in this process is used to form the high-energy molecules ATP and NADH. Glycolysis is a metabolic pathway that converts glucose to pyruvate. The overall reaction could be described as:

$$\text{Glucose} + 2\ \text{ADP} + 2\ \text{NAD}^+ + 2\ \text{Pi} \rightarrow 2\ \text{pyruvate} + 2\ \text{ATP} + 2\ \text{NADH} + 2\ \text{H}^+ + 2\ \text{H}_2\text{O}$$

Glycolysis plays a pivotal role in glucose metabolism. It not only plays a critical role in bioenergetic, but it is also involved in the biosynthesis of biomass and NADPH production. Glycolytic intermediates efflux provides precursors for biosynthesis of nucleotides, glycerol and some amino acids (As shown in Figure 2.2.1). Glucose-6-phosphate is used as a precursor of glycogenesis and ribose-5-phosphate (R5P) biosynthesis. Dihydroxyacetone phosphate (DHAP) is a precursor of the glycerol that combines with fatty acids to form lipids. 3-phosphoglycerate(3-PG) could be used as a precursor of serine and glycine biosynthesis, which can be further used as a source of NADPH

generating one-carbon cycle and nucleotides biosynthesis. Pyruvate can be converted to alanine catalyzed by ALT which is widely present in many tissues. Conversely, other sugars such as galactose and fructose, glycogen, glycerol, lactate, and some amino acids, as well as oxaloacetate (OAA) can replenish glycolytic intermediates through glucose-6-phosphate(G6P), dihydroxyacetone phosphate (DHAP), phosphoenolpyruvate (PEP) and pyruvate for various metabolic purposes.

As an oxygen-independent energy-generating process, glycolysis accelerated as mitochondria are not able to provide adequate ATP, cells are under the hypoxic condition and as mitochondria are not properly functioning. However, in cancer cells, glycolysis is overactive although oxygen is available, which enable cancer cell to produce ATP in the absence of oxygen and provide precursors for rapid biosynthesis.

In glycolysis, the reactions catalyzed by hexokinase (HK), phosphofructokinase (PFK), and pyruvate kinase (PK) are virtually irreversible due to thermodynamic restriction. The reverse glycolysis (gluconeogenesis) is carried out by other enzymes such as glucose-6-phosphatase and fructose 1,6-bisphosphatase. Additionally, HK, PFK, and PK are the primary regulatory sites of glycolysis. They are tightly controlled in response to hormonal signals, allosteric regulators and protein kinases. These actions regulate the feeding of glycolytic intermediates into connected pathways such as glycogenesis, pentose phosphate pathway (PPP), gluconeogenesis, glycerol synthesis.

A common metabolic feature of a cancer cell is increased glucose uptake and increased lactate secretion. This phenomenon is observed even in the presence of completely functioning mitochondria, and it is known as the Warburg Effect[42]. The Warburg Effect has been documented for over 90 years, and it has been extensively studied over the past ten years with thousands of papers reporting either its causes or its functions. Despite this intense interest, the role of the Warburg Effect remains unclear.

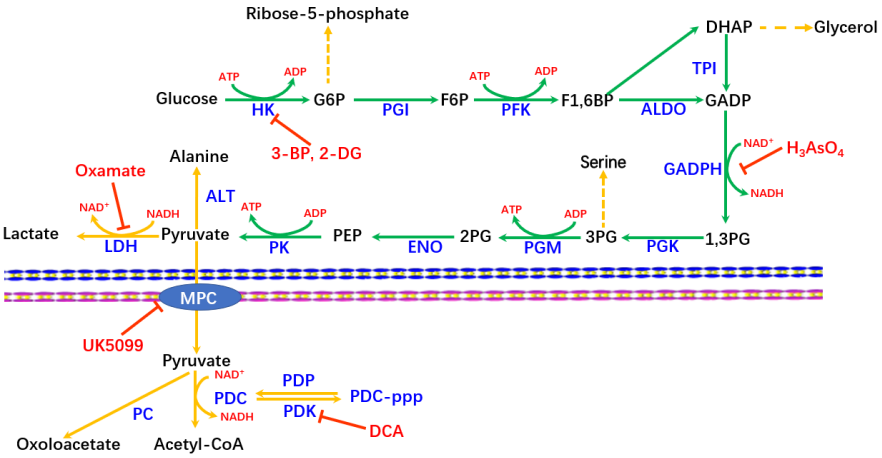

Figure 2.2.1 Glycolytic pathway and its metabolic interconnection with the pentose phosphate pathway. The green arrows indicate glycolytic reactions. The solid yellow arrows indicate further metabolism of pyruvate downstream of glycolysis, whereas the dashed yellow arrows show multiple reactions metabolism. HK, hexokinase; PGI, glucose-6-phosphate isomerase; PFK, phosphofructokinase; TPI, triosephosphate isomerase; ALDO, fructose-bisphosphate aldolase; GAPDH, glyceraldehyde-3-phosphate dehydrogenase; PGK, phosphoglycerate kinase; PGM, phosphoglycerate mutase; ENO, enolase; PK, pyruvate kinase; PDH, pyruvate dehydrogenase;

LDH, lactate dehydrogenase. PC, pyruvate carboxylase; PDC, pyruvate dehydrogenase complex; PDK, pyruvate dehydrogenase kinase; PDP, pyruvate dehydrogenase phosphatase;

2.2.2.2 Hexokinase

Hexokinase is a ubiquitously expressed enzyme that catalyzes the first committed step of glycolysis. HK irreversibly phosphorylates glucose and thus maintains concentration gradient, facilitating the entry of glucose. There are four isoforms of hexokinase (HK), differ in catalytic kinetic and regulator mechanism. They are referred as HK I, HK II, HK III, and HK IV respectively. HKI, HKII, and HKIII have high affinity (Km=∼0.02 mM) while HKIV has low affinity to glucose (Km=∼5 mM). HK1 is constitutively expressed and HK II is typically expressed in adipose, skeletal, and cardiac muscle. Both HK I and HK II are bound to the outer mitochondrial membrane through porin-like protein voltage-dependent anion channel (VDAC), so it has easier access to ATP due to its proximity to mitochondrial ATP/ADP translocase. Specifically, HK IV (also referred to as glucokinase) exclusively uses glucose as a substrate and primarily expressed in liver and pancreatic β-cells. However, other isoforms of HK are expressed in tissues. In glycolysis, HK I, HK II, and HK III are allosterically inhibited by glucose-6-phosphate, while HK IV (glucokinase) is regulated by insulin signaling.

In addition, it is notable that expression of HK II is commonly upregulated in various tumors. HKII is required in malignant transformation given the fact that deletion of HK II can halt RAS mutant driven oncogenic transformation regardless of the presence of HK I[43]. Interestingly, beyond acting as a glycolytic enzyme, HK II also inhibit mitochondrial-induced apoptosis and suppress cell death through the interaction with mitochondrial VDAC[44].

2.2.2.3 Phosphofructokinase (PFK)

Phosphofructokinase (PFK) is also a vital important regulatory point of glycolysis. And it is commonly upregulated in some tumors. Phosphofructokinase (PFK) can be unregulated by protein kinases in response to insulin or epidermal growth factor-induced PI3K/AKT activation[45]. Phosphofructokinase has two isoforms that exhibit very different in glycolysis. Phosphofructokinase 1 (PFK1) is a glycolytic enzyme that catalyzes the phosphorylation of fructose-6-phosphate to fructose 1,6-bisphosphate. However, phosphorylated phosphofructokinase 2 is an enzyme that catalyzes the conversion of fructose-6-phosphate to fructose-2,6-phosphate. Although phosphofructokinase 2 (PFK) have no direct contribution to glycolytic flux, fructose-2,6-bisphosphate (F-2,6-BP) plays a very significant role in allosteric activation of PFK1. As a result, dynamic phosphorylation and dephosphorylation PFK2 in response to deregulated signaling pathways such as hormonal signaling and AMPK signaling contribute to deregulation of PFK1, which would mostly alter glycolytic flux subsequently[46]. Besides, both PFK1 and PFK2 is allosterically regulated by AMP/ATP, phosphoenolpyruvate (PEP) and citrate. Notably, PFK can be inactivated by an elevated level of cAMP induced by glucagon and epinephrine. In this case, a high level of cAMP not only shuts down glycolysis but also stimulates gluconeogenesis through activation of fructose 2,6-bisphosphatase.

2.2.2.4 Fructose 1,6-phosphate aldolase (ALDO)

Fructose 1,6-phosphate aldolase (ALDO) is the enzyme catalyzes the split of fructose 1,6-phosphate into glyceraldehyde-3-phosphate (GA3P) and dihydroxyacetone phosphate (DHAP). It is upregulated in a large variety of tumors. It not only acts glycolytic enzyme, but it is also implicated in cancer metastasis by interaction with cytoskeleton and HIF-1α. Many studies have shown that ALDO can affect cytoskeletal dynamics, promoting cancer cells migration and metastatic

potential[47-51]. The binding of ALDO to the cytoskeleton and its effect on HIF-1α might be attributable to the effect[48, 52-55].

2.2.2.5 Pyruvate kinase (PK)

Pyruvate kinase catalyzes the final step in glycolysis by transferring the phosphate from phosphoenolpyruvate (PEP) to ADP, thereby generating pyruvate and ATP. It is the final regulatory site of glycolysis, and it acts as a gatekeeper for the metabolic fates of glucose carbon. Pyruvate kinase is encoded by the PKLR gene(1q22) and PKM (15q23). PKLR gene expresses two splice variants PKL and PKR which is mainly expressed in red blood cells and liver cells respectively. And PKM gene expresses two splice variants: constitutively active tetramer PKM1 and conditionally active PKM2**.** All other tissues studied express a product of the PKM gene, which generates either the PKM1 or PKM2 isoforms by including one of two mutually exclusive exons during mRNA splicing.

Although the prevalence of PKM1 is lower than that of PKM2 in tumors, it is reported to promote malignancy by upregulation of central carbon metabolism and autophagy[56]. However, some others argued that PKM1 expression suppresses malignancy given the fact that it suppresses nucleotides biosynthesis[57, 58].

It seems to be that PKM2 overexpression is necessary for aerobic glycolysis and to provide an advantage for tumor growth. However, many studies have shown PKM2 is dispensable in maintaining tumor growth[59-63]. The reconciling view was that lower pyruvate kinase activity (by either expression of PKM2 or loss of the enzyme altogether) in all cases was beneficial for anabolic metabolism and thus cell proliferation and tumor growth. In a word, PKM2 not justly simply promote Warburg effect and tumorigenesis by promoting glucose uptake and lactate secretion, but also revise Warburg effect to meet various metabolic requirements of malignancy[64]. The inactive state of PKM2 is associated with the proliferating cell population within tumors, whereas nonproliferating tumor cells require active pyruvate kinase[63].

Given that PKM is a very critical point of glycolysis, to meet the various metabolic purpose, PKM is tightly controlled through expression, post-translational modification, oligomerization, and allosteric regulation. PKM2 is expressed during development and in many adult tissues, including the spleen, lung. Particularly, PKM2 is the predominant isoform that has been frequently found in a large variety of tumors. The regulation of PKM splicing is dependent on multiple splicing factors that bind within the PKM1 and PKM2 exons to promote or suppress their inclusion in the mature transcript[63]. Metabolically, PKM2 have active tetramer, less active dimer, and inactive monomer. PKM2 tetramers support high ATP generation, while PKM2 dimers slow down glycolysis and initiating high biosynthetic rates. The differential oligomerization of PKM2 confers considerable metabolic flexibility and adaptation to meet the requirements of cancer cells. PKM2 catalytic activity could be downregulated by O-GlcNAcylation and phosphorylation[65]. Both O-GlcNAcylation and phosphorylation of pyruvate kinase destabilized the active tetrameric PKM, reduced its catalytic activity and led to nuclear translocation of PKM2[66]. This post-translational modification enhances lipid and DNA synthesis, indicating that O-GlcNAcylation promotes the Warburg effect[67]. Moreover, increases of upstream glycolytic intermediate fructose-1,6-biphosphate(F-1,6-BP) levels allosterically activate PKM2, while ATP inactivates PKM2. This regulatory mechanism enables cells to respond to alterations of glucose availability and energy state by increasing glycolytic rate.

Interestingly, PKM has multiple functions beyond acting as a glycolytic enzyme. Non-glycolytic

functions of PKM2 have been intensively studies, including acting as a protein kinase, the interaction with HIF-1α, epigenetic regulation and nuclear translocation. These findings highlight the role of PKM2 as a protein kinase in its nonmetabolic functions of histone modification[68]. PKM2 as an intriguing new interacting partner for HIF, revealing a potential mechanism for the Warburg effect, an elevation in aerobic glycolytic metabolism frequently observed in cancer[69, 70]. The less active PKM2 dimer, whose structure is favored upon phosphorylation at Tyr105, can also translocate to the nucleus and act as a transcription factor upon stimulation with epidermal growth factor in certain cancer cell lines[71].

2.2.3 Lactate production

A notable characteristic of the Warburg effect is elevated lactate secretion, and it has been long recognized that lactate contributes to aggressive behaviors. Excessive lactate secretion leads to favorable microenvironment for cancer cells. Excessive lactate also leads to low immune cell accessibility, consequently resulting in cell resistance to immunity. Moreover, lactate production sustains glycolysis through cytosolic NAD^+ regeneration together with the reduction of oxaloacetate to malate (malate shuttle). As a result, lactate flux usually responds to alteration of glycolytic flux actively. Thus, it has been commonly used as a marker of glycolytic rate although it is not equivalent to glycolytic flux.

Lactate dehydrogenase (LDH) catalyzes the conversion from pyruvate to lactate in hyperactive glycolytic cells. Lactate dehydrogenase (LDH) is composed of four subunits (tetramer). The two most common subunits are the LDHA (M) and LDHB (H) which share the same active site. There are five isoforms of lactate dehydrogenase in human: LDH1(4H), LDH2 (3H1M), LDH3 (2H2M), LDH4 (3H1M) and LDH5 (4M) depending on the constitution of subunits. These five isoforms are functionally similar but show different tissue distribution.

According to some studies, lactate can be recycled and be utilized by the cancer cell[72-74]. The metabolic symbiosis between cancer cells and stromal cells indicates that lactate could be used as a metabolic fuel under a specific condition[41]. Monocarboxylate transporters (MCTs) is a family 14 members of plasma membrane transporters involved in lactate release and lactate uptake in response to different metabolic stress. MCT1 and MCT4 are the two significant MCTs expressed in tumor cells and represent promising targets for therapy[75].

2.2.4 Pentose phosphate pathway (PPP)

The pentose phosphate pathway (PPP) has been shown to play an essential role in cancer cell growth by providing both nucleotide precursors, which is required for proliferation. And NADPH produced in oxidative PPP could be used for both intracellular ROS detoxification and anabolic metabolism. Pentose phosphate pathway (PPP) is a major NADPH generating pathway in the cytosol, which has profound implication to many critical processes such as lipid biosynthesis, nucleic acid biosynthesis, and GSH regeneration.

Pentose phosphate pathway (PPP) is linked with glycolysis through several points. Glycolytic intermediate glucose-6-phosphate (G6P) feeds into oxidative PPP, producing NADPH and ribulose 5-phosphate through oxidative reactions. While fructose-6-phosphate (F6P) and glyceraldehyde-3-phosphate (GA3P) can be used to produce ribose-5-phosphate through non-oxidative PPP, reversibly, pentoses can feed back into glycolysis by the generation of glyceraldehyde 3-phosphate (GA3P) and fructose-6-phosphate (F6P).

Oxidative PPP could be described as:

Glucose-6-phosphate + 2 $NADP^+$ + H_2O → ribulose-5-phosphate + 2 NADPH + H^+ + CO_2

Non-oxidative PPP could be described as:

3 ribulose-5-phosphate →1 ribose-5-phosphate + 2 xylulose-5-phosphate ↔ 2 fructose-6-phosphate + glyceraldehyde-3-phosphate

G6PDH catalyzes the rate-limiting step of oxidative PPP, and it has been found that it is regulated by a variety of proliferative and survival signals. Some studies have suggested that it is can be positively regulated by PI3K/AKT/mTOR in response to proliferative signals[76], and by sterol element binding protein (SREBP) under conditions of increased need for NADPH for fatty acids synthesis[77], as well as by transcription factor Nrf2 that regulates several antioxidant response element genes[78]. Moreover, it is negatively regulated by Sirt 2 through deacetylation[79].

Besides, thiamine diphosphate-dependent transketolases (TKL) catalyzes multiple reversible non-oxidative reactions in non-oxidative PPP.

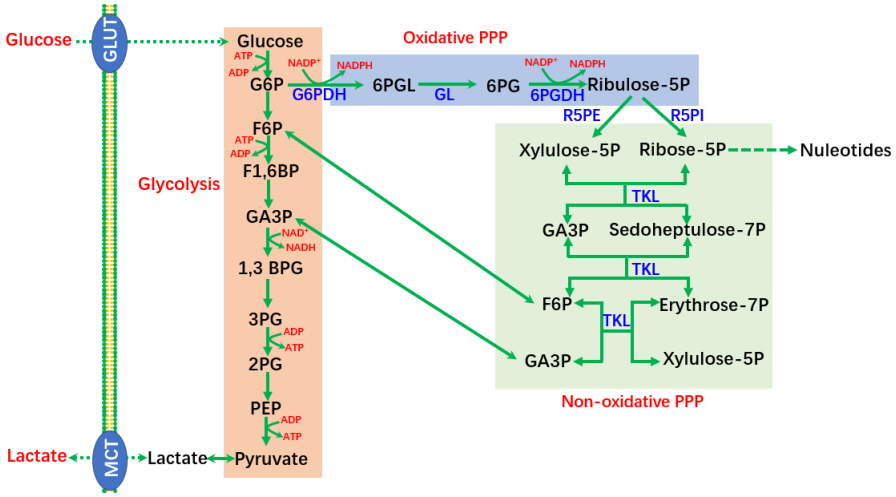

Figure 2.2.2 Schematic representation of pentose phosphate pathway and the interaction of glycolysis with the pentose phosphate pathway. G6P, glucose-6-phosphate; F6P, fructose-6-phosphate; F1,6P, fructose-1,6-phosphate; GA3P, glyceraldehyde-3-biphosphate; 1,3-biphosphoglycerate; 3PG, 3-phosphoglycerate; 2-PG, 2-phosphoglycerate; PEP, phosphoenolpyruvate; 6-PGL, 6-phosphogluconolactone; 6-PG, 6-phosphogluconate; G6PDH, glucose-6-phosphate dehydrogenase; GL, gluconolactonase; 6-PGDH, 6-phosphogluconate dehydrogenase; R5PE, ribulose-5-phosphate 3-epimerase. R5PI, ribulose-5-phosphate isomerase; TKL, transketolase;

2.2.5 Targeting glucose metabolism

Unsurprisingly, glycolysis plays a pivotal role in cancer energy metabolism given that it is an ATP generating pathway. Although glucose is commonly preferred as the fuel for ATP production, other fuels such as glycogen, glycerol, lactate and some amino acids can participate energy metabolism through feeding into glycolytic intermediates such as glucose-6-phosphate (G6P), dihydroxyacetone phosphate (DHAP), phosphoenolpyruvate (PEP) or pyruvate under certain conditions (As shown in Figure 2.2.3). Moreover, glycolytic flux contributes to the biosynthesis of biomass. Besides, glycolytic flux to pentose phosphate pathway and one carbon cycle contribute to NADPH production which is significant for biosynthesis and antioxidative defense.

Above all, one of the most prominent metabolic alterations in cancer cells is the increased dependency on the glycolytic pathway for ATP generation regardless of oxygen availability, known as the Warburg effect. As this metabolic alteration is frequently seen in tumors of various tissue origins, targeting the glycolytic pathway may preferentially kill the malignant cells, and likely have

broad therapeutic implications. Although the biochemical and molecular mechanisms leading to increased aerobic glycolysis in cancer cells are rather complex, and can be attributed to multiple factors such as mitochondrial dysfunction, hypoxia, and oncogenic signals, this metabolic feature has led to the hypothesis that inhibition of glycolysis may severely abolish ATP generation in cancer cells and thus may preferentially kill the malignant cells[80].

Depletion of fuels or essential impairment of energy generating machinery would inevitably lead to bioenergetic depletion. There is a bidirectional interaction of energy metabolism and cell division[81, 82]. Since bioenergetic stress could be sensed by AMPK, which consequently inhibits cell cycle checkpoint mediator p53 and cyclin-dependent kinase inhibitor proteins such as p21 and p27[83, 84]. Besides, phosphorylated AMPK activates TSC and inactivate mTORC1, mTORC1 downstream targets of S6K1 and 4EBP1/eIF4E downregulate protein synthesis which marked by reduced cell mass and cell size. When bioenergetic stress passes a certain threshold, cells commit to programmed cell death (PCD). Above all, the commitment of apoptosis might be attributable to the link of ATP and mitochondrial membrane potential(ψm). Besides, energetic stress is also associated with autophagy; then amino acids could be recycled for promoting cell survival. Since cancer cells are capable of compensating ATP production from alternative fuels or energy-generating pathways, this may relieve energetic stress and confer cancer cells adaptive resistance to bioenergetic depletion. When glycolysis is inhibited, the cells with intact mitochondria enable them to use alternative fuels such as fatty acids and amino acids to produce metabolic intermediates channeled to the TCA cycle for ATP production through respiration. As such, cells with healthy mitochondria are expected to be less sensitive to agents inhibiting glycolysis. Conversely, defective mitochondrial bioenergetics can sensitize cancer cells to glycolytic inhibition.

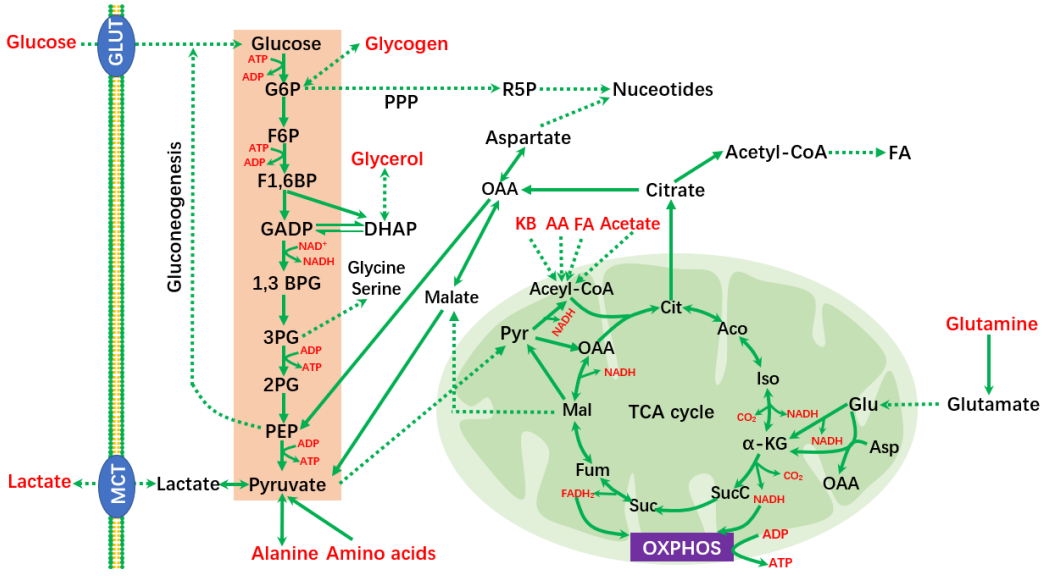

Figure 2.2.3 Schematic representation of cancer energy metabolism. Glycolysis is one of ATP production sites which was highlighted with orange background; While mitochondria is the other ATP production site which was green; Red texts indicate fuels and energetic substances involved in cancer bioenergetics; Solid green arrows indicate the conversions and movements of metabolites; Dashed arrows indicated multiple steps of reactions or transmembrane movement of metabolites; G6P, glucose-6-phosphate; F6P, fructose-6-phosphate; fructose-1,6-phosphate; GADP, glyceraldehyde-3-phosphate; DHAP, dihydroxyacetone phosphate 1,3BPG, 1,3-biphosphoglycerate; 3PG, 3-phosphoglycerate; PEP, phosphoenolpyruvate; Pyr, pyruvate; Cit, citrate; Aco, aconitate; Iso,

isocitrate; KG, ketoglutarate; SucC, succinyl-CoA; Suc, succinate; Fum, fumarate; Mal, malate; OAA, oxaloacetate; FA, fatty acids; AA, amino acids; KB, ketone bodies; Glu, glutamate; OXPHOS, oxidative phosphorylation;

Overexpression of GLUT1 is prevalent in tumors, and it lays a foundation of using GLUT1 expression as a prognostic biomarker[85, 86]. Many studies have shown that the overexpression of GLUT1 leads to the poor prognosis of cancer. 2-^{18}F-2-deoxy-glucose positron emission tomography (PET) has been used in clinical practice. Glucose influx into a cell is the first rate-limiting process involved in glucose metabolism. This characteristic of GLUTs expression makes it a very logical target for any pathological condition that involves the metabolism of glucose. In particular, cancer takes advantage of a cell's ability to generate energy from numerous pathways, and this flexibility in energy derivation is also a leading target in the development of therapeutic agents. It raises a lot of interests in the discovery and development of inhibitors of glucose transporters [87-89]. Although glucose uptake is elevated in various tumors, differential expression profiles and dependence of GLUTs makes it challenging to target GLUTs specifically. Cytochalasin B a potent GLUTs inhibitor used in many studies, while it inhibits cell division by blocking the formation of microfilament. Moreover, numerous natural products such as resveratrol, phloretin, curcumin, caffeine, apigenin, genistein, and silybin have been found to have an inhibitory effect on glucose uptake and tumor growth. However, mechanisms of their effects beyond metabolic modulation may also contribute to their efficacies. Glucose transporters are cell surface proteins, making it feasible to inhibit glucose uptake specifically by using antibody[90, 91] or antisense RNA[92, 93]. However, the discovery of potent and specific GLUTs inhibitor remains to be solved.

Since many types of tumors manifest a high dependency on glycolysis, glycolytic enzymes are proposed as anti-cancer targets. Numerous agents such as 2-deoxyglucose (2-DG)[94, 95]. 3-bromopyruvate[96] and lonidamine has reported being effective to mediate glucose metabolism by inhibiting hexokinase (HK) catalytic activity[97]. Whereas, 3-bromopyruvate(3-BP) also inhibit glyceraldehyde-3-phosphate dehydrogenase (GAPDH) through alkylation. Moreover, 3-bromopyruvate trigger the dissociation of HKII from mitochondria, thus promoting apoptosis. Some evidence has proven that lonidamine also inhibits mitochondrial pyruvate carrier (MPC) and monocarboxylic acid transporter (MCT)[98].

The regulation of pyruvate kinase (PK) is a critical diversion to active glycolysis to anabolism by using glycolytic intermediates. Because most normal tissues express an isoform of pyruvate kinase other than PKM2, selective targeting of PKM2 provides an opportunity to target cell metabolism for cancer therapy. PKM2 has an identical catalytic site as the related M1 splice variant (PKM1)[99]. However, isoform-selective inhibition is possible as PKM2 contains a unique region for allosteric regulation. Inhibition of the glycolytic activity of PKM results in reduced glycolytic flux and energetic depletion. And inhibition of inactive PKM2 can inhibit anabolism.

Pyruvate kinase (PK) confers multifaceted benefits on cancer cells. Active pyruvate kinase contributes to glycolysis, and inactive pyruvate kinase contributes to the anabolic pathway. Inhibition of PKM2 alters nucleotide synthesis to impact cell proliferation[57].

Pentose phosphate pathway is found upregulated in many types of tumor given the fact that higher demand of NAPDH and ribose-6-phosphate in cancer cells. Thus, inhibition of PPP has been proposed as a promising anti-cancer strategy. G6PDH is a gate-keeping enzyme of the pentose phosphate pathway. Inhibition of G6PDH considerably reduces oxidative PPP flux and reduced NAPDH regeneration, leading to perturbed GSH/GSSH ratio. Although specific G6PDH inhibitor

has not been identified yet, recent studies have shown that combination of a G6PD inhibitor DHEA and a hexokinase inhibitor 2-DG caused a remarkable decrease of the cellular glutathione level[100, 101]. Besides, transketolase 1 (TKTL1) has an essential role in carcinogenesis, being overexpressed in multiple tumors. Inhibition of transketolase (TKL) can result in the oxidative generation of ribose-5-phosphate, as well as NADPH[102-105], leading to an anti-proliferative effect.

Reversing overactive lactate release, by either inactivation of LDH or activation of pyruvate PDH, appears to be specifically toxic to cancer cells in comparison to normal cells, given the fact that cancer cells are exhibiting very distinctive metabolic phenotype. Many reports have discovered that inhibition of lactate dehydrogenase (LDH) is sufficient to suppress cancer growth in vitro and in vivo model[106-109]. In addition to the acceleration of glycolysis, it is found that the pyruvate dehydrogenase is inactivated and lactate dehydrogenase (LDH) is activated in many malignancies. Moreover, pyruvate dehydrogenase complex (PDC) and lactate dehydrogenase (LDH) reversal are widely regarded as a promising anti-cancer target[110]. Interestingly, an inhibitor of pyruvate dehydrogenase kinase dichloroacetate (DCA) is reported to be useful to revert Warburg effect[111-113], DCA has recently been proposed as a novel and relatively non-toxic anti-cancer agent that can reverse the glycolytic phenotype in cancer cells through the inhibition of pyruvate dehydrogenase kinase (PDK). Inhibition of LDH has been suggested a promising anticancer strategy[107, 114, 115]. Oxamate has been shown a promising inhibitor of LDH *in vitro*[116]. Moreover, Cexitumab has been reported to reverse the Warburg effect by inhibiting HIF-mediated LDH-A[41].

Inhibition of glycolysis represents a great perspective in cancer therapy. Thus, the development of new generations of glycolytic inhibitors with high potency, stability, and reasonable safety profiles represent an essential research area in this field. It is also significant to evaluate the synergic effect of glycolytic inhibitors and other therapeutic modalities such as chemotherapeutic agents and radiation therapies, as well as develop optimal combination regimens for effective treatment of cancer.

Table 2 Enzymes and inhibitors involved in glucose metabolism

Targets	Inhibitors	Drug development
HK	2-deoxy-D-glucose	Clinical trial I/II
	3-bromopyruvate	Preclinical
	Lonidamine	Clinical trial III
	Imatinib	Clinical use for leukemia
GPI	D-fructose-6-phosphate	Preclinical
PFK	3-(3-pyridinyl)-1-(4-pyridinyl)-2-propen-1-one	Preclinical
ALDO	3-deoxyglucose/4-deoxyglucose	Preclinical
TPI	2-Carboxyethylphophonic acid	Preclinical
	2-phosphoglyceric acid	Preclinical
GAPDH	3-bromopyruvate	Preclinical
	Pentavalent arsenic compound	Clinical use for Leukemia
	Iodoacetate	Preclinical
	Koningic acid	Preclinical
PGM	Benzene hexacarboxylic acid	Preclinical
Enolase	Sodium fluoride	Preclinical
PKM	Fluorophosphate,	Preclinical
	pyridoxal-5'-phosphate,	Preclinical

	creatine phosphate	Preclinical
	L-phosphonoacetate	
	CAP-232/TLN-232	
G6PDH	Dehydropiandrosterone	Preclinical
	Aminonicotinamide	Preclinical
	α-Chlorohydrin	Preclinical
	Polydatin	Preclinical
TKL	Oxythiamine	Preclinical
LDH	Oxamate	Preclinical
	Oxalate	Preclinical
	Galloflavin	Preclinical
	N-hydroxyindole based	Preclinical
	EGCG	Preclinical
PDK	Dichloroacetate	Clinical
MCTs	AZD3965	Preclinical
	Coumarin carboxylic acids	Preclinical

2.3 Glutamine metabolism

2.3.1 General introduction of glutamine metabolism

Cancer cells reprogramed their metabolism towards aerobic glycolysis and elevated glutaminolysis, which contributes to the aggressive phenotype. Understanding how glutamine metabolism is regulated may provide potential targets for therapeutic intervention. Glutamine is the most abundant amino acid in the blood, and it plays a critical role in cancer energy metabolism. Glutamine is also involved in multiple anabolic pathways. As a proteinogenic amino acid, so it is involved in protein synthesis. In particular, glutamine also serves as critical sources of acetyl-CoA which is an indispensable precursor of lipid synthesis and steroids synthesis. Moreover, as one of the most crucial nitrogen sources, glutamine is also involved in purine and pyrimidine synthesis and glutathione synthesis. Besides, Glutamine also plays a role in the anti-oxidative defense. Glutamine produce NADPH for glutathione (GSH) regeneration from glutathione disulfide (GSSH). Besides, Glutamine is also one of the critical precursors for gluconeogenesis and neurotransmitters such as glutamate and γ-aminobutyrate (GABA).

Many oncogenes or suppressors such as Myc, Ras, and p53 have been suggested to be attributable to the deregulation of glutamine metabolism[117]. Specifically, Myc is considered as a master regulator of glutamine metabolism Myc is usually upregulated and it contributes to the metabolic transformation in various cancers in response to mitogenic signals such as Wnt, PI3K, MAPK/ERK *et, al*. Myc manipulates glutamine metabolism both directly and indirectly. As a transcription factor, Myc directly binds the promoters and stimulates expression of genes involved in glutamine metabolism. Many studies have shown that the expressional pattern of glutamine transporters is positively regulated by Myc[118]. In addition, it is worthwhile to point out that Myc which is a transcriptional factor regulating multiple target genes involved in glutaminolysis, which may dominate the upregulation of transcriptional level of glutaminolytic enzymes. On the other hand, Myc also promotes glutaminase activity indirectly by repressing expression of miR-23a/b which targets GLS1[119, 120].

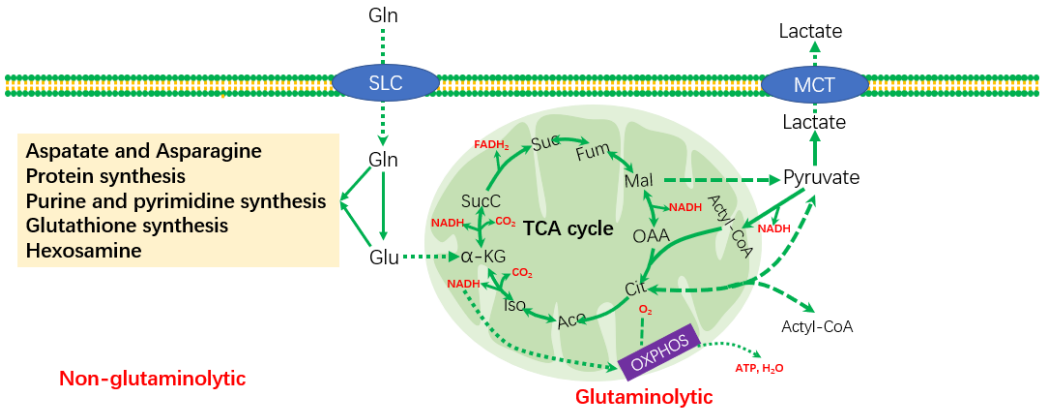

Figure 2.3.1 Major metabolic fates of glutamine in proliferating or cancer cells. Green arrows indicated conversions and movements of metabolites. Gln, glutamine; Glu, glutamate; α-KG, α-ketoglutarate; SucC, succinyl-CoA; Suc, succinate; Fum, fumarate; Mal, malate; OAA, oxaloacetate; Cit, citrate; Iso, isocitrate; SLC, solute carriers; MCT, monocarboxylate transporter;

Glutaminase metabolism is flexible and intricate, and metabolomic approaches could be developed to study a specific metabolic pathway in order to gain better insights into the metabolic fates of glutamine. To date, isotopic labeling together with mass spectrometry or NMR is the most common way to explore the metabolic fates of glutamine. The reductive glutamine metabolism can be traced by 1-^{13}C-glutamine because isotopically labeled carbon is lost during oxidative decarboxylation but retained on metabolites in the reductive pathway. Conversely, 5-^{13}C glutamine can be used to assess oxidative metabolism because it incorporates an isotopic label into TCA intermediates produced by oxidative metabolism except for acetyl-CoA. This method is intensively used in metabolic flux analysis even though it can only be used as a tool for steady-state metabolism[33].

2.3.2 Glutamine transporters and glutamine uptake

Glutamine is a hydrophilic amino acid. Thus, glutamine is not able to diffuse across the plasma membrane freely. Cells rely on transporters for taking up glutamine into the cell membrane. To date, 14 transporters have been identified that can transport glutamine across the cell membrane. Many transporters are involved in spontaneous passive transport of glutamine, and they belong to four genetically different families: SLC1, SLC6, SLC7 and SLC38[121]. Although there are 14 glutamine transporters, none of them is exclusive to glutamine transport.

For example, ASCT2 (SLC1A5) is the most commonly expressed glutamine transporter. This transporter is an obligatory exchanger of Na^+/glutamine to another Na^+/amino acid. It is selective for alanine, serine, cysteine, threonine, and glutamine. The transport through ASCT2 is passive transport because it is electroneutral. As a result, blocking of glutamine transporter would inevitably affect absorption of other amino acids, as well as downstream metabolism of another amino acid

LAT1 (SLC7A5), L-type amino acid transporter, is a member of solute carrier family 7 that is associated with chaperone subunit during the translocation to the plasma membrane. It has been found that it is highly expressed in many tumors[122]. This type of transporter can interact with neutral amino acids, but it prefers long chain amino acids such as leucine, isoleucine, valine, tyrosine, phenylalanine, tryptophan, glutamine and methionine[121].

Coupling of ASCT2 and LAT1 can export intracellular glutamine and import leucine. This bidirectional transportation promotes cell growth and suppresses autophagy via activation of mTORC1[123]. Many studies have revealed that mTORC1 is an amino acids sensor which

coordinates amino acids supply and protein synthesis. The exchange of glutamine and leucine activates mTORC1, although the underlying molecular mechanism remains unclear. Some studies have shown the import of branched-chain amino acids such as leucine might facilitate the GTP loading to mTORC1 though Rag protein instead of Rheb GTPase[124-126], which subsequently promote the translocation of ribosomal Ragulator complex. However, some others argue that leucine alone is not sufficient to activate mTORC1. It is the exchange of glutamine and leucine is necessary for the activation of mTORC1. Besides, leucine is an allosteric activator of glutaminase dehydrogenase (GDH), which suggests that leucine activate mTORC1 through mediating glutaminolysis[127]. Moreover, many studies have found that the cell membrane permeable α-ketoglutarate can suppress autophagy in the absence of glutamine and leucine, indicating that α-ketoglutarate might be the metabolite responsible for the activation of mTOR[128, 129]. Interestingly, some evidence has shown that mTOR is activated by α-ketoglutarate in a prolyl domain hydroxylase (PDH) dependent manner[130].

Previous work has suggested that glutamine influx via ASCT2 triggers essential amino acids entry via the LAT1 exchanger, thus activating mechanistic target of rapamycin complex 1 (mTORC1) and stimulating growth. ASCT2's pro-tumoral role and indicate that the proposed functional coupling model of ASCT2 and LAT1 is not universal across different cancer types[131]. In a word, mTORC1 is acting as an amino acids sensor, and it also serves as the master coordinator of metabolism and cell growth, autophagy as well as apoptosis. L-glutamine and EAAs alone have little effect, but together they synergize to activate mTORC1 [124]. Addition of cell-permeable α-ketoglutarate stimulated lysosomal translocation and activation of mTORC1[128, 130].

XCT or SNAT, a glutamate-cysteine antiporter, plays a critical role in oxidative homeostasis. Because cysteine is one of the indispensable precursors of glutathione (GSH) synthesis, and sulfhydryl group (SH) of cysteine serves as a proton donor and is responsible for its biological activity. And cystine is one of the semi-essential amino acids that need to be supplied from a diet. Thus, it is conceivable that the exchange of glutamate and cysteine plays a very significant role in the anti-oxidative defense.

Table 3 Glutamine and glutamate transporters and its properties

Family	Genes	Proteins	Substrates	Direction	Ion dependence
SLC1	SLC1A5	ASCT2	**Gln**, Glu, Asp, Ala, Ser, Cys and Thr	Influx/efflux	Na^+ dependent
SLC6	SLC6A14	ATB^{0+}	Cationic and neutral amino acids; Glutamine, neurotransmitters	Influx	Na^+/Cl^- dependent
	SLC6A19	ATB^{0+}	Glu, Arg, Ser, and Gly, neurotransmitters; All 9 essential amino acids;	Influx	Na^+ dependent
SLC7	SLC7A5	LAT1	Gln, Phe, Val, Thr, Trp, Met, Leu, Ile, His and all neutral amino acids	Influx/efflux	Na^+-dependent;
	SLC7A6	y^+LAT1	Influx of neutral amino acids; efflux of cationic amino acids (Lys, Arg)	Influx/ efflux	Na^+-dependent;
	SLC7A7	y^+LAT2	Influx of neutral amino acids; efflux of cationic amino acids (Lys, Arg)	Influx/efflux	Na^+-dependent;
	SLC7A8	LAT2	Gln, Phe, Val, Thr, Trp, Met, Leu, Ile, His and all neutral amino acids	Influx/efflux	Na^+-independent;
	SLC7A9	$b^{0,+}$	Influx of Lsy, Arg, Cys; Efflux of neutral amino acids	Efflux	Na^+-independent;
	SLC7A11	SANT	Influx of Cys; efflux of Glu	Influx/efflux	Na^+-independent;
SLC38	SLC38A1	SANT1(SA2)	Gln, neutral amino acids excluding aromatic amino acids	Influx	Ion independent
	SLC38A2	SANT2(SA1)	Gln, neutral amino acids excluding aromatic amino acids	Influx	Ion independent
	SLC38A3	SN1	Gln, Asp, His	Influx/efflux	Na^+/ H^+ dependent
	SLC38A5	SN2	Gln, Asp, His	Influx/efflux	Na^+/H^+ dependent
	SLC38A7	System N	Gln, Asp, His, Glu, Asp, Arg	Influx	Ion independent
	SLC38A8	System A	Gln, Asp, His, Glu, Asp, Arg	Influx	Ion independent

2.3.3 Glutaminolysis

Glutaminolysis commonly used to convert glutamine to all TCA intermediates through TCA intermediates interconversion. It can be sequentially broken down into five carbon carboxylates, four carbon carboxylates, and then three carbon carboxylates through decarboxylation and dehydrogenation (As shown in the figure). The catabolism glutamine could be divided into three phases: phase I, conversion from glutamine to α-ketoglutarate; Phase II, The conversion of α-ketoglutarate to pyruvate; Phase III, the oxidation of pyruvate. Glutamine to α-ketoglutarate is commonly referred as glutaminolysis. But it is often confused with some other relevant metabolic pathways. It is referred as canonical glutaminolysis in this study.

Phase I, Glutamine + H_2O + $NAD(P)^+$→ α-ketoglutarate + 2 NH_3 + NAD(P)H,

This process could be defined as glutaminolysis. The α-ketoglutarate fueled by glutamine can be converted to other TCA cycle intermediates which could be further used for bioenergetic and biosynthetic purposes.

(1) Glutamine + H_2O + $NAD(P)^+$→ α-ketoglutarate + NAD(P)H + 2 NH_3

(2) Glutamine + Aspartate+ H_2O → α-ketoglutarate + Oxaloacetate + NH_3

Phase II, conversion of ketoglutarate to pyruvate. The process has not been well defined yet. The system of metabolic reactions involved in oxidative phosphorylation through succinate dehydrogenase, it is referred as “OXPHOS glutaminolysis” hereafter. This term points out to its essential dependence on succinate dehydrogenase (Complex II) and hence on respiration and OXPHOS[132, 133]. Thus, the rate of OXPHOS glutaminolysis could be measured by the reduction of oxygen consumption rate (OCR) or ATP generation under the glutamine deprived condition[134-137]. 1 NADH, 1NAD(P)H, 1 FADH2, and 1 GTP are produced in this process, indicating this process contributes to both bioenergetics and NADPH dependent antioxidative system. In contrast, when the reductive carboxylation of α-ketoglutarate by $NADP^+$ dependent isocitrate dehydrogenase 1/2 (IDH1/2) (in the counter Krebs cycle direction) consuming NADPH, we define that system “anoxic glutaminolysis”, denotes the absolute independence of oxygen or respiration. Although the conversion of glutamine to pyruvate is presumably carried through multiple pathways, it is notable that malic enzymes 1/2 (ME1/2) is indispensable because it could not be bypassed.Translocation of the glutamine-derived TCA intermediates can be accieved by citrate carrier (CIC) or malate carriers (MC).

Phase III, oxidation of pyruvate. The glutamine-derived pyruvate can be converted to lactate. It could also enter mitochondria and then be fully oxidized through TCA cycle and OXPHOS. 4 NADH, 1 FADH2 and 1 GTP, which is equivalent to 14 ATP in total.

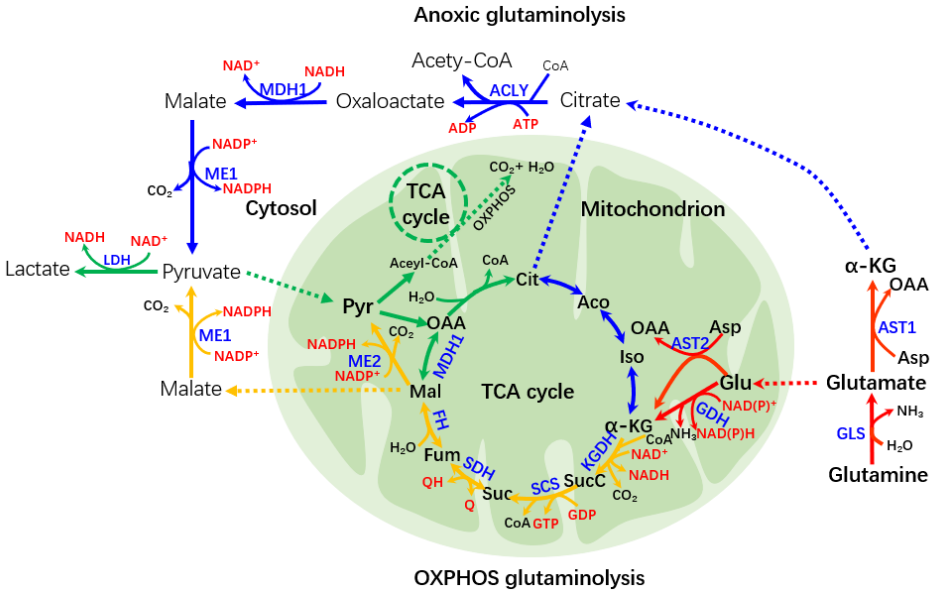

Figure 2.3.2 Schematic illustration of glutaminolysis. Yellow arrows indicated OXPHOS glutaminolysis pathway, and blue arrows indicated anoxic glutaminolysis. While other metabolic reactions were indicated by green arrows. Dashed arrows indicate transmembrane movements of metabolites; Bidirectional arrows indicated reversible reactions; GLS, glutaminase; GDH, glutamate dehydrogenase; AST, aspartate transaminase; KGDH, ketoglutarate dehydrogenase; SCS, succinyl-CoA synthase; SDH, succinate dehydrogenase; FDH, fumarate dehydrogenase; ME1, malic enzymes 1; ME2, malic enzyme 2; LDH, lactate dehydrogenase. Pyr, pyruvate; Cit, citrate; Aco, cis-aconitate; Iso, isocitrate; α-KG, α-ketoglutarate; SucC, succinyl-CoA; Suc, succinate; Fum, fumarate; Mal, malate; OAA, oxaloacetate;

Glutaminase is a critical enzyme that catalyzes the hydrolysis of glutamine. It is the first step of glutaminolysis, which provide glutamate that can be further used to support either energy generation or anaplerosis. To date, three glutaminase isoforms have been identified: kidney-type glutaminase (KGA) and glutaminase C (GAC) are two splice variants both encoded by gene Gls1, and those two isoforms are referred as GLS. One liver type glutaminase (KGB) encoded by Gls2 is also referred to as GLS2[138]. The kidney-type glutaminase (KGA) a type with high activity and low Km. The glutaminase (KGB) is a type with low activity and allosteric regulation; its activity could be allosterically altered in response to ATP/ ADP ratio or NAD^+/ NADH ratio.

The three isoforms of glutaminase play different roles in cancer cell metabolism. GLS1 splice variant glutaminase C which is reportedly compartmentalized in the mitochondria has been found upregulated in various cancer cells[121, 138]. It is supposedly localized on the mitochondrial membrane due to the absence of mitochondrial glutamine transporter. Besides, a study has shown that transient knockdown of GLS1 splice variant GAC had the most detrimental effect on cancer cell growth[139]. In addition, mitochondrial glutaminases are mostly found as inactive dimers in the organelle and tetramerization is required for enzyme activation[140, 141]. Some studies have shown that the accumulation of inorganic phosphate in the mitochondria is the trigger for increased GAC-based glutaminolysis[140]. GLS1 is involved in the transcriptional repression of thioredoxin-interacting protein (TXNIP), which is a potent negative regulator of glucose uptake and aerobic glycolysis. Moreover, it has been shown that the loss of GLS1 function by RNA interference or pharmacological inhibition diminished the rates of glucose utilization, growth, and invasiveness of

prostate cancer cells. Therefore, GLS1 may positively regulate glucose uptake in addition to operating glutaminolysis[142].

GLS2, another isoform of glutaminase mainly expressed in the liver, acting as controller of glutamate flux through glutamine hydrolysis. Thanks to its contribution to glutamate flux, it has been shown that GLS2 is involved in glutathione (GSH) generation and anti-oxidative defense in response to p53[143-145]. Besides, it appears to be a functional tumor suppressor due to its negative regulation of PI3K/AKT signaling in human hepatocellular carcinoma[146]. However, the role of GLS2 in cancer metabolism remain to be further elucidated.

Glutamate dehydrogenase 1 (GDH1) is the isoform ubiquitously expressed in life, while glutamate dehydrogenase 2 (GDH2) is tissue-specific isoform. Both of two isoforms are localized to the mitochondrial matrix. It can be classified into three classes depending on its preference to NAD^+ or $NADP^+$: NAD^+ dependent GDH, $NADP^+$ dependent GDH and $NAD(P)^+$ dependent GDH, regardless of they have not been identified yet. Glutamate dehydrogenase (GDH) is a significant regulatory enzyme, together with aspartate transaminase (AST) and alanine transaminase (ALT), keeping the entry gate of glutamine/glutamate into mitochondria. In addition, GDH also acts as an energy sensor because glutamine is an alternative source for energy generation. Mammalian GDH1/2 is allosterically regulated, with chemically diverse compounds shown to influence the enzyme's activity. A wide range of allosteric regulators includes purine nucleotides (ATP/ADP or GTP/GDP), NAD^+/NADH, L-leucine, palmityl CoA, spermidine, steroid hormones and neuroleptic drugs[147]. Those allosteric regulators alter GDH activity and control glutamate flux into mitochondria for energy generation or anaplerosis in response to specific metabolic stresses[148, 149]. Moreover, the regulation is carried out by SIRT 4 through ATP-ribosylation is also very significant regulatory mechanism on glutamate dehydrogenase (GDH). This regulation acts as a restriction of mitochondrial glutamine metabolism.

Aspartate transaminase 1 (referred to as GOT1 or cAST) and aspartate transaminase 2 (referred as GOT2 or mAST) is used as an alternative enzyme to catalyze the conversion from glutamate to α-ketoglutarate. Thus, inhibition of aspartate has been proven to inhibit glutamate flux into mitochondria. Alanine transaminase 1 (SGT1 or cSGT) and alanine transaminase 2 (referred as SGT2 cSGT) also involved in the conversion from glutamate to α-ketoglutarate in the same way.

Besides, the entry and flux of glutamine through the TCA cycle requires the continual regeneration of mitochondrial NAD^+ through the activities of the mitochondrial electron transport chain and availability of multiple metabolites due to its dependency on malate shuttle.

2.3.4 Glutamine metabolism through reductive carboxylation

Anaplerosis is the metabolic process of replenishing TCA cycle intermediates that have been extracted for biosynthesis. Glutamine can be converted to α-ketoglutarate through glutaminolysis due to the interconversion pool of TCA intermediates. Oxaloacetate, citrate, ketoglutarate, and succinyl-CoA are usually used as a processor for macromolecules synthesis. Normally, glutamine can feed into the pool of TCA intermediate either through oxidative decarboxylation pathway or reductive carboxylation pathway. Whereas, as mitochondrial impaired or cells are under hypoxic condition, glutamine-derived anaplerosis is predominantly used to conduct reductive carboxylation due to a rendered oxidative pathway or limited input of Acetyl-CoA[150, 151].

Glutamine anaplerosis plays a multifaceted role in cancer cell proliferation and survival. A recent study has shown that glutamine anaplerosis suppresses pancreatic cancer growth through mTORC1 activated autophagy[152]. Despite that, TCA reductive carboxylation has been intensely studied due

to its contribution to the proliferation of cancer cells with mitochondrial defects. It is notable that reductive carboxylation is predominant glutamine-derived anaplerosis and could be carried out both in cytosol and mitochondria. There are three isoforms of IDH, namely IDH1 (cytosolic, $NADP^+$ dependent), IDH2(mitochondrial, $NADP^+$ dependent) and IDH3 (mitochondrial, NAD^+ dependent)[153]. However, it has been proven that transient knockdown of IDH1 or IDH2 diminished the reductive flux and cancer cell proliferation and IDH3 silencing did not affect reductive flux, indicating only NADPH-dependent isoforms IDH1 and IDH2 are capable of operating reductive carboxylation[154, 155]. Furthermore, nicotinamide nucleotides transhydrogenase (NNT) knockdown reduced mitochondrial NADPH production and TCA reductive flux, suggesting that NNT is required to maintain mitochondrial redox state and reductive carboxylation[150, 156, 157].

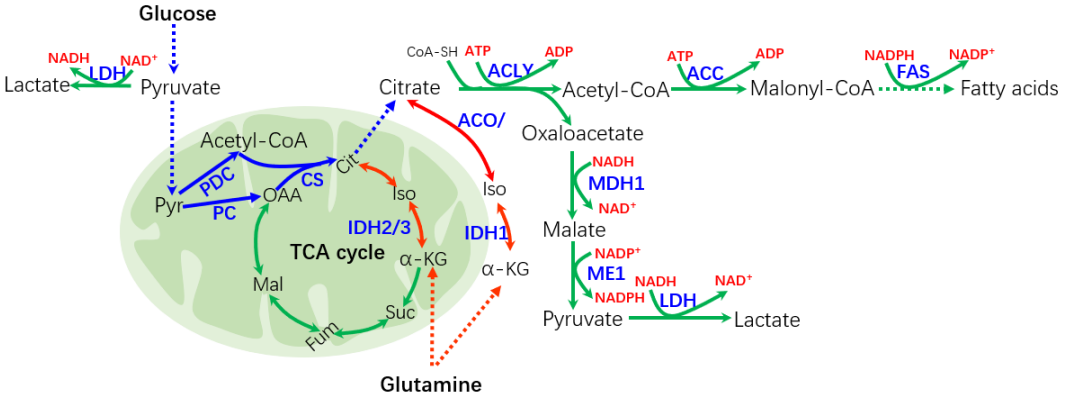

Figure 2.3.3 Glutamine derived anaplerotic pathway in proliferating cells. Green arrows indicate the conversions and movements of metabolites. GLS, glutaminase; GDH, glutamate dehydrogenase; IDH1, isocitrate dehydrogenase 1; IDH2/3, isocitrate dehydrogenase 2/3; AST, aspartate transaminase; ACLY, ATP citrate lyase; ACC, acetyl-CoA carboxylase; MDH, malate dehydrogenase; ME, malic enzymes; LDH, lactate dehydrogenase; ATP, adenosine triphosphate; ADP, adenosine diphosphate; NAD^+, nicotinamide adenine dinucleotide. NADH, reduced nicotinamide adenine dinucleotide; $NADP^+$, nicotinamide adenine dinucleotide phosphate; NAPDH, reduced nicotinamide adenine dinucleotides phosphate;

2.3.5 Glutamine and glutathione biosynthesis

Glutamine metabolism is also involved in oxidative homeostasis. Glutathione is synthesized in the cytoplasm of liver cells. First, gamma-glutamyl-cysteine is synthesized from L-glutamate and cysteine via the enzyme gamma-glutamyl-cysteine synthetase (γGCS). This reaction is the rate-limiting step in glutathione synthesis. Second, glycine is added to the C-terminal of gamma-glutamyl-cysteine via the enzyme glutathione synthase (GS) (As shown in Figure 2.3.4).

Glutamine is associated with NADPH production through $NADP^+$-dependent GDH and $NADP^+$ dependent Malic enzymes. NADPH production contributes to the reduction of GSSH.

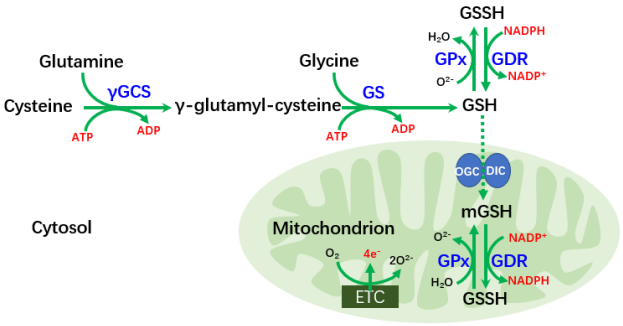

Figure 2.3.4 Glutathione synthesis and antioxidative effect of glutathione. GSH, glutathione; mGSH, mitochondrial glutathione; GSSH, glutathione disulfide; γ-GCS, γ-glutamylcysteine synthase; GS, glutathione synthase; GPx, glutathione peroxidase; GDR, glutathione reductase; OGC, oxoglutarate carrier; DIC, dicarboxylate carrier; ETC, electron transport chain;

2.3.6 Ammonia and urea cycle

Urea cycle occurs mainly in the liver and, and in the kidneys to a smaller extent. More specifically, the urea cycle takes place in mitochondria and cytosol. Unlike pyrimidine biosynthesis, carbamoyl phosphate is synthesized in mitochondria instead of cytosol.

The breakdown of amino acids generate ammonia, and it can be excreted by producing urea.

The overall reaction could be described as:

$NH_3 + CO_2 + \text{aspartate} + 3\ ATP + 2\ H_2O \rightarrow \text{urea} + \text{fumarate} + 2\ ADP + 2\ Pi + AMP + PPi$

It is worthwhile to mention that cytosolic fumarate production in this process could be converted to malate by cytosolic fumarate hydratase (FH1) and go back to the TCA cycle through mitochondrial malate transporters. Another fate of fumarate is to produce oxaloacetate though fumarate hydratase 1(FH1) and malate dehydrogenase1 (MDH1). And the product oxalacetate can be further used for gluconeogenesis and aspartate synthesis.

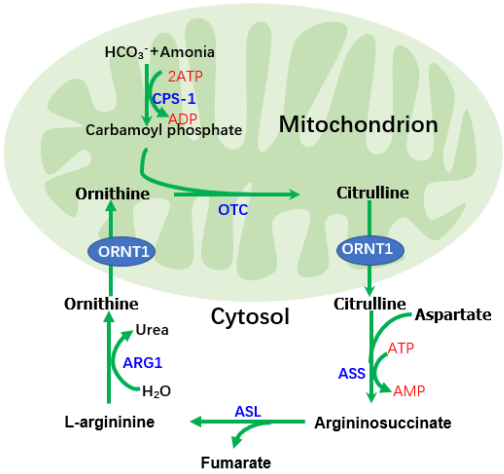

Figure 2.3.5 Schematic illustration of the urea cycle. CPS-1, carbamoyl phosphate synthase 1; OTC, Ornithine transcarbamoylase; ASS, Argininosuccinate synthetase; ASL, Argininosuccinate lyase; ARG1, arginase 1; ORNT1, ornithine translocase 1.

2.3.7 Targeting glutamine metabolism

Glutamine is engaged in multiple cellular processes. It is a precursor of protein, purine, pyrimidine, and glutathione synthesis. On the other hand, it is also used as a carbon source for many metabolic pathways through glutaminolysis. It has been long perceived that many types of tumor are addicted

to glutamine. Thanks to this addiction to glutamine, inhibitors of glutamine metabolism have been found to possess an anti-neoplastic effect. Therefore, targeting glutamine metabolism have been suggested to be a promising anti-cancer strategy. Because of the multiple fates of the glutamine, inhibitors in specific pathways have been developed, particularly in glutaminolysis. According to its effect on various targets, they could be classified into several classes: glutamine analogs, glutamine transporter inhibitors, glutaminase inhibitors, glutamate dehydrogenase inhibitors, and aminotransferase inhibitors.

Overexpression of glutamine transporters has been found in many tumors, indicating cancer cell's reliance on glutamine transporters. Thus, blocking glutamine transporters have been proposed to be an anti-cancer strategy[158-162]. Particularly, ASCT2 (SLC1A5) is viewed as a promising anti-cancer target due to its considerable contribution to tumor aggressiveness. Some studies have shown small molecules such as GPNA, phenylglycine, y-FBP, benzylserine[160] are sufficient to inhibit ASCT2 which would lead to reduced glutamine uptake and cell cycle progression.

Moreover, L-type amino acids transporter 1 (LAT1, SLC7A5) is also proposed as an anti-cancer target since LAT1 has involved the exchange of glutamine and essential amino acids (EAAs). Many studies have shown that inhibition of LAT1 by 2-aminobicyclo-(2,2,1) heptanecarboxylic acid (BEH) leads to inactivation of mTORC1[163, 164].

And XCT (SLC7A11), a glutamate-cystine antiporter, is essential for the uptake of cystine required for intracellular glutathione (GSH) synthesis and maintenance of the intracellular redox homeostasis. Inhibition of XCT reduces the concomitant influx of cystine and efflux of glutamate, resulting in perturbation of oxidative stress[165]. Therefore, the inhibition of XCT may sensitize cancer cells to radiotherapy[166]. However, inhibition of XCT alone does not necessarily suppress tumor growth, since the inhibition blocks glutamate export which could potentially promote glutaminolysis[167].

Glutaminase is a very critical metabolic enzyme that converts glutamine to glutamate. It acts as a gatekeeper of glutaminolysis. It has been found upregulated in many tumors due to the high demand for glutamine flux into mitochondria. Notably, highly specific expression of the splice variant glutaminase C (GAC) in cancers lays a foundation for the selective suppression of tumor growth without affecting healthy cells. Glutamine analogs have been found effective to inhibit cancer cell proliferation both in vitro cell culture and xenograft model. Many studies have shown their more significant activity in inhibiting the glutamine-dependent enzymatic steps in nucleotides biosynthesis. Numerous glutamine analogs such as 6-diazo-5-oxo-norleucine (Don), azaserine, acivicin are found effective to inhibit GLS1. Besides, BPTES and CB-839 have been proven effective to inhibit GLS1, which are structurally similar. However, CB-839 is an orally bioavailable allosteric inhibitor of both glutaminase 1 (GLS1) splice variants, KGA and GAC. Treatment of CB-839 has been demonstrated to increase the intracellular concentration of glutamine, but remarkably decrease levels of glutamate and TCA intermediates in various cancer cells[168-170]. It suggested that glutamine might be the predominant replenishment for TCA intermediates pool in some cancers. CB-839 has been shown to block the growth or kill cancer cells across a range of tumor types. CB-839 has demonstrated antitumor activity in several different tumor models. Compound 968 is cell permeable antagonist that can selectively inhibit GLS1 splice variant C (GAC) which is found to be upregulated in the various tumor[141], which raises a prospect in suppressing tumor growth safely.

Table 4 Small-molecule inhibitors of glutaminolysis

Class	Compounds	Status
Glutamine analogs	DON [171-175]	Preclinical study

	Azaserine [176-178]	Preclinical study
	Acivicin [176, 179]	Preclinical study
ASCT2（SLC1A5） inhibitor	GPNA [158, 180]	Preclinical study
	Phenylglycine[181]	Preclinical study
	γ-FBP [182]	Preclinical study
	Benzylserine [158, 183]	Preclinical study
	Tamoxifen [184]	Clinical use for breast cancer
LAT1（SLC7A5）inhibitors	BCH [164, 185]	Preclinical study
XCT (SLC7A11) inhibitors	Sulfasalazine [186-189]	Clinical use for arthritis
	Erastin [190-192]	Preclinical study
GLS inhibitors	BPTES [193-196]	Clinical trial
	CB-839 [197, 198]	Phase I clinical trial
	Compound 968 [199, 200]	Preclinical study
GDH inhibitors	EGCG [201-205]	Preclinical study
	R162 [205, 206]	Preclinical study
Transaminase inhibitor	AOA [207-210]	Clinical use for tinnitus

Owing to the vital role that glutamate dehydrogenase (GDH) plays in the glutamine associated catabolic pathways, inhibition of GDH have been considered as a potential anti-cancer strategy. Many studies have demonstrated that the green tea polyphenol epigallocatechin gallate (EGCG) can effectively inhibit glutamate dehydrogenase [46,52]. Recently, the purpurin analog R162 (2-allyl-1-hydroxy-9,10-anthraquinone) was identified as a potent inhibitor of GDH1.

As described above, aminotransferases such as AST and ALT are critical to facilitate glutamate into mitochondria through aspartate-glutamate carrier 1/2 (AGC1/2). Thus, inhibition of AST or ALT blocks the anaplerotic influx of glutamate. Many studies have shown that aminooxyacetate (AOA), an inhibitor of aspartate aminotransferase (AST) have been found effective inhibit glutaminolysis dependent cancers[211].

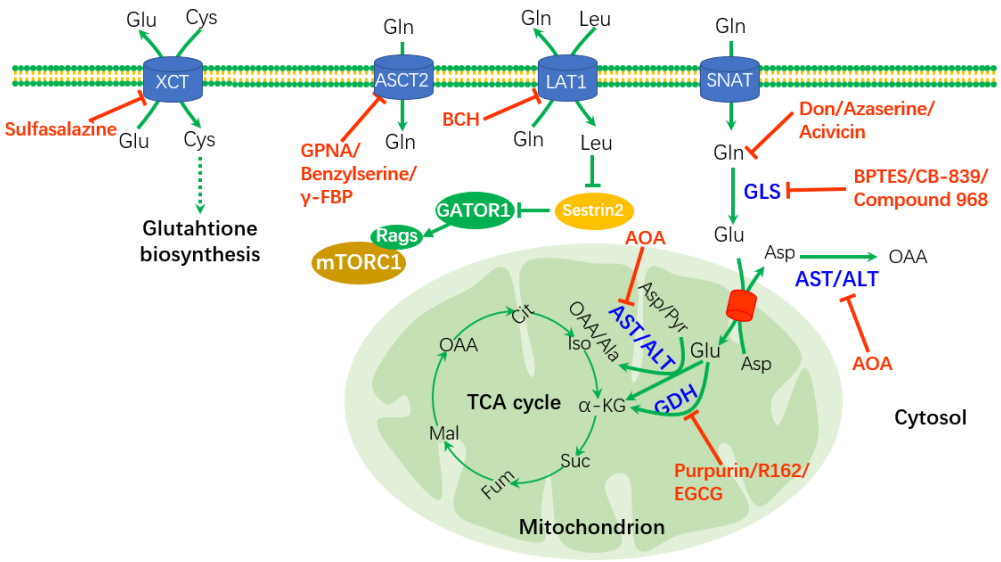

Figure 2.3.6 Inhibition of glutamine uptake and glutaminolysis. Green arrows indicated conversions and movements of metabolites, as well as activation of a certain protein. Red bar-headed lines indicate inhibition of metabolic enzymes or biological processes. Gln, glutamine; Leu,

leucine; Cys, cysteine; Inhibitors were shown with red texts, while metabolic enzymes shown with blue texts. γ-GPNA, L-γ-glutamyl-p-nitroanilide; Don, 6-diazo-5-oxo-norleucine; BEH, 2-aminobicyclo-(2,2,1)-heptanecarboxylic acid; BPTES, Bis-2-(5-phenylacetamide-1,3,4-thiadiazol-2-yl) ethyl sulfide; CB-839, N-(6-(4-(5-((2-Pyridine-2-ylacetyl)amino)-1,3,4-thiadiazol-2-yl)butyl)pyridazine-3-yl)-2-(3-(trifluoromethoxy)phenyl) acetamide; Compound 968, 5-(3-Bromo-4-(dimethylamino)phenyl)-2,2-dimethyl-2,3,5,6-tetrahydrobenzo[a]phenanthridin-4(1H)-one;
AOA, aminooxyacetic acid, R162, 2-allyl-1-hydroxy-9,10-anthraquinone; EGCG, Epigallocatechin gallate; GLS, glutaminase; AST, aspartate transaminase; GDH, glutamate dehydrogenase;

2.4 Mitochondrial metabolism

2.4.1 Mitochondrial carriers

Mitochondrial carriers (MCs) are mostly members of the solute carrier family (SLC). And the common function of mitochondrial carriers is to provide a link between mitochondria and cytosol by facilitating the flux of a large variety of solutes through the permeability barrier of the inner mitochondrial membrane. This link is indispensable as many physiological processes require the participation of both intramitochondrial and extramitochondrial enzyme reactions. Besides this basic function, some MCF plays an important role in regulating and maintaining a balance between cytosol and mitochondrial matrix, for example, the phosphorylation and redox potentials. It is fundamental to understand mitochondrial carriers in order to gain a better understanding of the link of mitochondrial metabolism to cytosolic metabolism.

Mitochondrial carriers (MCs) are localized to the inner membranes of mitochondria mitochondrial carriers (MCs) mostly belong to a family of carrier proteins, the *SLC25* or mitochondrial carrier family (As shown in Table 5). Whereas, mitochondrial pyruvate carrier encoded by *MPC1/2* is an exception.

Moreover, mitochondrial metabolism plays a pivotal role in crosstalk with glucose metabolism, glutamine metabolism, and fatty acids metabolism. And this crosstalk between the cytosolic compartment and the mitochondrial compartment is essential to cancer cell proliferation. Many shuttles are responsible for the exchange of biosynthetic precursors and bioenergetics. There are many proteins that are responsible for the bidirectional translocation of metabolic intermediates from cytosol to mitochondria.

Because of the low permeability of inner mitochondrial membrane, mitochondrial transporters including malate-α-ketoglutarate antiporter (MKA), glutamate-aspartate antiporter (GAA), mitochondrial pyruvate carrier (MPC) and mitochondrial citrate carrier (MCT) allow metabolites to import from cytosol to mitochondrion, maintaining metabolites homeostasis. In particular, malate shuttle plays significant role in facilitating cytosolic NAD^+ regeneration and mitochondrial influx of glutamate. Malate shuttle consists of malate-ketoglutarate antiporter, aspartate-glutamate antiporter and malate dehydrogenase 1/2(MDH1/2), and aspartate aminotransferase 1/2(AST).

It is worthwhile to point out that many mitochondrial carriers such as aspartate-glutamate carrier (AGC), ornithine carrier (ORC), phosphate carrier (PIC), glutamate carrier (GC), pyruvate carrier (MPC) concomitantly pump H^+ into mitochondrial matrix while importing metabolites[212]. This might dissipate mitochondrial potential. Nevertheless, these carriers allow mitochondria to transport their corresponding substrate against concentration gradient without consuming ATP.

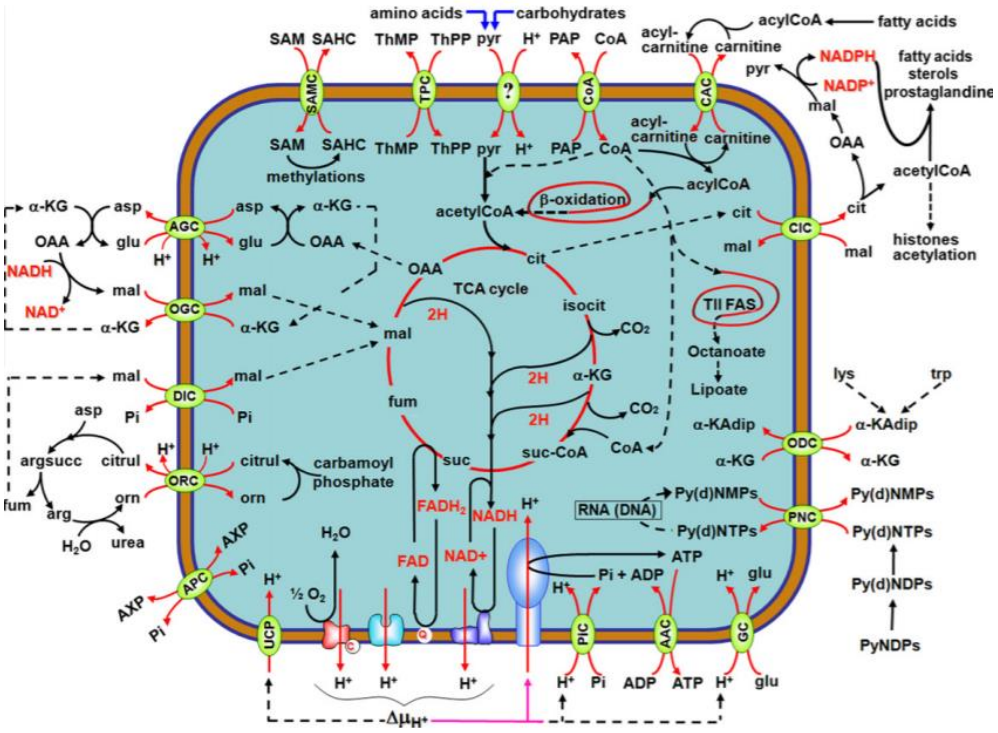

Figure 2.4.1 Representative mitochondrial carriers involved in metabolites translocation across mitochondrial membrane. CIC, citrate-isocitrate carrier; DIC, Dicarboxylate carrier; OGC, 2-oxoglutarate carrier; ODC, 2-oxodicarboxylate carrier; OAC, dicarboxylate carrier (*SLC25A10*); ORC, Ornithine carrier; GC, Glutamate carrier; AGC, aspartate/glutamate carrier; 9, citrate carrier; CAC, carnitine carrier; Asp, aspartate; Glu, glutamate; Cit, citrate; Isocit, isocitrate; α-KG, α-ketoglutarate; Suc, succinate; Fum, fumarate; Mal, malate; OAA, oxaloacetate; Pyr, pyruvate; DIC, dicarboxylate; Pi, phosphate.

Table 5 Mitochondrial carriers in *SLC25* family

Genes	Proteins	Predominant substrates
SLC25A1	Citrate carrier	Cit, Iso, Mal, PEP
SLC25A2	Ornithine carrier 1	Ornithine
SLC25A3	Phosphate carrier	Phosphate
SLC25A4	ATP/ADP carrier 1	ATP/ADP
SLC25A5	ATP/ADP carrier 2	ATP/ADP
SLC25A6	ATP/ADP carrier 3	ATP/ADP
SLC25A7	Uncoupling protein 1	H^+
SLC25A9	Uncoupling protein 2	H^+
SLC25A9	Uncoupling protein 3	H^+
SLC25A10	Dicarboxylate carrier	Succinate, malate
SLC25A11	Oxoglutarate carrier	Oxoglutarate
SCL25A12	Aspartate/glutamate carrier 1	Aspartate/glutamate
SLC25A13	Aspartate/glutamate carrier 2	Aspartate/glutamate
SLC25A14	Uncoupling protein 5	H^+
SLC25A15	Ornithine carrier 1	Ornithine
SLC25A16	Graves' disease carrier	CoA

SLC25A17	Adenine nucleotide carrier	ATP, ADP, AMP
SLC25A18	Glutamate carrier 2	Glutamate
SLC25A19	Deoxynucleotide carrier	Deoxynucleotide
SLC25A20	Carnitine/acylcarnitine carrier	Carnitine, acylcarnitines
SLC25A21	oxoadipate carrier	Oxoadipate, oxoglutarate
SLC25A22	Glutamate carrier 1	Glutamate

2.4.2 TCA cycle

The typical TCA cycle started with the input of acetyl-CoA. The two-carbon unit incorporates into carboxylic acid oxaloacetate to form citrate. It turns back to oxaloacetate after eight TCA intermediate interconversions. Every turn of this cycle produces one molecule of H_2O, two molecules of CO_2, one molecule of GTP, 3 NADH and 1 FDH_2, without consuming a single carboxylic acid from TCA intermediates pool.

The overall reaction could be described as:

$CH_3C{=}O\text{-}CoA + 2\ H_2O + 2\ NAD^+ + NAD(P)^+ + GDP + Pi \rightarrow GTP + 2\ CO_2 + 2\ NADH + CoA + FADH2 + NAD(P)H + H^+$

Metabolic rearrangements in the TCA cycle are very common in cancer cells. Cancer cells exploit metabolic rearrangements for sustaining their high proliferation rate and energy demand. Thus, dysregulation of the TCA cycle flux is frequently observed in cancers. The identification of mutations in several enzymes of the TCA cycle in human tumors demonstrated a direct connection between this metabolic pathway and cancer occurrence. Moreover, changes in the expression or activity of these enzymes were also shown to promote metabolic adaptation of cancer cells. Particular attention should be given to metabolic roles of TCA cycle enzymes and metabolites underlying in the reprogramming of cancer metabolism.

There are nine TCA cycle intermediates, namely citrate, aconitate, isocitrate, α-ketoglutarate, succinyl-CoA, succinate, fumarate, malate, and oxaloacetate. TCA intermediates are essential to cancer cells, and they are involved in many biological processes. TCA cycle is highly plastic to maintain both bioenergetics, biosynthesis and redox state. The conventional clockwise cycling supply NADH for oxidative phosphorylation. On the other hand, TCA cycle intermediates such as malate, oxaloacetate (in specific tissue) and citrate *et, al*, could be extruded to the cytosol for biosynthesis of biomass. Moreover, citrate acts as a junction between the TCA cycle and de novo lipogenesis, alfa-ketoglutarate acts as a junction between glutaminolysis and TCA cycle, oxaloacetate is the junction of gluconeogenesis with the TCA cycle. Citrate is not only an essential intermediate located at several branch points of metabolic pathways[33], but it also acts as an "energy gauge", a powerful sensor and regulator of cellular energy production, adjusting both output and need. Since citrate promotes histone acetylation, it could also play a role in coordinating the level of some key regulatory enzymes.

There are two reactions out of all eight reactions are thought to be irreversible due to unfavorable thermodynamics: the condensation of acetyl-CoA and oxaloacetate to form citrate and the conversion of α-ketoglutarate to succinyl-CoA. Reactions in the TCA cycle is tightly controlled by NAD+/NADH ratio, ATP/ADP ratio, and Ca^{2+} levels *et, al* in order to maintain the balance of the loading of TCA intermediates and energy generation,. The affinities of the substrate to the corresponding enzyme can be altered by the level of energy molecules such as ADP/ATP and NAD^+/NADH.

TCA cycle is primarily regulated at several key regulatory sites: isocitrate dehydrogenase (IDH) and ketoglutarate dehydrogenase (KGDH). It is notable that those regulatory sites control C3 carboxylates, C4 carboxylates, C5 carboxylates, and C6 carboxylates interconversions because those commitments determine metabolic fates of those carboxylates.

Firstly, isocitrate dehydrogenase (IDH) is a critical metabolic enzyme that catalyzes the reversible conversion of isocitrate to α-ketoglutarate. Three are three isoforms of IDH: IDH1, IDH2, and IDH3. IDH1 is localized in the cytosol, while IDH2 and IDH3 are localized in mitochondria. IDH1 and IDH2 are obligate homodimers and depend on $NADP^+$ as a cofactor. Whereas IDH3 structurally differs IDH1 and IDH2 which is a heterotetramer consisting of two alpha, one beta, and one gamma subunit, utilizing NAD^+ as a cofactor. Some studies have suggested that IDH3 and activated IDH2 catalyze oxidative decarboxylation which generates reducing equivalents NADH and NADPH respectively. Interestingly, activation of IDH2 by SIRT3 deacetylation responsible for TCA cycle derived mitochondrial NADPH generation, which partly contributes to redox homeostasis[213], $NADP^+$ dependent IDH1 and IDH2 catalyze reductive carboxylation which largely contribute to *de novo* lipogenesis in various tumors. To maintain the exquisite equilibrium of citrate depletion and clockwise TCA cycling, IDH is also carefully controlled by allosteric regulators.

Secondly, α-ketoglutarate dehydrogenase complex (KGDC) is another significant regulatory point of TCA cycle. Similar to pyruvate dehydrogenase complex (PDC), α-ketoglutarate dehydrogenase complex (KGDC) consists of subunit E1, E2, and E3 which is responsible for decarboxylation, CoA transfer, and dehydrogenation respectively. The regulation of the KGDC highlights a dynamic interplay between the enzyme and the OXPHOS to adjust mitochondrial metabolism through cell energy status sensing[214]. Both the E1 and the E3 subunits are inactivated by NADH and activated by ADP/ATP ratio and Pi. And it is noteworthy that KGDC is complex that has three redox centers and has numerous thiol groups are on subunit E2. As a result, KGDC only contributes to mitochondrial ROS generation; it also acts as a redox sensor which mediates clockwise TCA cycling to counter mitochondrial ROS generation[214-216]. Given the fact that α-ketoglutarate is at the crossroad of numerous metabolic pathways, deregulation of KGDC would have a profound impact on linked metabolic pathways. Glutamine anaplerosis feeds into TCA cycle through α-ketoglutarate (α-KG), so downregulation of α-ketoglutarate dehydrogenase complex (KGDC) and pyruvate dehydrogenase complex (PDC) mostly drive reductive carboxylation of α-KG, which contribute to anabolic pathways and cancer proliferation. Besides, accumulation α-KG led by KGDC inactivation is also involved in downregulation of malate-aspartate shuttle[217].

Notably, succinate dehydrogenase (SDH) catalyzes the dehydrogenation of succinate TCA cycle and contribute to electron flux to the respiratory chain.

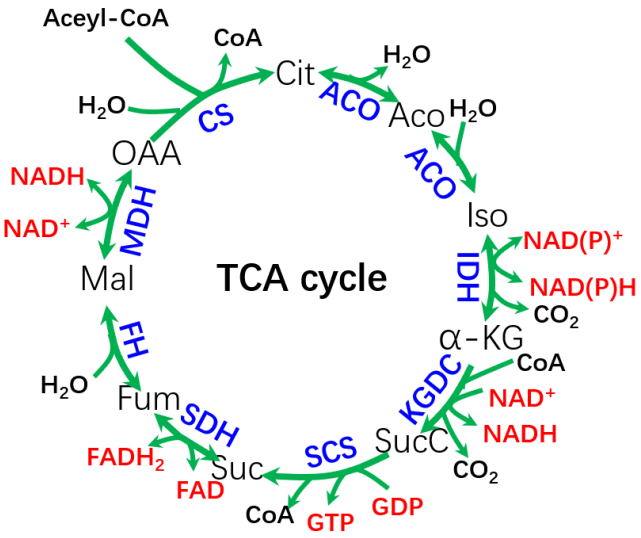

Figure 2.4.2 Schematic representation of typical TCA cycle. Cit, citrate; Aco, aconitate; Iso, isocitrate; α-KG, α-ketoglutarate; SucC, succinate; Suc, succinate; Fum, fumarate; Mal, malate; OAA, oxaloacetate; CS, citrate synthase; Aco, aconitase; IDH, isocitrate dehydrogenase; KGDH, α-ketoglutarate dehydrogenase; SCS, succinyl-CoA synthase; SDH, succinate dehydrogenase; FH, fumarate hydrolase; Malate dehydrogenase;

2.4.3 Anaplerotic and cataplerotic metabolism

Anaplerotic and cataplerotic metabolism is essential since it retains the TCA intermediates homeostasis.

Firstly, the incorporation of acetyl-CoA and oxaloacetate to produce citrate is one of the most significant anaplerotic reaction. And this anaplerotic flux is essentially dependent on the feed of pyruvate or alternative sources of acetyl-CoA. Above all, pyruvate dehydrogenase complex (PDC) is structurally similar to ketoglutarate dehydrogenase complex (KGDC) that controls the pyruvate flux to acetyl-CoA, together with mitochondrial pyruvate carrier (MPC). It is notable that the regulation of pyruvate dehydrogenase complex (PDC) largely depends on the phosphorylation by pyruvate dehydrogenase kinase (PDK) and dephosphorylation by pyruvate dehydrogenase phosphatase (PDP). The entry of acetyl-CoA largely contributes to bioenergetics and biosynthesis of fatty acids.

The conversion of pyruvate to oxaloacetate is a very significant anaplerotic flux. And mitochondrial oxaloacetate and malate can be translocated to cytosol directly or indirectly, and then could be used as the precursor of gluconeogenesis and aspartate synthesis, or for some other metabolic purposes. Besides, pyruvate carboxylase (PC) is a critical enzyme that replenishes oxaloacetate from pyruvate. It catalyzes the first committed step of gluconeogenesis. On top of that, it also has been implicated with cancer cell survival, particularly when the glutamine-derived TCA intermediates are inadequate[218-221].

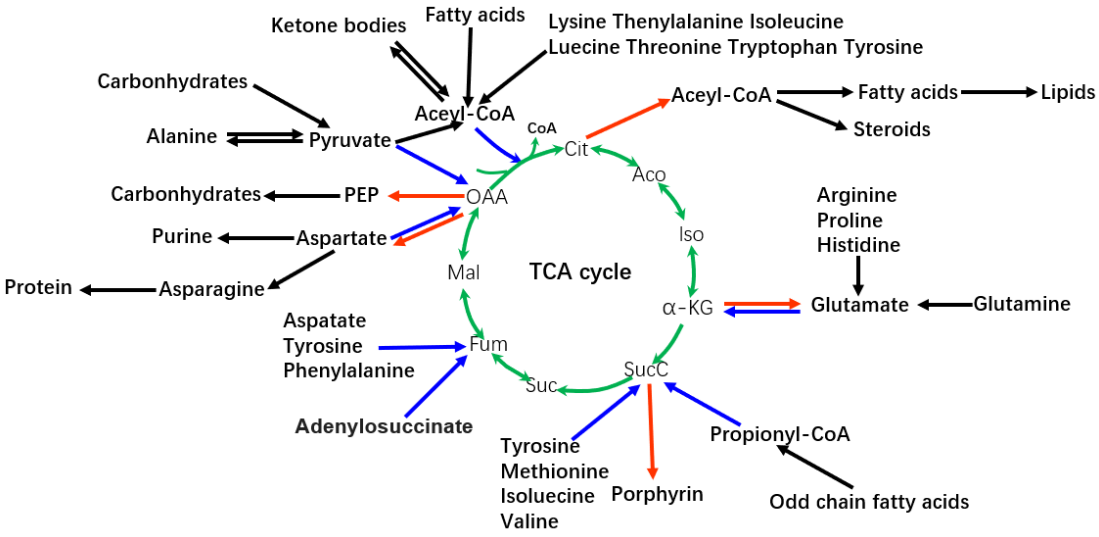

Figure 2.4.3 Predominant Anaplerotic fluxes and cataplerotic fluxes. Green arrows indicated TCA cycle; blue arrows indicated anaplerotic reactions; red arrows indicated cataplerotic reactions. Cit, citrate, Aco, Aconitate; Iso, isocitrate; KG, ketoglutarate; SucC, succinyl-CoA; Suc, succinate; Fum, fumarate; Mal, Malate; OAA, oxaloacetate;

This reprogramming in energy metabolism includes a shift from oxidative phosphorylation to aerobic glycolysis (commonly known as "Warburg effect"), and, in many tumors, an increased glutaminolysis (referred to as "glutamine addiction") that feed anaplerosis or bioenergetics. Together, glucose and glutamine support the rapid proliferation of cancer cells, which actively coordinate the metabolism of these nutrients.

Among all cataplerotic pathways, enhanced *de novo* lipogenesis is the primary hallmark of various types of tumor. Depending on the tumor type, tumor cells synthesize up to 95% of saturated and mono-unsaturated fatty acids (FA) *de novo* by using acetyl-CoA or acetate regardless of sufficient dietary lipid supply[222]. And the cytosolic citrate is the predominant precursor that could be primarily derived from glucose or glutamine.

Fatty acids synthesis takes place in the cytosol and cytosolic citrate, either derived from glucose or glutamine, is the predominant precursor of *de novo* lipogenesis, although acetate can be used to produce fatty acids. The contribution of glutamine and glucose have been investigated in many studies by using isotopic labeling glucose or glutamine. According to many reports, the contribution of glucose and glutamine varied under different condition.

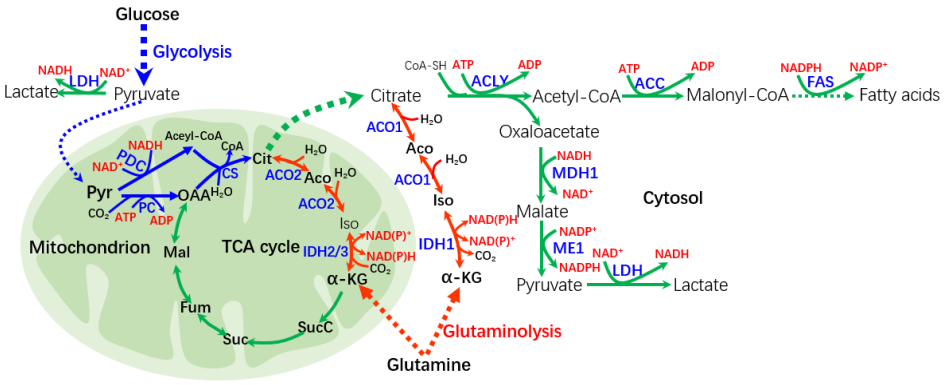

Figure 2.4.4 Contribution of glucose derived citrate and glutamine-derived citrate to fatty acids synthesis. Solid arrows indicate conversions and movements of metabolites. Dashed arrows indicate multiple reactions or transmembrane movements of metabolites; glucose derived citrate generating process was indicated by blue color, glutamine-derived citrate generating process was indicated by red color; The remaining reactions were indicated by green color; PDC, pyruvate dehydrogenase complex; PC, pyruvate carboxylase; CS, citrate synthase; IDH2/3, isocitrate dehydrogenase 2/3; IDH1, isocitrate dehydrogenase 1; ACO1, aconitase 1; ACO2, aconitase 2; ACLY, ATP-citrate lyase; ACC, acetyl-CoA carboxylase; FAS, fatty acids synthesis; MDH1, malate dehydrogenase 1; ME1, malic enzymes 1; LDH, lactate dehydrogenase; Pyr, pyruvate; Cit, citrate; Aco, aconitate; Iso, isocitrate; KG, ketoglutarate; SucC, succinyl-CoA; Suc, succinate; Fum, fumarate; Mal, malate; OAA, oxaloacetate;

Lipogenesis requires translocation of citrate from mitochondria to cytosol. Citrate-isocitrate carrier (CIC, SLC25A1) is the mitochondrial carrier responsible for this translocation. Citrate can be subsequently converted to cytosolic acetyl-CoA which is an indispensable precursor of fatty acids biosynthesis and mevalonate pathway, as well as acetylation of histone. Besides, Citrate-isocitrate carrier (CIC) plays a crucial role in maintaining the mitochondrial pool of citrate homeostasis and redox balance in cancer cells. Thus, inhibition of CIC would result in disrupted oxidative stress[223, 224]**.**

ATP-citrate lyase (ACLY) is a metabolic enzyme that cleaves cytosolic citrate to acetyl-CoA and oxaloacetate. Interestingly, Citrate and ATP-citrate lyase (ACLY) is involved in the acetylation of histone, which links citrate metabolism with epigenetic regulation[225, 226]. A recent study has shown histone acetylation critically depends on citrate and acetyl-CoA levels. And acetylation of histone stabilizes ATP-Citrate lyase, resulting in promoted lipid biosynthesis and tumor growth[227]. Moreover, Ruiting Lin and his coworkers found that SIRT2 inhibitor deacetylates and subsequently destabilizes ATP citrate lyase (ACLY) and hydroxy-citrate (HG) is used as a competitive inhibitor of ATP citrate lyase (ACLY)[228].

Acetyl-CoA carboxylase (ACC) is another critical regulatory point in *de novo* lipogenesis[229]. Inhibition of ACC through pharmacological approaches or genetic approaches can inhibit cancer cell proliferation both *in vitro* and *in vivo*.

Cataplerosis also plays a significant role in purine biosynthesis other than its role in *de novo* lipogenesis. Aspartate formed by oxaloacetate is primarily utilized as one of the precursors for *de novo* purine biosynthesis in cancer cells.

2.4.4 Oxidative phosphorylation

There is a longstanding assumption that cancer cells have upregulated glycolysis compared with normal cells, which has led to the plausibility that oxidative phosphorylation (OXPHOS) is downregulated in all cancers. However, more and more evidence has shown that OXPHOS can also be exceptionally upregulated in numerous tumors. Till now, it has wildly been recognized that oxidative phosphorylation is highly variable due to dysfunctional mitochondria, hypoxia or NADH supply at different stages of cancer progression. Those cancer cells intrinsically featured by hyperactive OXPHOS might render high susceptibility to OXPHOS inhibitors, conferring potential anti-cancer targets for cancer therapy.

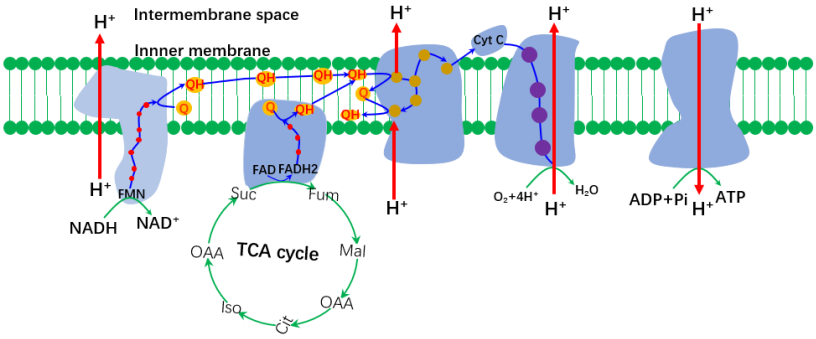

Figure 2.4.5 Schematic diagram of oxidative phosphorylation (OXPHOS) and inhibition of oxidative phosphorylation. Green arrows indicate the conversion or movement of the metabolite, while blue arrows indicate movement of electrons. Red bar-headed lines indicate inhibition of metabolic enzymes or biological processes. Suc, succinate; Fum, fumarate; Mal, malate; OAA, oxaloacetate; Cit, citrate; Iso, isocitrate; α-KG, α-ketoglutarate; I, complex I; II, complex II; III, complex III; IV, complex IV; Cyt c, cytochrome c; Q, CoQ10; QH, reduced CoQ10; H^+, proton; NAD^+, nicotinamide adenine dinucleotides; NADH, reduced nicotinamide adenine dinucleotides; FCCP, Carbonyl cyanide-4-(trifluoromethoxy)phenylhydrazone;

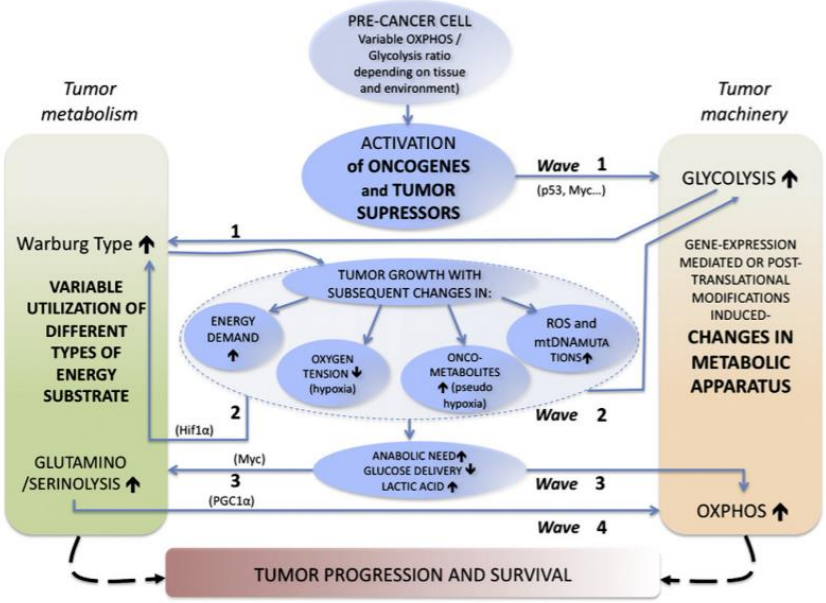

Figure 2.4.6 Schematic illustration of deregulation of oxidative phosphorylation during tumor progression.

2.4.5 Metabolism associated mitochondrial defects

2.4.5.1 General introduction of metabolism associated mitochondrial Defects

Mitochondrial defects have been long implicated with tumorigenesis. Dysfunctional mitochondria may account for the varied OXPHOS in cancer. Despite that mitochondrial dysfunction not solely contribute to this metabolic reprogramming. Relatively low stability of the mitochondrial genome, mitochondrial gene mutations is more likely to occur. All respiratory complexes have proteins encoded by mitochondrial genes. Deficiencies of respiratory complexes are frequently occurring, which has been associated with malignant transformation. However, it is challenging to identify a causal relationship between mitochondrial defects and cancer occurrences. Oxidative

phosphorylation contributes to ROS production. Oxidative phosphorylation has a profound impact on metabolic reprogramming. Firstly, oxidative phosphorylation is critical ATP producing process together with glycolysis. Experimental evidence is currently very limited that dysfunctional mitochondria are solely responsible for the onset of aforementioned pathophysiological conditions. According to a review, mitochondrial defects involved in energy metabolism can be generally grouped into the following five categories:

1. Isolated defects of OXPHOS subunits or assembly factors.
2. Defects of mitochondrial DNA, RNA and protein synthesis (including replication, nucleotide metabolism, RNA processing, and modification and translation).
3. Disorders in the substrate-generating upstream reactions of OXPHOS (pyruvate dehydrogenase complex, Krebs cycle, fatty acid beta-oxidation, substrate import, and anaplerosis).
4. Defects in cofactors of OXPHOS and other enzymes of mitochondrial energy metabolism.
5. Defects in the homeostasis of mitochondria, including their biogenesis, lipid processing, protein import, fission/fusion, and quality control.

Mitochondrial dysfunction somatic mutations could be a mitochondrial membrane or mitochondrial matrix, deregulated mitochondrial dynamics, mitochondrial dysfunction has been implicated with cancer resistance[230, 231].

2.4.5.2 Mutant Isocitrate dehydrogenase 1/2 (mIDH1/2)

Several underlying mechanisms of deregulated cellular energetics are associated with mitochondrial dysfunction caused by mitochondrial DNA mutations, mitochondrial enzyme defects, or altered oncogenes/tumor suppressors.

A recent study has shown that more than 75% of low-grade gliomas and approximately 20% of acute myelocytic leukemia (AML) have mutations in IDH1 or IDH2, and mutations are also found in other solid tumors such as chondrosarcoma, cholangiocarcinoma, colon, pancreatic and prostate cancer to varying extents[232]. It also has been demonstrated that the heterozygous mutations frequently occur at the R132 position of IDH1 and R140 or R172 of IDH2[232].

IDH1/2 represent one pathway for cellular NADPH generation in most tissues, together with other NADPH generating pathways. Conversion of isocitrate to α-ketoglutarate (α-KG) by IDH1/2 simultaneously produces one equivalent of NADPH, an essential reducing equivalent that controls cellular defense mechanisms against oxidative damage through reduction of glutathione and thioredoxins, as well as the formation of activated catalase. Therefore, it is conceivable that loss or reduction of IDH1/2 function in cancerous cells could impair detoxification mechanisms, leading to DNA damage and genome instability[233].

Unlike wild type IDH1/2, mutant IDH1/2 can convert ketoglutarate to D-2-hydroxyglutarate (D-HG) and L-2-hydroxyglutarate (L-HG) by using NADPH as a cofactor, resulting in accumulation of the oncogenic metabolite and reduction of NADPH. D(L)-Hydroxyglutarate deregulate tricarboxylic acid cycle (TCA) to a large scale. Besides, hydroxyglutarate which is an α-ketoglutarate (α-KG) competitive antagonist can inhibit α-ketoglutarate (α-KG) dependent dioxygenases, leading to genome-wide histone and DNA methylation alterations (as shown in the figure). Therefore, oncometabolite D-HG or L-HG is usually used as the marker of mutant IDH1/2.

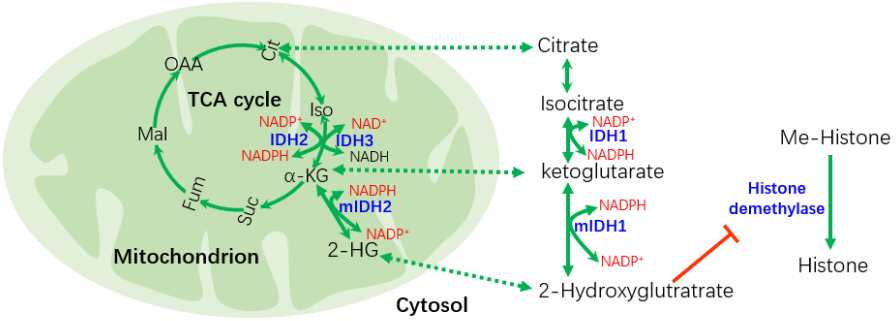

Figure 2.4.7 Mutant isocitrate dehydrogenase 1/2 (IDH1/2) and accumulation of D(L)-2-hydroxyglutarate. Solid arrows indicate conversions and movements of metabolite; Dashed arrows indicate translocation of metabolite; Bidirectional arrows indicate reversible reactions. Cit, citrate; Iso, isocitrate; α-ketoglutarate; Suc, succinate; Fum, fumarate; Mal, Malate; OAA, oxaloacetate; IDH1, isocitrate dehydrogenase 1(cytosolic isoform, $NADP^+$ dependent); IDH2 isocitrate dehydrogenase (mitochondrial isoform, $NADP^+$ dependent); IDH3, isocitrate dehydrogenase (mitochondrial isoform, NAD^+ dependent); mIDH1, mutant isocitrate dehydrogenase 1; mIDH2, mutant isocitrate dehydrogenase 2;

2.4.5.3 Mutant succinate dehydrogenase (mSDH) and fumarate hydrolase (mFH)

Succinate dehydrogenase (SDH) and fumarate hydratase (FH) catalyze sequential reactions in the TCA cycle. Succinate dehydrogenase A (SDHA) mutations and fumarate hydrolase mutations have been long implicated with tumorigenesis[234, 235]. And this is attributable to deregulation of prolyl domain hydrogenases (PDHs). Prolyl domain hydrogenase (PDHs) catalyzed hydroxylation, and subsequent ubiquitination is required for degradation of HIF-1α. And the prolyl domain hydrogenases (PDHs) activity is dependent on the availability of oxygen (O_2), Fe^{2+}, and cytosolic α-KG (As shown in **Figure 2.4.8**). Therefore, the accumulation of succinate can inactivate prolyl domain hydrogenases (PDH) due to its structural similarity to α-KG. As a consequence, mutant SDH or complex II (succinate: ubiquinone oxidoreductase) leads to HIF-1α stabilizations, which can promote tumor progression. Likely, deficient fumarate hydrolase can also result in HIF-1α stabilization due to succinate accumulation. They might be associated with activation of α-ketoglutarate (α-KG) dependent prolyl domain hydrogenases (PDHs). It is worthwhile to mention that a significant source of cytosolic α-ketoglutarate (α-KG) is from transamination catalyzed by aspartate transaminase 1 (cytosolic, AST1) and alanine transaminase 1(cytosolic, ALT1). Gottlieb *et al.* showed that amino acid starvation led to α-KG depletion and thereby inactivation of PHDs[236].

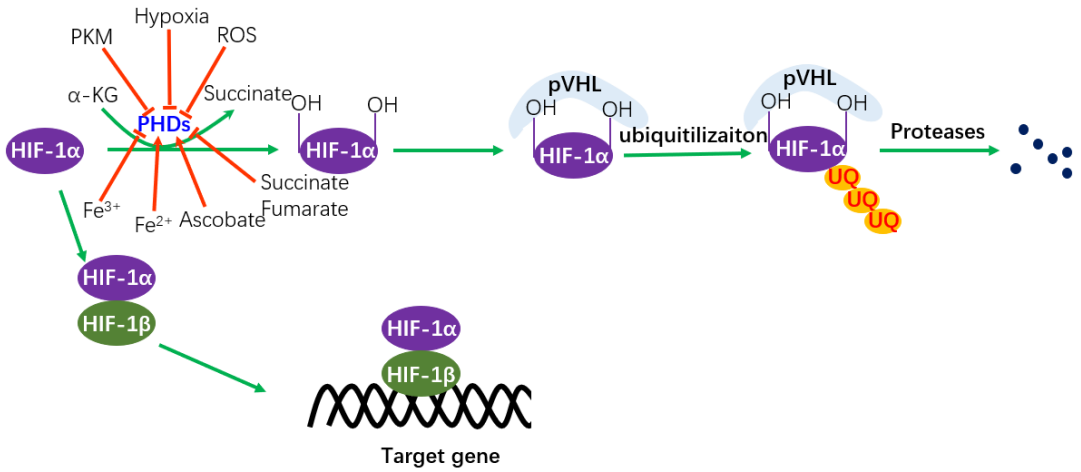

Figure 2.4.8 Succinate accumulation induces stabilization of HIF-1α by inactivating prolyl domain hydrogenases(PDHs). Green arrows indicate conversion and movements of metabolites. Red bar-headed lines indicate inhibition of a c protein. HIF-1α, hypoxia-inducible factor-1α; HIF-1β, hypoxia-inducible factor-1β; ROS, reactive oxidative species; α-ketoglutarate;

3.4.5.4 Defective respiratory chain

More than 250 gene defects have been reported to date, and this number continues to grow. Mitochondrial diseases can be grouped into disorders of oxidative phosphorylation (OXPHOS) subunits and their assembly factors, defects of mitochondrial DNA, RNA and protein synthesis. Mitochondrial DNA mutations can be induced by endogenous or exogenous DNA-damaging agents such as ROS[237]. Defective respiratory is frequently occurring since the mtDNA codes 7 subunits for complex I, a cytochrome b for complex III, 3 cytochrome c oxidase (COX) subunits for complex IV, and 2 ATPase (ATPase6/8) for complex V[237].

2.4.5.5 Deregulated mitochondrial dynamics

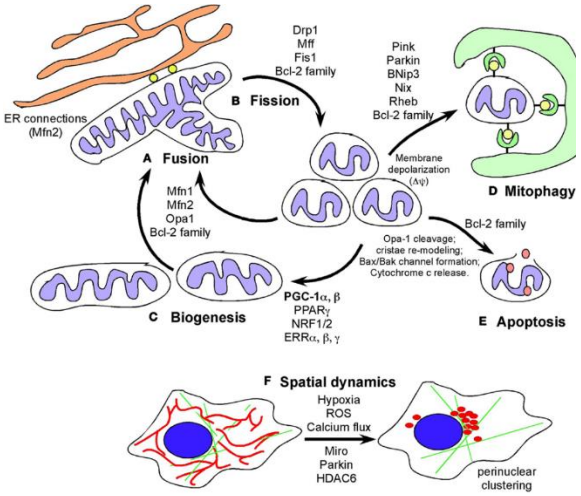

Figure 2.4.9 Defining mitochondrial dynamics.

Mitochondria are highly dynamic organells undergo coordinated dynamics of fussion and fission. Mitochondrial dynamics have an impact on mitochondrial metabolism. The mitochondiral fusion is primarily coodinated by sevral fusion proteins such as OPA-1, Mitofusin 1 and Mitofusion2. Specifically, Opa-1 work on inner mitochondral membrane while Mitofusin I and Mitofusin 2 work on outter mitochondrial membrane. According to literatures, mitochondrial fusion is selective for polarized mitochondria and supported by growth on oxidative carbon sources, increased cristae

density, and formation of respiratory chain supercomplexes and increased OXPHOS. Mitochondrial fusion likely also contributes to OPHOXS activity and mitochondrial metabolism by promoting increased diffusion of intermediate metabolites and reducing agents. Besides, mitochondrial fusion inhibits mitophagy and apoptosis.

On the other hand, mitochondrial fission is mainly promoted by the GTPase activity of the dynamin-related protein (DRP1). DRP1 can be recruited to mitochondria in response to hypoxia, where DRP1 interacts with its mitochondrial receptors, susequently pinch off mitochondria into smaller units. Generally, mitochondrial fission induces depolarization of mitochondrial membrane potential due to impact on mitochondrial bioenergetics.

Besides, mitochondrial biogenesis is induced by nutrient deprivation and in response to oxidative stress. Transcription factors NRF1/2, PPARγ, ERRα, β, γ, and PGC-1α are primary regulators of mitochondrial biogenesis. Mitochondrial biogenesis is required for cell growth to produce increased metabolites and energy.

Additionally, mitophagy is a specialized form of autophagy in which mitochondria are phagophores and autophagosomes that fuse with lysosomes, leeding to degradation of mitochondria. Mitochondrial fragmentation is required for mitophagy and mitochondrial fusion protects mitochondria from degradation, leeding to deregulated mitochondrial metabolism[238].

Mitochondrial fusion allows efficient mixing of mitochondrial content, and it generates extended mitochondrial networks. Both effects are advantageous under conditions of high energy demand, and disruption of mitochondrial fusion results in mitochondrial dysfunction and loss of respiratory capacity both in yeast and in mammalian cells.

2.4.6 Targeting mitochondrial metabolism

2.4.6.1 Inhibitors of mitochondrial complexes

There are a handful of ways of inhibiting mitochondrial respiration. Firstly, inhibition of respiratory complexes directly. There are many inhibitors of respiratory complexes such as rotenone, malonate, antimycin A, cyanide and oligomycin et, al. Although they are extensively used as tools to study oxidative phosphorylation, it does not show too many prospects to be used as an anti-cancer drug due to the unsuitable therapeutic index. Because most of the respiratory inhibitors lack specificity, inhibition of ETC inevitably affects the bioenergetics of normal healthy cells. Besides, they are very likely to induce ROS, which could be damaging to normal cells.

However, accumulating evidence has shown that some moderate inhibitors of oxidative phosphorylation (OXPHOS) have shown a better therapeutic index than those are very potent OXPHOS inhibitors. Interestingly, biguanides such as metformin are drugs commonly used to treat type 2 diabetes, which has been found to show an effect of prevention or repression of certain cancers[239-242]. While the underlying mechanisms are still controversial, it has been a longstanding hypothesis that that metformin inhibits cancer growth indirectly by mediating insulin and insulin-related growth factors as well as AMPK signaling pathway, more and more evidence have shown that metformin inhibits mitochondrial complex I, and eventually result in altered bioenergetics[243-245]. Besides, the combination of metformin and glycolytic inhibitor 2-deoxyglucose (2-DG) has achieved a desirable effect on cancer cell proliferation *in vitro* and *in vivo* due primarily to the synergy effect on bioenergetics[246-250].

Interestingly, upregulated oxidative phosphorylation has been found frequently as an adaptive response to B-RAF and BCR-ABL inhibition, conferring resistance to kinase inhibitors[251]. It

suggested that oxidative phosphorylation could be used as a synergic treatment with a kinase inhibitor. OXPHOS is upregulated or to alleviate tumor hypoxia to improve treatment outcomes.

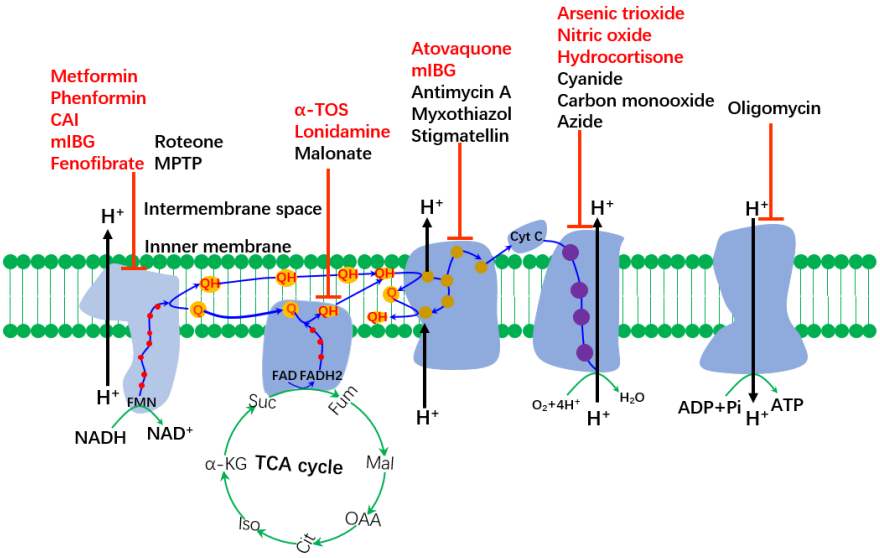

Figure 2.4.10 Schematic diagram of oxidative phosphorylation (OXPHOS) and inhibition of oxidative phosphorylation. Green arrows indicate the conversion or movement of the metabolite, while blue arrows indicate movement of electrons. Red bar-headed lines indicate inhibition of metabolic enzymes or biological processes. Suc, succinate; Fum, fumarate; Mal, malate; OAA, oxaloacetate; Cit, citrate; Iso, isocitrate; α-KG, α-ketoglutarate; I, complex I; II, complex II; III, complex III; IV, complex IV; Cyt c, cytochrome c; Q, CoQ10; QH, reduced CoQ10; H^+, proton; NAD^+, nicotinamide adenine dinucleotides; NADH, reduced nicotinamide adenine dinucleotides; FCCP, Carbonyl cyanide-4-(trifluoromethoxy)phenylhydrazone; CAI, carboxyamidotriazole; mIBG, meta-iodobenzylguanidine; MPTP, 1-methyl 4-phenyl 1,2,3,6 tetrahydropyridine; α-TOS, α-tocopheryl succinate;

2.4.6.2 Blockade of mitochondrial carriers

Aminooxyacetic acid (AOA) is commonly used as the inhibitor of aspartate-glutamate transaminase which is a critical component of malate-aspartate shuttle. The influx of glutamate and pyruvate depend on the malate-aspartate shuttle directly and indirectly. Moreover, translocation of glutamate to mitochondria relies on the malate-aspartate shuttle. Moreover, malate-aspartate shuttle and lactate production are two major pathways of cytosolic NAD^+ regeneration, when the malate shuttle is inhibited, pyruvate would convert to lactate for regeneration of cytosolic NAD^+. In this way, glycolysis could be maintained. However, the flux of pyruvate into mitochondria would be reduced. Therefore, inhibition of malate-aspartate shuttle (AST) deprives two of the mitochondrial fuels to mitochondria. Thus, it induces mitochondrial bioenergetics failure.

1,2,3-benzenetricarboxylate, a citrate analog which is not permeable, might be a competitive inhibitor of the citrate-isocitrate carrier (CIC). N-ethylmaleimide, p-chloromercuribenzoate and 4-Chloro-3-[[(3-nitrophenyl)amino]sulfonyl]-benzoic acid[252] are the inhibitors of citrate-isocitrate carrier (CIC, SLC25A1)[223, 228, 253]. Although inhibition citrate-isocitrate carrier (CIC) may not be able to fully deplete cytosolic citrate due to citrate supply from plasma membrane citrate transporters (PMCT)[252]. Moreover, cytosolic glutamine anaplerotic pathway could be an alternative pathway for cytosolic citrate generation. And a recent study has demonstrated that newly developed CIC inhibitors CTPI-1 and CTPI-2 can inhibit NSCLC cell growth in vivo[224].

Mitochondrial pyruvate carrier (MPC) is a unidirectional transporter. In cancer cells, it has been implicated with metabolic switch oxidative phosphorylation to the glycolysis. UK5099 is reportedly used as a blocker of MPC. However, inhibition of mitochondrial pyruvate carrier, surprisingly, does not affect the TCA intermediates pool[254]. It suggested that compensations generated TCA intermediates could occur such as glutamine when MPC was inhibited[255].

Carnitine shuttle confers metabolic plasticity to cancers considering that it provides mitochondria alternative fuels. Thus, carnitine palmitoyltransferase I (CPT I) is proposed as a possible therapeutic target for cancer[256]. A study reported that etomoxir which is an irreversible inhibitor of carnitine palmitoyltransferase-1 (CPT-1) could induce cancer cell death due partly to ATP depletion[257].

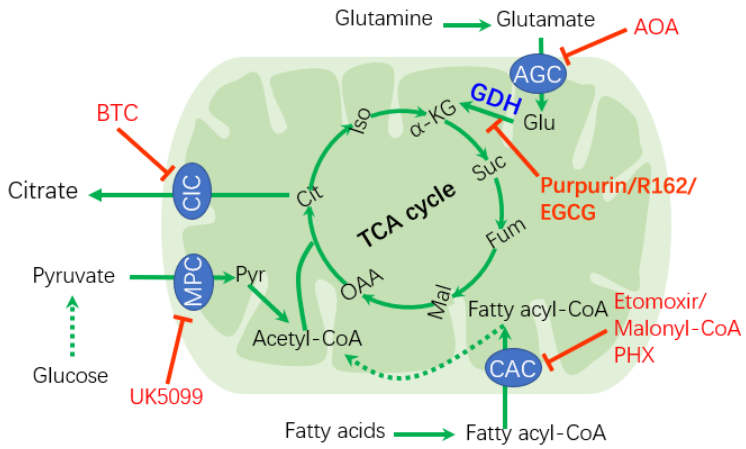

Figure 2.4.11 Schematic illustration of blocking mitochondrial carriers. CIC, citrate isocitrate carrier; MPC, mitochondrial pyruvate carrier; CAC, carnitine/acylcarnitine carrier; GDH, glutamate dehydrogenase; AGC, aspartate/glutamate carrier; BTC, 1,2,3-benzene-tricarboxylate; UK5099, 2-Cyano-3-(1-phenyl-1H-indol-3-yl)-2-propenoic acid; AOA, Aminooxy-acetic acid; Etomoxir, R(+)-2-[6-(4-Chlorophenoxy) hexyl]-oxirane-2-carboxylic acid. R162, 2-allyl-1-hydroxy-9,10-anthraquinone; EGCG, Epigallocatechin gallate; Cit, citrate; Iso, isocitrate; α-KG, α-ketoglutarate; Suc, succinate; Fum, fumarate; Mal, malate; OAA, oxaloacetate;

2.4.6.3 Targeting mutant metabolic enzymes in the TCA cycle

Furthermore, mutant IDH1/2 lead to the accumulation of 2-hydroxyglutarate (2-HG), which is very common oncogenic metabolites that have been found in many tumors. Thus, mutant isocitrate dehydrogenase 1/2 (IDH1/2) has been suggested as a novel anti-cancer target[258, 259]. To date, many pieces of evidence have shown that mutant IDH1 and IDH2 in gliomas and myeloid malignancies acute myeloid leukemia (AML), which indicated that mutant IDH could be a potential anti-cancer target. Indeed, high levels of D-2HG inhibit α-ketoglutarate-dependent dioxygenases, including histone and DNA demethylases, leading to histone and DNA hypermethylation and finally a block in cell differentiation[260]. Therefore, some compounds were demonstrated to inhibit mutant isocitrate dehydrogenase (IDH) such as AG120，AG221，AG881，IDH305，BAY 143603 and FT2012 in a recent clinical trial.

2.4.6.4 Targeting mitochondrial dynamics

Mitochondrial bioenergetics is associated with mitochondrial biogenesis and mitochondrial connectivity. Mitochondria is in dynamics of fission and fusion. Instead of mediating respiratory complexes, regulation of mitochondrial biogenesis or mitochondrial network might be more promising approach to inhibit mitochondrial respiration. Oxidative phosphorylation plays a critical

in tumor progression. Recent evidence has shown that oncogenic signaling can promote oxidative phosphorylation through activate PGC-1.

2.5 Association of cancer metabolism with redox state

Free radicals are considered by-products of metabolism, and it is associated with redox reactions taking place in cells. For example, the primary reactive oxygen species (ROS) production site such as complex I, complex III, ketoglutarate dehydrogenase complex (KGDC) and pyruvate dehydrogenase complex (PDC) which are metabolic enzymes[261]. In return, ROS production is also vital in redox signaling that can regulate metabolism.

NADPH which shares a similar chemical structure with NADH. Both NADPH and NADH can be used as electron donor and receptor. NAPDH is closely connected to metabolism because of $NADP^+$. Unlike NADH, NADPH can't be used as an electron donor of the electron transport chain. However, NADPH plays an indispensable role in cellular antioxidative defense and many biosynthetic pathways such as nitrogenous bases biosynthesis, fatty acids synthesis, steroids synthesis and so on. Given that cancer cells are usually undergoing active more active anabolism. It is conceivable that cancer cells produce NADPH in a faster way.

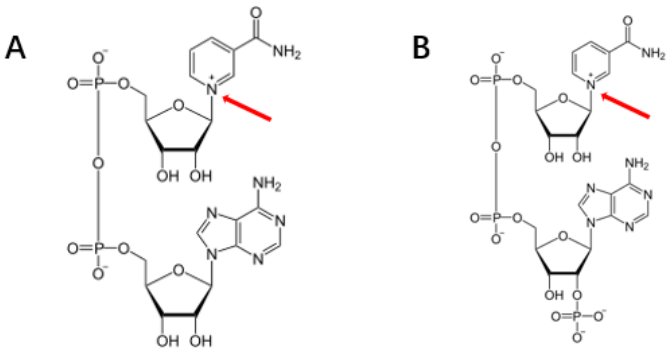

Figure 2.5.1 Chemical formula of nicotinamide dinucleotide (NAD^+, A) and nicotinamide dinucleotide phosphate ($NADP^+$, B)

Like NAD^+, $NADP^+$ which shares same active quaternary amine that can receive an electron from some hydrides, subsequently form an NADPH molecule. These redox reactions are usually catalyzed by dehydrogenases. Specifically, there are a handful of metabolic enzymes account for cellular NADPH production. There are couples of enzymes that can produce NADPH. Metabolic enzymes including glucose-6-phosphate dehydrogenase (G6PD) and 6-phosphogluconate dehydrogenase (6PGDH), malic enzyme(ME1 or ME2), methane-tetrahydrofolate dehydrogenase （MTHFD1 and MTHFD2， $NADP^+$-dependent isocitrate dehydrogenase (IDH1 and IDH2), $NADP^+$-dependent glutamate dehydrogenase (GDH) and nicotinamide nucleotides transhydrogenase (NNT). However, a recent study has shown the contribution of IDH, glutamate dehydrogenase and nicotinamide nucleotides transhydrogenase (NNT) is negligible HEK293T cells[262].

Nicotinamide adenine dinucleotide can transport across the inner mitochondrial membrane. It is also worthwhile to note that NADP(H) can not be transported across the intracellular membrane. A reporter system can be employed to trace cytosolic and mitochondrial pool of NADPH to gain a better understanding of the compartmentalization of NADPH[263].

The input of glucose, serine or glutamine is required for NADPH production (As shown in Figure 2.5.2). An output of lactate and glycine is usually accompanied. Thus, isotopic 3-^{2}H-glucose was

used as a tracer to study the contribution of the oxidative pentose phosphate pathway to NADPH. Similarly, U-^{13}C-glutamine, ^{2}H-serine can be used to quantify the NADPH production from serine and glutamine.

That is to say, the generation of NADPH is usually accompanied by deregulation of metabolic alterations which are involved in NAPDH production. It may be considered as antioxidant, because the constitutively expressed NADPH oxidase isoform-4, NOX4 [89, 90], can consume a significant portion of the excess NADPH and produce more superoxide and consequently release more H_2O_2 into the cytosol, the overall reaction scheme may be pro-oxidant.

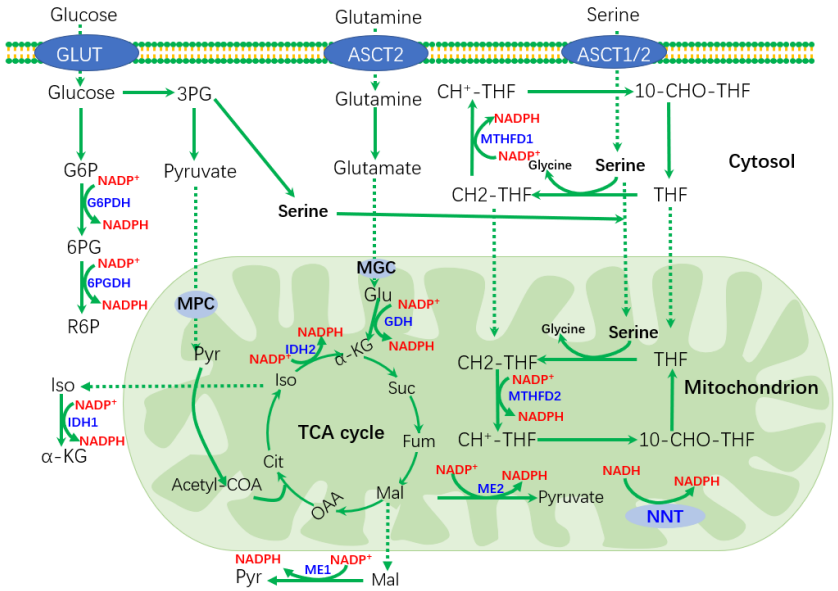

Figure 2.5.2 Schematic representation of NADPH generating metabolic pathways. Solid arrows represent conversion or movement of metabolites. Dashed arrows represent transmembrane movements of metabolites. Reducing equivalent were represented as red text. And enzymes associated with NADPH generation were displayed as blue text. G6P, glucose-6-phosphate; 6PG, 6-phosphogluconate; R6P, ribulose-6-phosphate; 3-PG, 3-phosphoglycerate; THF, tetrahydrofolate; CH2-THF, methylene-tetrahydrofolate; CH^{+}-THF, methenyl-tetrahydrofolate; 10-CHO-THF, 10-formyl-tetrahydrofolate; OAA, oxaloacetic acid; G6PDH, glucose-6-phosphate dehydrogenase; 6PGDH, 6-phosphogluconate dehydrogenase; IDH1, isocitrate dehydrogenase 1 (cytosolic isoform) ; IDH2, isocitrate dehydrogenase 2 (mitochondrial isoform); GDH, glutamate dehydrogenase; ME1, malic enzyme 1(cytosolic isoform) ; ME2, malic enzyme 2(mitochondrial isoform); MTHFD1, methylene-tetrahydrofolate dehydrogenase 1(cytosolic isoform); MTHFD2, methylene-tetrahydrofolate dehydrogenase 2 (mitochondrial isoform); NNT, nicotinamide nucleotides transhydrogenase; NAD^{+}, nicotinamide adenine dinucleotide; NADH, reduced nicotinamide adenine dinucleotide; NADP^{+}, nicotinamide adenine dinucleotide phosphate; NADPH, reduced nicotinamide adenine dinucleotide phosphate; Glut, glucose transporters; ASCT2, serine-, cysteine transporter; LAT1, L-type amino acid trnaporter1;

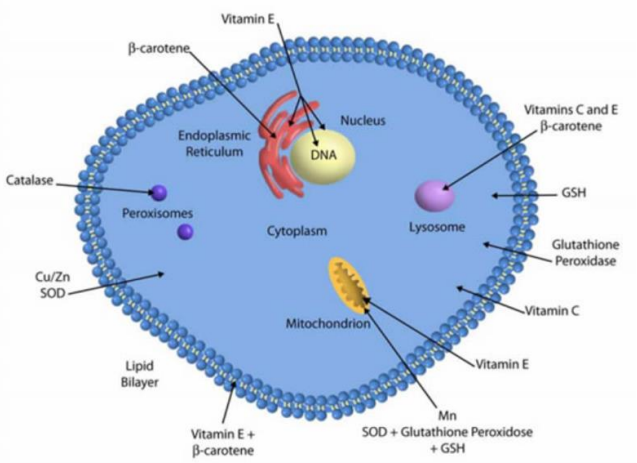

Figure 2.5.3 Enzyme antioxidants and non-enzymes antioxidant

Antioxidant enzymes include superoxide dismutase (SOD), catalase, glutathione reductase (GDH), thioredoxin (TXN), glutathione peroxidases (GPXs), NADPH quinone oxidase (NQO) need NADPH either to maintain active cofactor or for reduction. Although superoxide dismutase which has a heme coenzyme. Primarily, a reactive unpaired electron on free radicals necessarily receives an electron to be stabilized. To protect the cell from oxidative damage, NADPH is generated by the cell as an electron donor.

Part II Experiments

Chapter 1 Mitochondrial dysfunction induced by CoQ10 depletion

1.1 Materials and cell culture

1.1.1 Materials

a. DMEM high glucose (22.5 mM glucose), DMEM low glucose (5.5 mM glucose), modified DMEM (glucose, glutamine, bicarbonate and phenol red-free), glutamine (200 mM), pyruvate (100 mM), fetal bovine serum (FBS), EDTA-trypsin, calf serum and penicillin used in cell culture and passage were all purchased from Sigma Aldrich (MI, USA). Culture mediums were stored in a room at a temperature of 4 ºC and others were stored at -20 ºC.

Dialyzed FBS was prepared by using a semipermeable membrane, and it was stored at 4-8 ºC.

b. Lowry assay reagents: Reagent A consists of DOC (10% w/v) in H_2O; Reagent B consists fo sodium carbonate (10%, w/v), 0.5 N NaOH final concentration in water. Reagent C Na-K tartrate; Reagent D consists of $CuSO_4$; Reagent E consists of Folin-Ciocalteau reagent diluted in H_2O (50%, v/v). All reagents placed at room temperature. Bovine serum albumin (BSA) was used for calibration.

c. 4-nitrobenzoic acid (4NB) was dissolved in PBS (PH7.4, 200 mM), followed by sterilization with filtration. A volume of 1 mL aliquots was made, and they were stored at -20 ºf;

d. Coenzyme Q10 (CoQ10) was dissolved in ethanol and stored at -20 ºC. It was used for the calibration curve of Coenzyme Q10 quantification.

e. Cholesterol, cholesterol esterase, and cholesterol oxidase;

f. Adenosine triphosphate (ATP), Adenosine diphosphate (ADP) and adenosine monophosphate (AMP), nicotinamide adenine dinucleotide (NAD^+), nicotinamide adenine dinucleotide reduced (NADH), nicotinamide adenine dinucleotide phosphate ($NADP^+$) and Coenzyme A (CoA) were purchased from Sigma Aldrich (MI, USA). A solution should be freshly prepared since they are not stable. Once stock solutions were made, they could be stored in -20 ºC for a week. Ubiquinone 1 (CoQ1) and decylubiquinone (DUB) was dissolved in DMSO, and they were stored at -20 ºC.

g. Glutathione was purchased from Sigma Aldrich (MI, USA) and it is dissolved in 50 mM PBS (PH 7.4) freshly. N-ethylmaleimide (NEM) was kindly donated.

h. The stock solution of rotenone (2 mM), oligomycin (1.56 mM), antimycin A (AA, 1.56 mM), carbonyl cyanide-4-(trifluoromethoxy)-phenylhydrazone (FCCP) (2 mM) were dissolved in ethanol, and they have used study oxidative phosphorylation relevant experiments. Cyanide (KCN) was prepared freshly by dissolving deionized H_2O.

i. PBS buffer 1X consists of 137 mM of NaCl, 2.7 mM KCl, 10mM Na_2HP_4 and 1.8 mM KH_2PO_4, pH 7.4; Tris buffer consists of 50 mM Tris-Cl, 150 mM NaCl , pH 7.5; RIPA buffer consists of 50 mM Tris-HCl, pH 7.4, 150 mM sodium chloride, 1 mM ethylenediaminetetraacetic acid (EDTA), 1% NP-40, 1% Sodium Deoxycholic acid, 0.1% sodium dodecyl sulfate (SDS), 1 mM phenylmethylsulfonyl fluoride, (add fresh) Protease Inhibitors; PBS buffer (20 mM) and PBS(50mM) buffer was prepared by dilution of PBS buffer 1X.

j. Molecular probes JC-1 (5mM); Mitotracker Green; DAF-AM, H_2DCFDA 10 mM; Mitosox; BTP, Acetylacetonatobis [2-(29-benzothienyl)-pyridine-kN, kC3’] iridium (III). All of them were

dissolved in DMSO and stored under room temperature. 2-NBDG (44 mM) was dissolved in ethanol and stored in -20 ^{o}C and keep away from light.

Instruments

a. Cell culture incubator (Thermo Electron Corporation, MA, USA)

b. Inverted microscope (Carl Zeiss AG, Baden-Württemberg, Germany)

c. Biosafety chamber

d. Jasco V-750 Spectrophotometer (Japan Spectroscopic Corporation, Tokyo, Japan)

e. Millipore water purifying system (Merck Millipore, MA, USA)

f. Agilent 1100s High-performance liquid chromatography (Agilent Technologies, CA, USA) and and chromatographic columns with different static phase material (Phenomenex, CA, USA)

g. Multi-well plate reader (Perkin Elmer)

h. Confocal microscope

i. Bio-Rad S3e Cell sorter (Bio-Rad Laboratories, CA, USA)

j. YSI dissolved oxygen meter featured with an oxygen sensor and magnetic stirring system, water cycling temperature controlling system (Yellow Springs Instrument Co. OH, USA)

k. Stacking gel consists of 0.5M Tris-HCl (PH 6.8); 10% SDS (w/w); acrylamide (30%, w/w); 10% (w/v) ammonium persulfate; TEMED; Resolving gel: Acrylamide; 1.5 M Tris-HCl (pH=8.8); Loading buffer consists of 10% w/v SDS, 10 mM dithiothreitol (DTT) or 2-mercaptoethanol, 20 % v/v glycerol, 0.2 M Tris-HCl, pH 6.8, 0.05% w/v bromophenol blue; Running Buffer consists of 25 mM Tris-HCl, 200 mM glycine and 0.1% (w/v) SDS.

1.1.2 Cell culture

MCF7 breast cancer cells were cultured in Dulbecco's Modified Eagle Medium (DMEM, 22.5 mM glucose) supplemented with 10% fetal bovine serum (FBS), penicillin and 2 mM glutamine. HepG2 hepatic cancer cells were cultured in Dulbecco's Modified Eagle Medium (DMEM, 5.5 mM glucose) supplemented with 10% fetal bovine serum (FBS), penicillin and 2 mM glutamine. Cell morphology was monitored by an optical microscope. If not specially mentioned, the cells were exposed in 4 mM 4-nitrobenzoate for more than 4 days to deplete CoQ10 level.

1.2 Methods

1.2.1 CoQ10 content

3-6×10^{6} Cells were detached by trypsin. Cell pellets were suspended in 0.3 mL water and vortex vigorously until cells were disrupted. An aliquot of 2.1 mL mixture of ethanol and hexane (2:5, v/v) was added in an Eppendorf and vortex 3 min. Centrifuge at the speed of 5,000 rpm for 5 min. Upper hydrophobic layer hexene was collected. Repeat the extraction once and combine the supernatant. Then the supernatant was dried by nitrogen gas flow. The residue was reconstituted in 100 μL ethanol, and 50 μL was injected in the HPLC system.

CoQ10 was quantified by an Agilent 1100 series HPLC-UV system was equipped with a C18 column (100mm, 4.6 mm, 5 μm) was used to separate CoQ10. And 97% (v/v) ethanol in distilled H_2O was used as mobile phase and isocratic 0.4 mL/min elution flow rate. The wavelength was set at 275 nm.

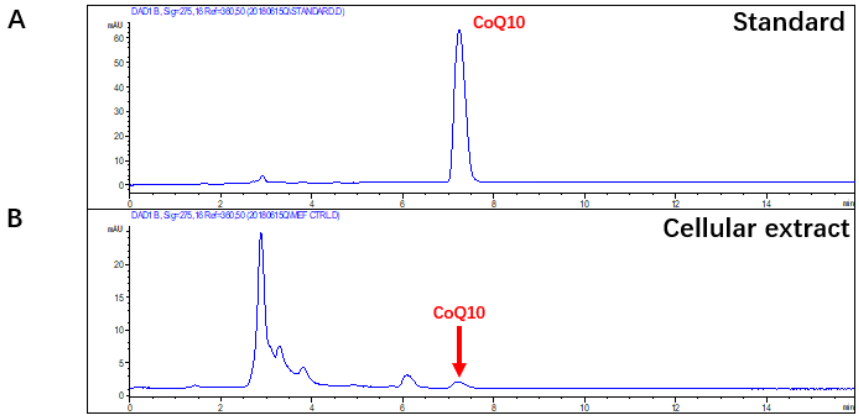

Figure 1.1.1 Representative chromatograms of CoQ10 of standard (A) and cellular extract(B). CoQ10 was measured at a wavelength of 275 nm**.**

1.2.2 Total cholesterol content

3-6×10^6 MCF7 cells were detached by trypsinization, followed by twice of PBS washing. A suitable amount of cells was withdrawn for protein determination. Then cell pellets were suspended in 0.3 mL water and vortex vigorously until cells were disrupted. Then, 100 µL of each sample with 10 µL of 1% Triton X-100 (either standard or cell solution containing 0.4 mg/mL of protein) was supplemented with 10 µL of a reaction mixture composed of 500 mM $MgC1_2$, 500 mM Tris buffer (pH 7.4), 10 mM dithiothreitol, 1% Triton X-100. The mixture of cholesterol esterase and cholesterol oxidase (both at a 0.8U/mL final concentration) and then the solution was incubated 37 ºC for 30 min. The reaction was stopped by adding 120 µL of a 1:1 methanol/ethanol (v/v) and incubated at 0 ºC for 30 min. Afterward, the samples were centrifuged at 14000 g for 10 min. Supernatants were collected and analyzed by HPLC-UV.

HPLC-UV analysis was carried out by Agilent 1100 system equipped with Kinetex reverse phase C18 (250 mm×4.6 mm×5.5 µm, Phenomenex, CA, USA). The oxidized cholesterol (cholest-4-en-3-one) was separated using 1:99 (v/v) acetic acid/methanol as the mobile phase at a flow rate of 1 mL/min. And the UV absorbance at a wavelength of 240 nm was recorded for quantification of total cholesterol. A calibration curve was obtained by diluting cholesterol standards in the same medium used for cell solubilization (0.1% Triton X-100) to obtain values ranging from 0 to 40 pg/mL.

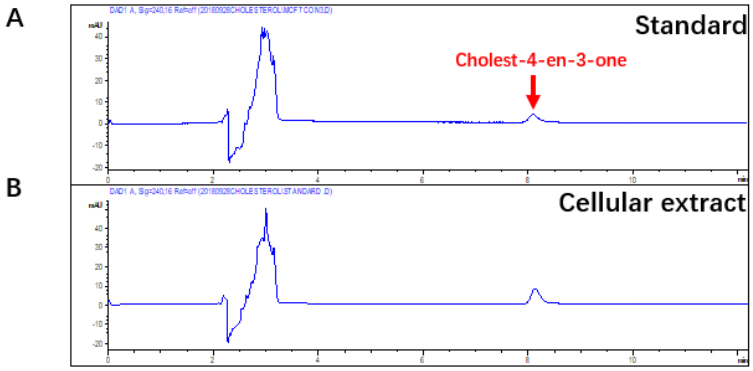

Figure 1.1.2 Measurement of total cholesterol by HPLC-UV after cholesterol esterase and cholesterol oxidase treatment. A. standard cholesterol treated with a mixture of cholesterol esterase and cholesterol oxidase; B, MCF7 cellular extracted treated with a mixture of cholesterol esterase and cholesterol oxidase. Cholest-4-en-3-one was measured at a wavelength of 240 nm.

1.2.3 Oxygen consumption rate (OCR)

Oxygen consumption rate was performed by YSI oxygen meter. At least 1×10^6 cells were used in every measurement. 1.6 mL of culture medium and incubated at 37 ºC in the chamber for 30 min. Afterward, an OCR baseline was monitored until it was stabilized. Cells were incubated at 37 ºC for 10 min to allow temperature and pH equilibration. After an OCR baseline measurement, cells were added to the chamber, and the endogenous oxygen consumption was measured. And then 1 μM oligomycin, 0.5 μM FCCP and 1 μM antimycin A was sequentially added to get the different phase of the oxygen consumption curve. And the slopes of traces relative to oxygen consumption were used to calculate the oxygen consumption rate. All the experiments were conducted three times and data are expressed as nanomoles of O_2 per minute per milligram of protein.

1.2.4 NADH autofluorescence by confocal microscopy

Oxidative phosphorylation was also assessed by alteration of NADH autofluorescence in response to various inhibitors. Although NADPH also has autofluorescence at approximately the same spectrum which could affect the specificity of autofluorescence, the NADPH autofluorescence could be negligible considering that it couldn't be altered correspond to inhibitors of oxidative phosphorylation. MCF7 cells and HepG2 cells were cultured in DMEM with or without 4 mM 4NB for more than 4 days. And then cells untreated with 4NB and treated with 4NB were seeded on coverslips in a 6-well plate. Multi-well plates were placed into the incubator (37 ºC, 5% CO_2) for more than 24 h stabilization. Prior to confocal microscopic measurement, cells on different coverslip were treated with vehicle (0.01% (v/v) ethanol, 5 min), rotenone (1 μM, 5 min) and FCCP (0.5 μM, 5 mM) respectively. Coverslips were washed by KRB buffer for three times before mounting on confocal microscopy. The excitation was natural light and the fluorescence was measured by the green channel.

1.2.5 Activity of respiratory complex I, II and IV

Remove the medium from about 5×10^6 cells and wash them once with PBS. Detach the cells using 0.05% (w/v) trypsin-EDTA, and after the cell detachment, blocks the trypsin by adding the removed medium. Transfer the cell suspension to a 15 mL conical tube. Wash the cells by centrifuging at 300 g for 3 min at 4 °C, discarding the supernatant and resuspending the cells in 3 mL of PBS. Centrifuge the cells at 300g for 3 min at 4 ºC and discard the supernatant. The cell pellets were flash-frozen in liquid nitrogen and it can be stored at -80 °C for weeks. Cell pellets were suspended in 0.4 mL of 20 mM hypotonic potassium phosphate buffer (pH 7.5). By using a 100 μL syringe, take up and expel the suspension several times until it has the appearance of a homogeneous solution. Snap-freeze the cell lysate in liquid nitrogen and thaw it at 37 °C for three cycles and keep it on ice for the activity analysis.

Add 100 μL of PBS buffer (0.5 M, pH 7.5), 60 μL of fatty acid-free BSA (50 mg/mL), 30 μL of KCN (10 mM) and 10 μL of NADH (10 mM). Adjust the volume to 994 μL with distilled water. Prepare, in parallel, a separate cuvette containing the same quantity of reagents and sample but with the addition of 10 μL of 1 mM rotenone solution. To avoid underestimation of rotenone-resistant activities, incubation of rotenone in a separate cuvette in parallel is crucial. Mix by inverting the cuvette covered with parafilm and read the baseline at 340 nm for a more than 2 min. Start the reaction by adding 6 μL of ubiquinone 1 (at a 10 mM final concentration), mix by inverting the cuvette using parafilm and follow the decrease of absorbance at 340 nm for 2 min. Specific complex I activity is the rotenone-sensitive activity.

To measure activity of complex II, an aliquot of 970 µL reaction solution that consists of 1 mg/mL fatty acid-free bovine serum albumin (BSA), 20 mM succinate, 2,6-dichlorophenolindophenol (DCPIP, at 80 µM final concentration), 20 mM potassium phosphate buffer (pH 7.5) was added in a quartz cuvette. Mix by inverting the cuvette and incubate inside the spectrophotometer at 37 °C for 10 min. Read the baseline activity at 600 nm for the last 2 min. Preincubation of the sample with succinate is mandatory to activate the enzyme. The reaction was started by adding 30 µL decylubiquinone (DUB, final concentration 60 µM) in the cuvette, and the decrease of absorbance was recorded at 600 nm for 3 min. Check the specificity of complex II activity by running the assay after the addition of 10 µL of carboxin before starting the reaction.

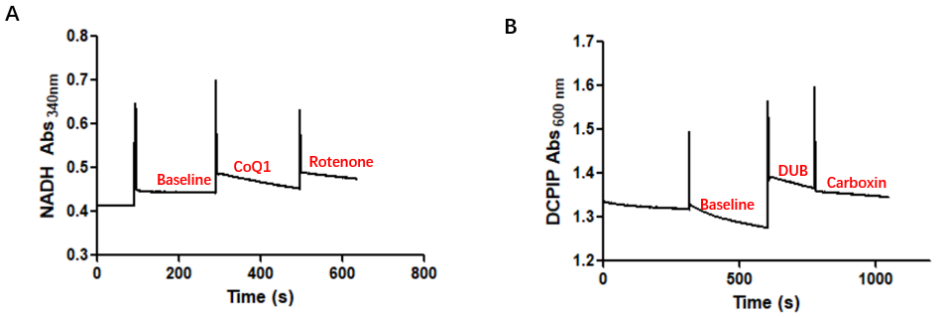

Figure 1.1.3 Spectrophotometric measurement of the kinetics of complex I and complex II.
A. Kinetics of complex I. The absorbance of NADH at 340 nm was recorded after adding CoQ1 and rotenone. Reaction rate at different phase was obtained by fitting linear regression(R^2>0.99).
B. Kinetics of complex II. The absorbance of DCPIC at 600nm has recorded Baseline after adding decylubiquinone (DUB, 60 µM) and carboxin. Reaction rate at different phase was obtained by fitting linear regression(R^2>0.99).

Complex IV activity was measured by using polarographic measurement. Briefly, cells were harvested and washed by PBS buffer. And cell pellets were resuspended in the respiratory buffer that consists of 300 mM mannitol, 10 mM KCl, 5 mM $MgCl_2$, and 10 mM K_2PO_4 (pH 7.4). An aliquot of 1.5 mL cell suspension was injected into the polarographic chamber ($1.5x10^6$ cell/mL) and the reaction was started by adding the 5 µL the mixture of ascorbate (at a 6mM final concentration) plus N, N, N', N'-tetramethyl-p-phenylenediamine (TMPD, at a 700 µM final concentration). The baseline oxygen consumption rate was recorded for 2-5 minutes and finally, 2 µL KCN (12 mM) was added to block specific complex IV activity. The final respiratory rate is obtained by subtracting the KCN-insensitive respiration. Data were normalized against the cellular protein content determined by the Lowry method, and complex IV activity was expressed as µmoles $O_2 \cdot min^{-1} \cdot mg^{-1}$.

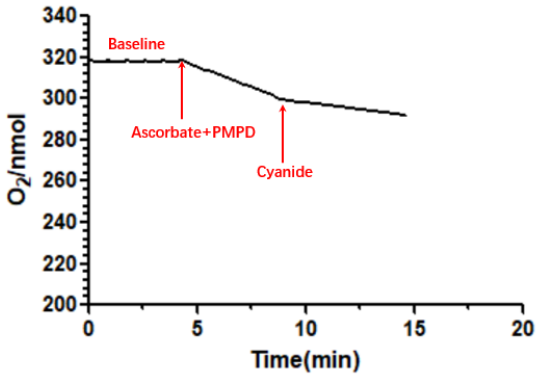

Figure 1.1.4 Polarimetric measurement of the kinetics of complex IV. Kinetics of complex IV followed by absorbance of NADH at 340 nm was recorded after baseline, adding ascorbate (10 mM) + PMPD (0.2 mM) and cyanide (700 µM). Oxygen consumption rate at different phase was obtained by fitting linear regression (R^2>0.99).

1.2.6 Characterization of mitochondria

1.2.6.1 Mitochondrial morphology

Sterile coverslips were placed in a 6-well plate, and MCF7 cells were seeded on coverslips at suitable density. Cells were placed in an incubator for at least 24 h. Before the confocal microscopy, the culture medium was replaced by 100 nM Mitotracker Green staining solution. After 30 min of staining, coverslips were washed three times by 100 nM Tris buffer (7.4) and then mounted on slides immediately. Mitochondria were visualized by confocal microscopy, the excitation wavelength was 488 nm, and fluorescence emission of Mitotracker Green was viewed by green channel. Confocal microscopic images were analyzed by ImageJ. The circularity and aspect ratio analyzed by ImageJ was used to characterize mitochondrial morphology.

1.2.6.2 Mitochondrial membrane potential

Coverslips were placed in a 6-well plate, and MCF7 cells were seeded on coverslips at suitable density. Cells were placed in an incubator for at least 24 h. Before the confocal microscopy, the culture medium was replaced by 5 µM JC-1 staining solution. After 30 min of staining, mitochondria were visualized by confocal microscopy. Green and red fluorescence of JC-1 were viewed by green and red channel. The intensity of green and red fluorescence was quantified by ImageJ respectively and the ratio of green to red fluorescence.

1.2.6.3 Mitochondrial Mass

MCF7 and HepG2 cell were cultured and treated or untreated with 4NB. Cells were trypsinized and cell density was adjusted to approximately 1×10^6/mL. Cells grown in high glucose or low glucose were exposed to 100 nM MitoTracker for 20 min. Afterward, cells were washed by PBS for twice and resuspended in PBS. Cells were injected in a flow cytometer for analysis, and FL1 fluorescence channel was chosen to measurement oxidized FL1. Histogram plot was used for the comparison of mitochondrial mass.

1.2.7 Evaluation of ROS and glutathione

1.2.7.1 Reactive oxygen species (ROS) production

MCF7 and HepG2 cell were cultured as described as above. Before reactive oxygen species (ROS) measurement, prolonged treatment of 4-nitrobenzoic acid (4NB). Cells were detached, and cell

density was adjusted to approximately 1×10^6/mL. Cells grown in high glucose or low glucose were exposed to10 µM H2DCFFDA for 20 min. Afterward, cells were washed by PBS for twice and then resuspended in PBS. Cells were injected in a flow cytometer for analysis, and FL1 fluorescence channel was chosen to measurement oxidized DCFDA.

1.2.7.2 Glutathione (GSH)

MCF7 cancer cells and MCF7 cancer cells treated with 4 mM 4NB were cultured in 10 cm dishes until they reached to approximately 70% confluence. The culture medium was replaced by fresh culture medium in the presence of 2 mM alkylating agent N-ethylmaleimide (NEM) for 10 min before cell harvest. Cells were trypsinized after the NEM treatment, followed by double washing of the cells with cold PBS solution containing 0.5 mM NEM. A suitable amount of cells was withdrawn from the tube for protein quantification. Afterward, cells were extracted by using 100 µL 15 % (w/v) trichloroacetic acid (TCA) in H_2O. The samples were centrifuged at 14000 g for 5 min, and the supernatants were transferred in Eppendorf before injection into the HPLC system.

A Phenomenex Kinetex C18 column (150 mm, 4.6 mm, 5 µm) was used for separation of conjugate GSH-NEM. The mobile phase composed of 94% acetonitrile (ACN) and 6% of 0.25% (v/v) acetic acid in H_2O was used, and isocratic elution was carried out at a flow rate of 1.25 mL/min. Run a standard GSH, NEM and standard GSH with NEM derivatization under the identical conditions before the analysis of cellular extracts. The conjugates GSH-NEM could be identified by comparing the chromatograms. Furthermore, the calibration curve was done by analyzing GSH-NEM of a series of GSH with NEM derivatization. Signal was recorded at a wavelength of 265 nm with 400 nm as a reference. After each injection, at the end of the run, flush the column with 100% mobile phase until then re-equilibrium of the system to the initial conditions before the next injection.

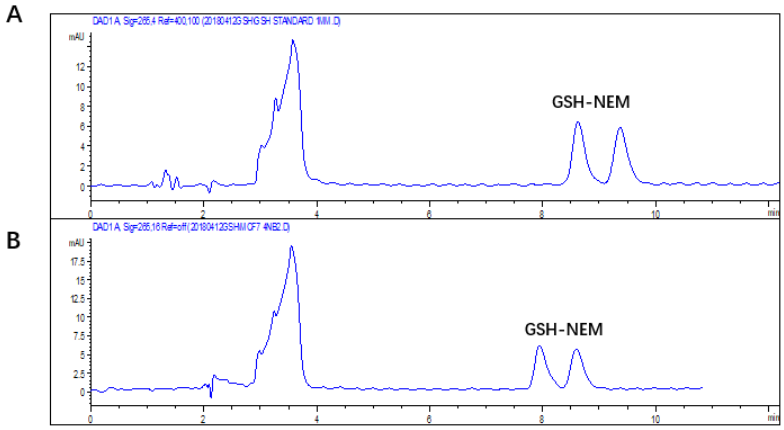

Figure 1.1.5 Representative chromatogram of the GS-NEM conjugate of standard GSH (A) and cellular GSH (B). The GSH-NEM conjugates were analyzed by HPLC with UV detection at a wavelength of 265 nm in the supernatant obtained from a cellular extract. GS-NEM conjugate separation resulted in two peaks with the same area at different retention time. These two peaks form as the consequence of the generation of diastereomers, which are separable under achiral chromatographic conditions.

1.2.8 The effect of 4NB on the energetic charge

Owing to the instability and the interconversion of those high-energy phosphates and reducing equivalents, stable and efficient way of extraction is required for measurement of cellular energetic charge. Specifically, adenine dinucleotides are readily broken into nicotinamide and ADP under a specific condition[264]. MCF7 cells were cultured in 6-well plates and cells in different wells were

treated with 0 mM, 2 mM, 4 mM, 6 mM and 8 mM for triplicates. After 4 days of 4NB treatment, cells were cultured detached by trypsinization. Cell pellets were washed by PBS for 2 times and resuspended in 1 mL PBS. A volume of 20 µL cell suspension was withdrawn for protein quantification. Then cell pellets were collected again by centrifuge at 300g for 3 min, and 100 µL ice-cold perchloric acid was added in cell pellets for the extraction of adenosine nucleotide triphosphate (ATP), adenosine nucleotide diphosphate (ADP) and adenosine nucleotide monophosphate (AMP). Samples were centrifuged 14000 g under a temperature of 4°C for 5 min. Supernatants were transferred into the Eppendorf and then neutralized using KOH. 20 µL of supernatant was injected for HPLC analysis.

Adenosine nucleotide triphosphate (ATP), adenosine nucleotide diphosphate (ADP) and adenosine nucleotide monophosphate (AMP) were simultaneously determined by HPLC-UV. A Phenomenex Kinetex C18 column (250 mm, 4.6 mm, 5 µm) was used for separation of ATP, ADP, and AMP. The mobile phase composed of 100 mM phosphate (pH 6.5) was used, and isocratic elution was carried out at a flow rate of 1 mL/min.

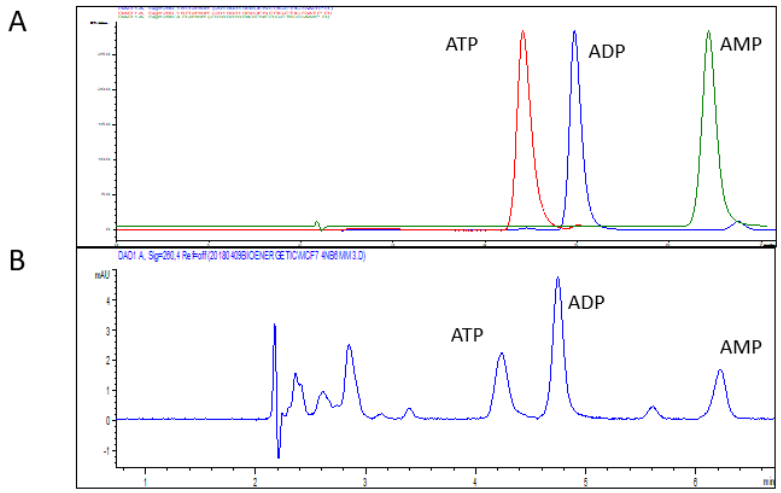

Figure 1.1.6 Representative chromatographs of ATP, ADP, and AMP. (A) Chromatograph of ATP, ADP, AMP standard. (B) Chromatograph of ATP, ADP AMP extracted from MCF7 cells. Energetic charge was calculated by equation: energetic charge=(ATP+ADP)/(ATP+ADP+1/2AMP).

1.2.9 Intracellular oxygen

Acetylacetonatobis-[2-(29-benzothienyl) pyridinato-kN, kC3'] iridium (III) (BTP) was served as a phosphorescent dye of intracellular oxygen. BTP is a compound that is phosphorescent in low oxygen conditions and is quenched in the presence of oxygen. The extent of quenching is dependent upon intracellular oxygen concentration. The endogenous oxygen was measured by the adaption of the approach has been described in a published paper[265]. BTP was utilized in all experiments at a concentration of 1 µM.

Besides, intracellular oxygen was measured by using flow cytometry. MCF7 and HepG2 cells were cultured in the corresponding culture medium. Then cells were detached and suspended in cell culture medium with 1 µM. Cells were then washed three times using PBS buffer. After, the cell suspension was subjected to flow cytometry. Excitation laser was 488/581 nm, and FL4 (650 LP) was chosen for BTP fluorescence. Fluorescence of various samples was compared by using histogram analysis.

We also visualized endogenous oxygen using confocal microscopy. MCF7 and HepG2 cells were

cultured in the corresponding culture medium. Then cells were seeded on coverslips in a 6-well plate at a suitable density. After 24 h incubation at 37°C and 5% CO_2, the culture medium was replaced by culture medium in the presence of 1 μM. Place the plates in at 37 °C for 2 h incubation. Afterward, coverslips were washed by Tris buffer for three times and mounted on the confocal microscope. Samples were viewed at the excitation wavelength 488nm and emission of BTP was by red channel.

1.2.10 Statistical analyses

All statistical analyses were performed using GraphPad Prism 5.0. Statistical significance was assessed using t-tests or ANOVA as indicated in figure legends, and the confidence interval was set at a 95% in every analysis. And error bars represent the standard deviation (SD) or standard error of the mean (SEM) as indicated in figure legends. Furthermore, when the $p<0.001$, statistical significance was indicated by ***; when the significance was $p<0.01$, it was indicated by**; when $p<0.05$, it was indicated by *; when $p > 0.05$, it was indicated by NS.

1.3 Results

1.3.1 CoQ10 content and total cholesterol content

Prolonged 4 mM 4-nitrobenzoic acid (4NB) treatment of MCF cells and HepG2 cells was found to inhibit CoQ10 biosynthesis effectively. Cellular CoQ10 reduced approximately 60% and 70% in MCF7 cells and HepG2 cells respectively when the cells were treated with 4 mM 4-nitrobenzoic acid for more than four days (As shown in Figure 1.3.1.A). CoQ10 primarily presents in the mitochondrial membrane, and it is one of the substrates of mitochondrial respiratory complex I (NADH: ubiquinone oxidoreductase) and complex II (succinate: ubiquinone oxidoreductase). Besides, ubiquinol is one of the substrates of complex III (ubiquinol: cytochrome c oxidoreductase). Therefore, it is conceivable that reduced CoQ10 pool may reduce the efficiency of the electron transport chain (ETC).

4NB, an analog of 4-hydroxybenzoate (4 HB), is an inhibitor of CoQ2 which catalyzes the particularly important connection of 4-hydroxybenzoate (4-HB) with an isoprenoid side chain. Thus, 4NB inhibited biosynthesis of CoQ10 as mentioned above. As a consequence, cells would switch to synthesize cholesterol due to the elevated level of isoprenoids. In our study, we measured total cholesterol level in both MCF7 cells and HepG2 cells by using HPLC-UV after hydrolysis and oxidation. We found that total cellular cholesterol level in cells with 4NB treatment was enhanced in comparison to that of the controls (As shown in Figure 1.3.1.B). It demonstrated that the blocking CoQ10 biosynthesis using 4-nitrobenzoate (4 mM) would switch CoQ10 synthesis to cholesterol biosynthesis because they share a common precursor farnesyl-pyrophosphate (FPP) (As shown in Figure 1.1.3 C).

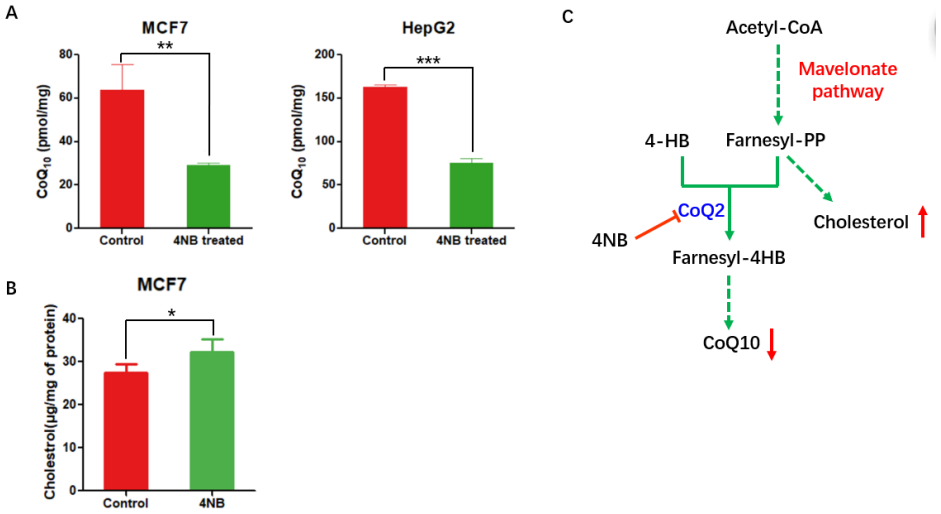

Figure 1.3.1 Reduction of CoQ10 and elevated total cholesterol level in MCF7 cells and HepG2 cells in the presence of 4 mM 4NB. (A). Cellular CoQ10 content measured by HPLC-UV at the wavelength of 275 nm. (B). Total cholesterol level in MCF7 cells in the absence and the presence of 4 mM 4NB. Total cellular cholesteryl esters were converted to cholesterol by cholesterol esterase. Cholesterol esters generated cholesterol, and free cholesterol was oxidized by cholesterol oxidase. Afterward. The product cholest-4-en-3-one was measured by HPLC-UV at the wavelength of 240nm. (C). Schematic illustration of CoQ10 biosynthesis and cholesterol biosynthesis. Farnesyl-pyrophosphate (FPP) is the common intermediates shared by CoQ10 biosynthesis and cholesterol biosynthesis. 4NB is an analog of 4-hydroxybenzoic acid (4HB) that can inhibit the farnesylation of 4-hydroxybenzoic acid. Therefore, inhibition of CoQ2 switches CoQ10 biosynthesis to cholesterol biosynthesis. Therefore, the isoprenoid unit farnesyl-pyrophosphate was shunted to cholesterol biosynthesis. (Mean±SD, n=3)

1.3.2 Measurement of oxygen consumption rate (OCR)

Cell permeable agents such as oligomycin (Oligo), FCCP and antimycin A (AA) were employed to work on ATP synthase, uncoupling protein and complex III respectively. Various stages of oxygen consumption rate (OCR) were obtained after sequential addition of oligomycin, FCCP and antimycin A. It was notable that basal oxygen consumption (Basal) of 4NB treated cells was reduced significantly in comparison to the controls. The difference between basal respiration and the oxygen consumption rate in the presence of oligomycin (Oligo) can be referred to the amount of oxygen consumed in phosphorylating conditions while oligomycin respiration accounts for non-phosphorylating OCR. The results reported in **Figure 1.3.2** showed that ATP synthase the rate of ATP synthesis was slower in cells treated with 4NB. The remaining oxygen consumption rate after addition of oligomycin have no significant difference between the controls and 4NB treated cells, which suggested 4NB treatment did not affect proton leak. In addition, uncoupling respiration was induced by using 0.5 μM FCCP. The oxygen consumption rate (OCR) of the control was elevated drastically in response to FCCP due to the proton movement into the mitochondrial matrix. Whereas, cells treated with 4 mM 4NB, either MCF7 cells or HepG2 cells, barely responded to the addition of FCCP. It was demonstrated that cells treated with 4NB may not be able to supply adequate oxygen or electron to for H_2O formation in cells added FCCP. Besides, it suggested maximum respiratory capacity was remarkably reduced in 4NB treated cells. All in all, the depletion of CoQ10 had a profound impact on oxidative phosphorylation (OXPHOS).

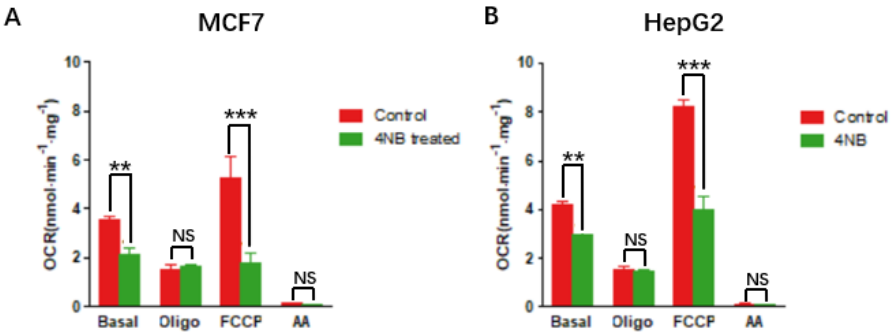

Figure 1.3.2 Oxygen consumption rate (OCR) of MCF7 cell line (A) and HepG2 cell line (B) after treatment of 4NB. After measurement of endogenous oxygen consumption (Basal), 1 μM oligomycin (Oligo), 0.5 μM FCCP and 4 μM antimycin A (AA) was sequentially added to get the different stages of the oxygen consumption rates. The statistical comparison was carried out by t-student analysis. (Mean±SD, n=3)

1.3.3 Activity of respiratory complex I, II and IV

To gain a better understanding of how 4NB treatment affects the activity of mitochondrial respiratory complexes. We measured the activity of complex I, complex II and complex IV. Respiratory complex I and respiratory complex II were measured by following NADH oxidation and DCPIP oxidation using cell lysate. While complex IV was measured by oxygen consumption using oxygen meter. We found that the activity of complex I was not affected by 4NB treatment. However, the activity of complex II reduced dramatically in the presence of 4NB. Besides, the activity of cytochrome c oxidase (complex IV) was slightly inhibited by 4NB treatment.

Overall, 4NB treatment has an inhibitory effect on some respiratory complexes such as complex II and complex IV. It suggested that the comprised oxidative phosphorylation in 4NB treated cells might be resulted from the inhibition of electron transport in addition to CoQ10 depletion.

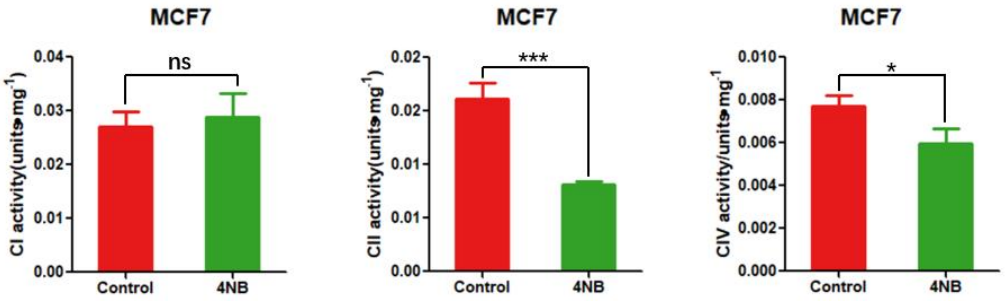

Figure 1.3.3 Activity of mitochondrial respiratory complex I, complex II and complex IV. The activity of complex I was indicated by oxidized NADH; The activity of complex II indicated by DCPIP; And the activity of complex IV was indicated by reduced oxygen. 1 unit=1 μmol·min^{-1}; The statistical comparison was carried out by t-student analysis. And when the $p<0.001$, significance was indicated by ***; when the significance was $p<0.01$, it was indicated by**; When the significance $p<0.05$, it was indicated by *; when there is no significant difference, it was indicated by NS. (Mean±SD, n=3).

1.3.4 NADH autofluorescence

NADH green autofluorescence was measured by confocal microscopy. It allowed us to assess the NADH level in living cells. We found that the autofluorescence of NADH was increased

significantly when complex I (NADH: ubiquinone oxidoreductase) was inhibited by rotenone, while the lower level was detected in the presence of FCCP. FCCP is an uncoupling agent that is used to access the maximum rate of the respiratory chain. These results confirmed that validity of this method. Although acitiivty complex I did not change, the rate of NADH oxidation was reduced by 4NB treatment due to CoQ10 depletion. Thus, NADH autofluorescence in 4NB treated cells increased more than that of the control. Moreover, FCCP was used to access the maximum rate of the respiratory chain. Although the maximum rate of oxidative phosphorylation was reduced, the NADH level in the 4NB treated cell has no significant increase after FCCP treatment. It might be resulted from less NADH generation by the TCA cycle. It might be attributable to the reduced activity of complex II (succinate dehydrogenase) in the 4NB treated cells.

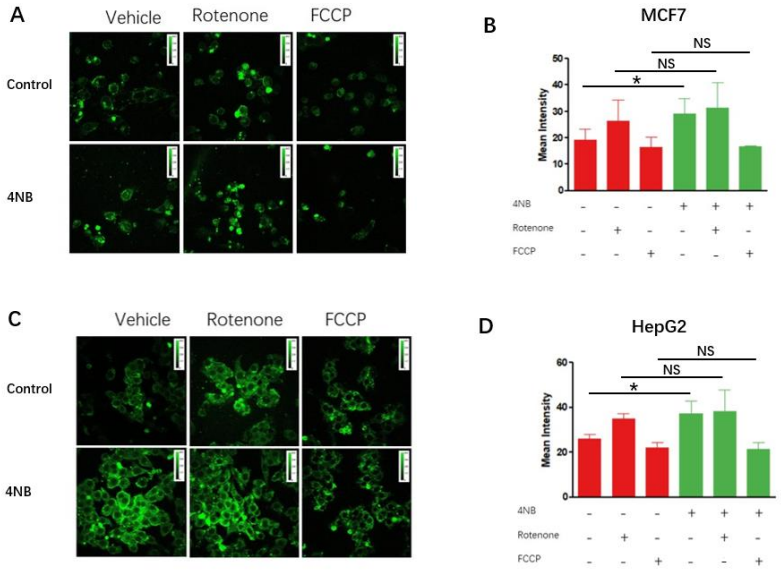

Figure 1.3.4 Measurement of NADH autofluorescence by confocal microscopy.

(A) Representative images of MCF cells untreated with 4NB (upper panels) and treated with 4NB (lower panels). Before observation by confocal microscopy, cells were treated with Rotenone for 10 min and FCCP (0.5 μM) for 5 min respectively.

(B) Quantification of NADH autofluorescence by ImageJ in MCF7 cells that untreated or treated with the 4NB. Before observation by confocal microscopy, cells were treated with Rotenone for 10 min and FCCP (0.5 μM) for 5 min respectively. (Mean ± SD, n=10)

(C) Representative images of HepG2 cells untreated with 4NB (upper panels) and treated with 4NB (lower panels). Before observation by confocal microscopy, cells were treated with Rotenone for 10 min and FCCP (0.5 μM) for 5 min respectively.

(D) Quantification of NADH autofluorescence by ImageJ in HepG2 cells that untreated or treated with the 4NB. Before observation by confocal microscopy, cells were treated with Rotenone for 10 min and FCCP (0.5 μM) for 5 min respectively. The statistical comparison was carried out by t-student analysis. And when the $p<0.001$, significance was indicated by ***; when the significance was $p<0.01$, it was indicated by**; When the significance $p<0.05$, it was indicated by *; when there is no significant difference, it was indicated by NS. (Mean ± SEM)

1.3.5 Characterization of Mitochondria

1.3.5.1 Mitochondrial network morphology

To know whether the 4NB treatment affected the mitochondrial morphology, we used a fluorescent probe to visualize mitochondrial network morphology. And images were taken by confocal

microscopy (As shown in **Figure 1.3.5**). Mitochondrial network was assessed by mitochondrial circularity and aspect ratio (AR) which were obtained from ImageJ analysis. We observed that mitochondrial circularity slightly increased, while mitochondrial aspect ratio (AR) was slightly reduced. It suggested an increased mitochondrial fragmentation in the cells were treated with 4-nitrobenzoic acid (4NB).

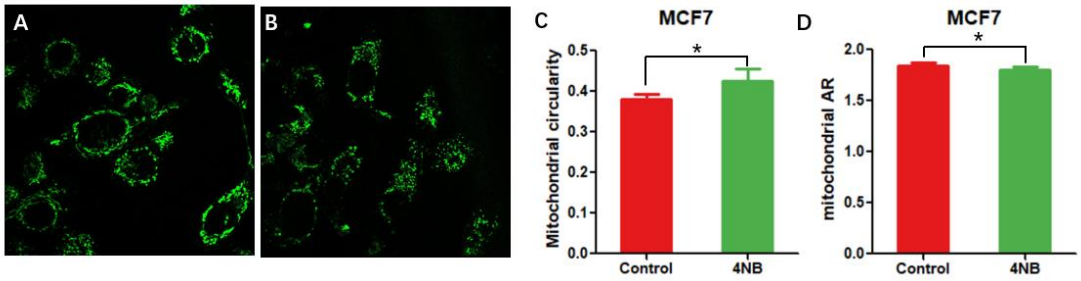

Figure 1.3.5 Mitochondrial morphology of MCF7 cells by confocal microscopy stained with Mito-Tracker green (100 nM). (A) Mitochondrial network morphology of MCF7 cells in the absence of 4NB; (B) Mitochondrial morphology of MCF7 in the presence of 4 mM 4NB; (Mean ± SEM) (C) Mitochondrial circularity analyzed by ImageJ (Mean ± SEM); (D) Analysis mitochondrial aspect ratio conducted by ImageJ. The statistical comparison was carried out by t-student analysis. And when the $p<0.001$, significance was indicated by ***; when the significance was $p<0.01$, it was indicated by**; When the significance $p<0.05$, it was indicated by *; when there is no significant difference, it was indicated by NS.

1.3.5.2 Mitochondrial membrane potential

Furthermore, mitochondrial membrane potential was evaluated by mitochondrial imaging. 4NB treated cells exhibited increased mitochondrial membrane potential.

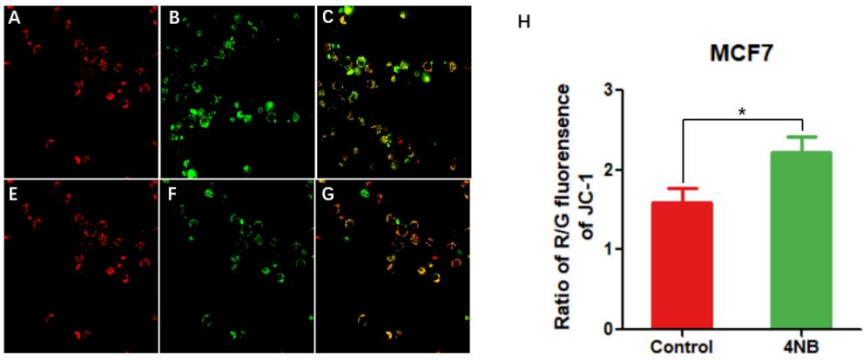

Figure 1.3.6 Polarization of mitochondrial membrane potential of MCF7 cells induced by 4NB treatment. Mitochondrial membrane potential was measured by confocal microscopy with JC-1 （5 μM) staining. And mitochondrial membrane potential was estimated by the ratio of red/green fluorescence.

A-C, Representative confocal microscopic images of red and green fluorescence of the control (Upper panels);

E-G, Representative confocal microscopic images of red and green fluorescence of the cells with 4 mM 4NB treatment (Lower panels).

(H) Ratios of red/green fluorescence were obtained from analyzing the intensity of red and green fluorescence by ImageJ. The statistical analysis was carried out by t-student analysis. (Mean ± SD)

1.3.5.3 Mitochondrial mass

Mitochondria were stained by MitoTracker Green and mitochondrial mass of a single cell was measured by flow cytometry in both MCF7 cells and HepG2 cells. In MCF7 cells, the fluorescence of MitoTracker Green in 4NB treated cells was reduced in comparison to controls. It suggested that the mitochondrial mass in 4NB treated cells might be reduced by CoQ10. It might be attributable to the deregulation of mitochondrial biogenesis. However, 4NB treatment had no significant effect on the mitochondrial mass in HepG2 cells. It indicated that the impact of 4NB treatment on mitochondrial mass was variable in different cell lines.

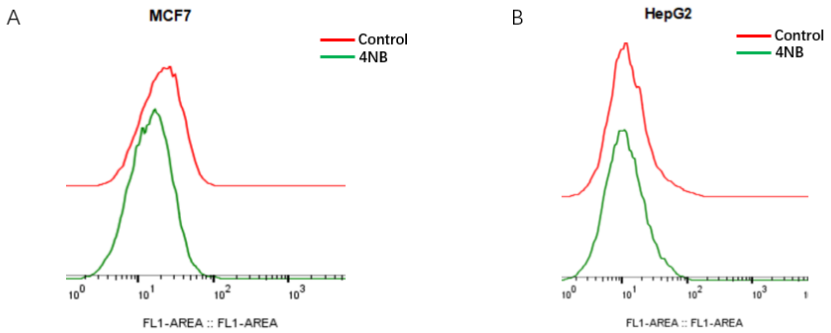

Figure 1.3.7 Mitochondrial mass measured by flow cytometry with 0.1 μM MitoTracker Green staining.

A. Histogram representation of fluorescence of MitoTraker Green in MCF7 cells. The X-axis represents the MitoTraker Green fluorescence intensity, while the Y-axis indicates the cell counts in corresponding fluorescence intensity.

B. Histogram representation of fluorescence of MitoTraker Green in HepG2 cells. The X-axis represents the MitoTraker Green fluorescence intensity, while the Y-axis indicates the cell counts in corresponding fluorescence intensity.

1.3.6 Evaluation of oxidative stress

1.3.6.1 ROS production

To estimate ROS production, a general ROS indicator H2DCFDA was employed to examine the ROS production in MCF7 cells with or without 4NB treatment. By using flow cytometry, we found that fluorescence of DCFDA was significantly higher in 4NB treated cells. It suggested that ROS production in 4NB treated cells was elevated.

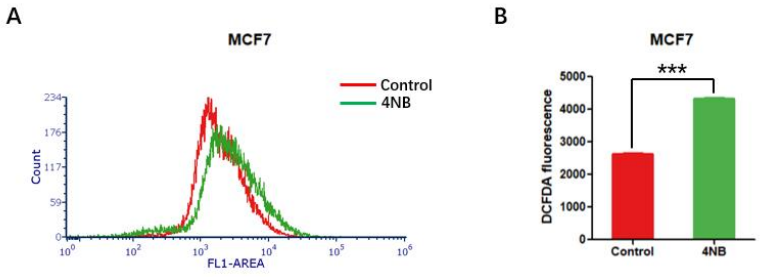

Figure 1.3.8 Flow cytometric measurement of ROS production in MCF7 cells with and without 4NB treatment

A. Histogram of DCFDA. It shows how many cells are at each intensity of H2DCFDA. The X-axis represents the DCFDA intensity, while the Y-axis indicates the cell counts in corresponding fluorescence intensity.

B. Fluorescence intensity of DCFDA in MCF7 cells in the presence of 4NB and in the absence of 4NB. The statistical comparison was carried out by t-student analysis. And when the $p<0.001$, significance was indicated by ***; when the significance was $p<0.01$, it was indicated by**; When the significance $p<0.05$, it was indicated by *; when there is no significant difference, it was indicated by NS. (Mean ± SEM)

1.3.6.2 Glutathione (GSH)

Glutathione is an endogenous antioxidant that can scavenge hydroperoxide (H_2O_2). We revealed that the glutathione level in 4NB treated cells was decreased significantly. It suggested that oxidative stress in cancer cells in the presence of 4NB was increased.

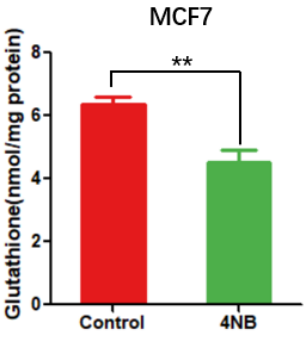

Figure 1.3.9 Glutathione in MCF7 cells measured by HPLC-UV

The measurement of glutathione was measured after derivatization with N-Ethylmaleimide (NEM). And the conjugates (GSH-NEM) were quantified by HPLC-UV. Statistical comparison was carried out by t-student analysis. And when the $p<0.001$, significance was indicated by ***; when the significance was $p<0.01$, it was indicated by**; When the significance $p<0.05$, it was indicated by *; when there is no significant difference, it was indicated by NS. (Mean ± SD)

1.3.6 Energetic charge

When the respiratory chain was impaired, it would affect ATP generation because the respiratory chain is one of the particularly important pathways responsible for ATP production. The cellular concentrations of ATP, ADP, and AMP are simultaneously determined by HPLC-UV, and the energetic charge was calculated by using the following equation:

$$\text{Energetic charge}=(ATP+1/2ADP)/(ATP+ADP+AMP).$$

As we mentioned above, oxidative phosphorylation (OXPHOS) was impaired in cells treated with 4NB. However, we found that energetic charge oscillated mildly despite less ATP generation from oxidative phosphorylation (OXPHOS) in cancer cells treated with 4NB. Specifically, we noted that 2 mM and 4 mM 4-nitrobenzoate (4NB) treatment had no significant effect on energetic charge. When cells were treated with 6 mM, the energetic charge decreased by approximately 2%. When cells were treated with 8 mM 4-nitrobenzoate (4NB), the energetic charge decreased by approximately 5% (As shown in Figure 1.3.10). Therefore, cells treated with very high concentrations of 4NB suffered from mild energetic stress. Consequently, we estimated that the ATP production could be compensated from glycolysis during treatment of 4NB. As an alternative, we can speculate that the energy demand in the 4NB treated cell was lower as we observed slower proliferation when cells treated with 4NB.

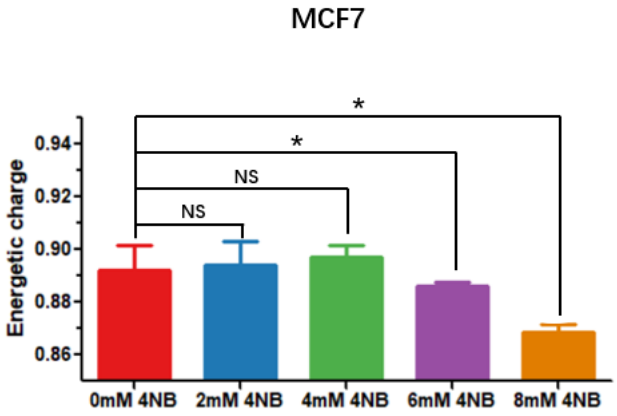

Figure 1.3.10 Energetic charge of MCF7 cells with prolonged 4NB treatment. ATP, ADP, and AMP were quantified by HPLC-UV. The energetic charge was used to assess energetic stress and it was calculated by the equation: Energetic charge=(ATP+1/2ADP)/(ATP+ADP+AMP). (Mean ± SD, n=3)

The statistical analysis was carried out by using the t-student test. And when the $p<0.001$, significance was indicated by ***; when the significance was $p<0.01$, it was indicated by**; When the significance $p<0.05$, it was indicated by *; when there is no significant difference, it was indicated by NS.

1.3.7 Hypoxia-induced by 4NB treatment

Firstly, we measured intracellular oxygen by flow cytometry with iridium (III) complex BTP staining. BTP phosphorescence could be quenched by intracellular oxygen. In both MCF7 cells and HepG2 cells, we found that BTP fluorescence was higher in 4NB treated cells (As shown in **Figure 1.3.11**). It indicated that endogenous oxygen level in 4NB treated cells was relatively lower than the controls.

Furthermore, we verified this finding by using confocal microscopy. Similarly, we noted that the BTP phosphorescence was significantly increased (As shown in **Figure 1.3.12**). It suggested that 4NB treatment led to hypoxia regardless of lower basal consumption rate as well mentioned above.

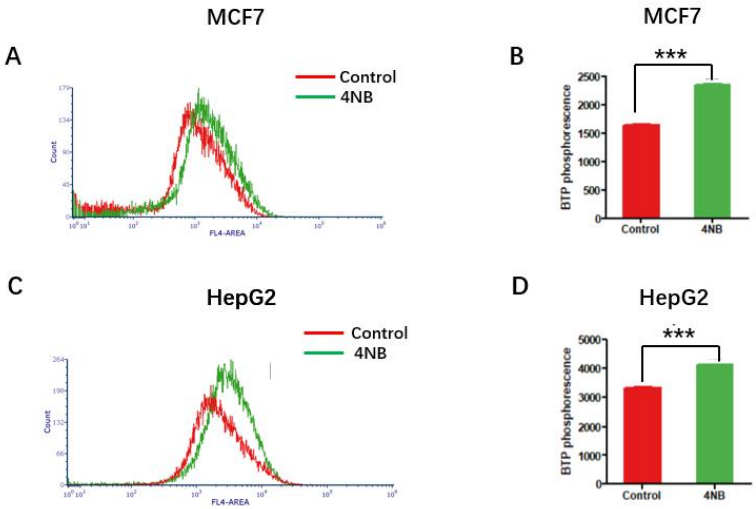

Figure 1.3.11 Intracellular oxygen of MCF7 cells and HepG2 cells traced by 1 μM iridium (III) complex (BTP)

(A) MCF7 cells with and without 4NB treatment were stained with BTP and then subjected to flow cytometry. It shows how many cells are at each intensity of BTP. The X-axis (FL4) represents the BTP intensity, while the Y-axis indicates the cell counts in corresponding fluorescence intensity.
(B) Fluorescence intensity of BTP in MCF7 cells in the presence of 4NB and the absence of 4NB. (Mean ± SEM)
(C) MCF7 cells with and without 4NB treatment were stained with BTP and the subject to flow cytometry. It shows how many cells are at each intensity of BTP. The X-axis represents the BTP intensity, while the Y-axis indicates the cell counts in corresponding fluorescence intensity.
(B) Fluorescence intensity of BTP in MCF7 cells in the presence of 4NB and the absence of 4NB. The statistical comparison was carried out by t-student analysis. And when the $p<0.001$, significance was indicated by ***; when the significance was $p<0.01$, it was indicated by**; When the significance $p<0.05$, it was indicated by *; when there is no significant difference, it was indicated by NS. (Mean ± SEM)

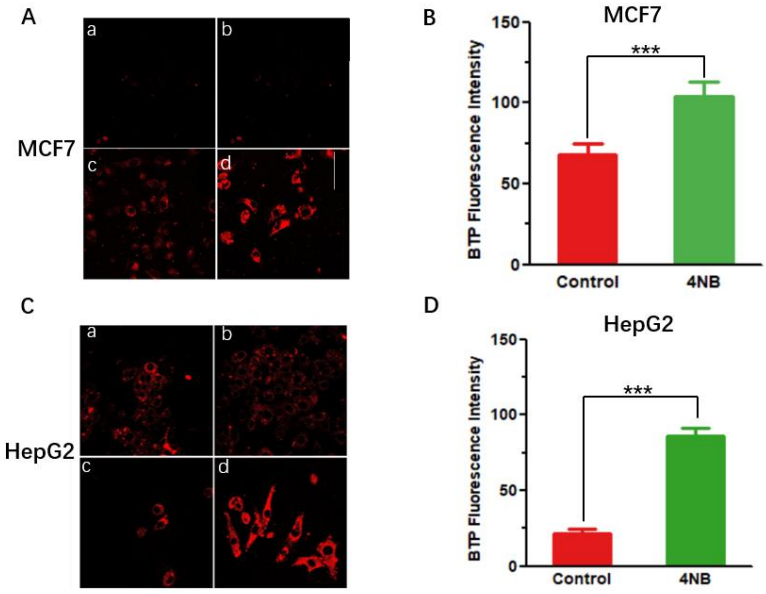

Figure 1.3.12 Intracellular oxygen measured by confocal microscopy MCF7 cell and HepG2 cells stained with 1 μM iridium (III) complex (BTP)
(A) Representative images of MCF7 cells with and without 4NB treatment were stained by iridium (III) complex BTP, and fluorescence was viewed by a confocal microscope. (a) The controls without BTP staining; (b) The 4NB treated cells without BTP staining; (c) The controls with BTP staining; (d) The 4NB treated cells with BTP staining.
(B) Fluorescence intensity of BTP in MCF7 cells with and without 4NB treatment was stained with iridium (III) complex (BTP), and fluorescence was viewed by a confocal microscope. Fluorescence intensity in cells with iridium (III) complex BTP was analyzed by ImageJ. And fluorescence without staining was subtracted from fluorescence intensity. Statistical analysis was performed by t-test. (Mean ± SD, n=10)
(C) Representative images HepG2 cells with and without 4NB treatment were stained by iridium (III) complex BTP and fluorescence was viewed by a confocal microscope. (a) The controls without BTP staining; (b) The 4NB treated cells without BTP staining; (c) the controls with BTP staining; (d) The 4NB treated cells with BTP staining.

(D) Fluorescence intensity of BTP in HepG2 cells with and without 4NB treatment was stained with iridium (III) complex (BTP), and fluorescence was viewed by a confocal microscope. Fluorescence intensity in cells with iridium (III) complex BTP was analyzed by ImageJ. And fluorescence without staining was subtracted from fluorescence intensity. Statistical analysis was performed by t-test. (Mean ± SD, n=10)

1.4 Discussion

4-nitrobenzoate (4NB) was chosen to inhibit CoQ10 biosynthesis since 4-nitrobenzoate (4NB) is an analog of 4-hydroxybenzoate (4HB). And 4-hydroxybenzoate is a significant precursor of CoQ10. As CoQ10 biosynthesis shares a common biosynthetic precursor with cholesterol biosynthesis, inhibition of CoQ10 using 4NB resulted in a diminished level of cellular cholesterol. The diminished level of cellular cholesterol would have a profound impact on biomembrane properties since cholesterol is one of the critical constituents in biomembranes, particularly in the cytoplasmic membrane. The underlying mechanism has been discussed in depth in a previous study. CoQ10 biosynthesis requires farnesyl-pyrophosphate (FPP) which is a shared precursor with cholesterol biosynthesis. Therefore, the inhibition of CoQ10 biosynthesis by 4-nitrobenzoate (4NB) induced elevated cholesterol level, which subsequently altered the makeup of the cytoplasmic membrane. Thus, the cytoplasmic membrane permeability to the oxygen has been altered.

Moreover, it is conceivable that reduced CoQ10 content would have an impact on the mitochondrial respiratory chain and thereby led to compromised oxidative phosphorylation (OXPHOS), considering that CoQ10 play the indispensable role in the electron transport chain. Specifically, CoQ10 is the substrate of mitochondrial complex I (NADH: ubiquinone oxidoreductase), complex II (succinate: ubiquinone oxidoreductase). The CoQ10 deficiency would decrease the rate of reactions catalyzed by the mitochondrial complex I and the mitochondrial complex II. In our study, we demonstrated that CoQ10 reduced oxidative phosphorylation (OXPHOS) rate. Furthermore, we proved that CoQ10 depletion by 4NB treatment decreased activity of complex II and complex IV. Taken together, we can conclude that CoQ10 deficiency induced by 4NB treatment resulted in impaired complex II and complex IV, as well as compromised oxidative phosphorylation.

Since oxidative phosphorylation was diminished in the 4NB treated cancer cells, the NADH level was remarkably increased in 4NB treated cells. The defective OXPHOS might be attributable to diminished rate NADH oxidation catalyzed by the mitochondrial complex I. As a consequence, the elevated level of NADH would have a profound impact on a broad variety of dehydrogenases.

In addition to defective respiratory chain, cells treated with 4NB showed fragmented mitochondrial network and increased mitochondrial membrane potential. Mitochondrial network fragmentation indicated perturbed mitochondrial fission/fusion dynamics in 4NB treated cells. And increased mitochondrial membrane potential suggested the demand for energy might be low. Thus, it is conceivable that dysfunctional mitochondria induced by CoQ10 deficiency would have a profound impact on bioenergetics. In some previous studies, mitochondrial respiration defects could be induced by respiratory chain complex I inhibitors such a metformin[266, 267], or mtDNA mutations[268, 269]. Mitochondrial abnormalities could be elicited directly or indirectly by CoQ10 deficiency. Notably, a cellular respiration injury was induced by cellular CoQ10 depletion (As shown in Figure 1.3.2), suggesting that cellular CoQ10 deficiency led to the loss of efficiency in the electron transport chain (ETC).

Firstly, endogenous oxygen was reduced regardless of the diminished basal oxygen consumption rate in 4NB treated cells. We verified this finding by using an endogenous oxygen tracer. As we can

see from the results, the intracellular oxygen level was reduced significantly in 4NB treated cells (As shown in Figure 1.3.11 and Figure 1.3.12). Besides, the oxygen consumption rate could be stimulated by FCCP in cancer cells without 4NB treatment. While oxygen consumption remained to be the same as basal oxygen consumption in cells with 4NB treatment (As shown in Figure1.3.2). This somewhat suggested that diffusion of oxygen across the plasma membrane was shifted to be the rate-limiting step. Secondly, stabilization of HIF-1α might be resulted from inactivation of prolyl domain hydrogenases (PDHs) by elevated ROS and deficient complex II. Many studies have shown that elevated ROS and deficient complex II can inactivate prolyl domain hydrogenases (PDHs)[235]. Moreover, the inactivation of complex II possibly accounts for the HIF-1α stabilization since succinate accumulation can inactivate prolyl domain hydrogenases (PDHs). And PDH is involved in the degradation of HIF-1α. However, the accumulation of succinate remains to be investigated. Although glycolysis accelerated in the 4NB treated cells, ATP production from the glycolytic pathway is not sufficient to compensate defected respiratory chain. Additionally, with deficient respiratory chain, NADH accumulated in mitochondria as well. As results of metabolic reprogramming, the 4NB treatment altered the energy generation and cellular redox status remarkably.

Chapter 2 Metabolic alterations in response to mitochondrial dysfunction

2.1 Materials and cell culture

2.1.1 Materials

a. DMEM high glucose (22.5 mM glucose), DMEM low glucose (5.5 mM glucose), modified DMEM (glucose, glutamine, bicarbonate, and phenol red-free). Fetal bovine serum (FBS), EDTA-trypsin, Calf, Penicillin, glutamine, pyruvate for cell culture and passage were all purchased from Sigma Aldrich (MI, USA). And they all stored under 4 ºC.

b. 2-(N-(7-Nitrobenz-2-oxa-1,3-diazol-4-yl)-amino)-2-Deoxyglucose (2-NBDG) was dissolved in ethanol (44 mM), and it was stored at -20 ºC

c. Metabolites including glucose, glutamine, glutamate, phosphoenolpyruvate (PEP), pyruvate, lactate, α-ketoglutarate, citrate, isocitrate, succinate; malate, oxaloacetate (OAA) were used as the substrate in various enzymatic assays. The stock solutions were prepared by dissolving in ddH_2O, following by neutralization with KOH. There were stored under the temperature of -20 ºC before using.

d. Pyruvate/lactate dehydrogenase (PK/LDH), lactate dehydrogenase (LDH, 2000 units/mL); glutamate dehydrogenase (GDH, 700 units/mL) were in glycerol and stored at 4-8 ºC. Powder of glucose oxidase (GO), horseradish peroxidase (HRP), cholesterol esterase and cholesterol oxidase were dissolved in deionized H_2O and stored at -20 ºC.

e. Adenosine triphosphate (ATP), Adenosine diphosphate (ADP) and adenosine monophosphate (AMP), nicotinamide adenine dinucleotide (NAD^+), nicotinamide adenine dinucleotide reduced (NADH), nicotinamide adenine dinucleotide phosphate ($NADP^+$) and coenzyme A (CoA) were purchased from Sigma Aldrich (MI, USA). The solution should be freshly prepared since they are not stable. Stock solution can be stored in -20 ºC for weeks.

f. A Stock solution of Amplex red at a concentration of 5 mM was prepared by dissolving in deionized H_2O, and aliquots were split and stored -20 ºC before using. Amplex Red reagent is somewhat air sensitive. Once the aliquots of Amplex red is opened, use the reagent promptly.

g. Resazurin was dissolved in deionized H_2O and stored at -20 ºC before using.

h. Microsyringe, liquid nitrogen, protease inhibitors cocktail; hypotonic PBS buffer (20 mM, pH7.4) were used to prepare cell lysate in the enzymatic assay.

i. RNA extraction: 100% ethanol; 70% ethanol; SDS 1%; 2-mercaptoethanol; Commercial RNA extraction kit consists of RNA lysis buffer, washing buffer I, RNase-free water, washing buffer II and spin cartridge with a removable collection tube; Nanodrop spectrophotometer. All of them were purchased from Bio-Rad.

j. Reverse transcription: Oligo-dT primers; RNase-free H_2O; Buffer; RNase inhibitor; Deoxynucleotides; Dithiothreitol (DTT); Transcriptase.

k. Primary Antibody of GLUT1 and GLUT3 and corresponding secondary antibodies.

l. Paraformaldehyde was used for cell fixation.

m. Pyruvate kinase/lactate dehydrogenase (PK/LDH) and lactate dehydrogenase (LDH) catalyzed

reactions were carried out in reaction buffer consists of 100 mM KCl, 50 mM Tris 7.5, 5 mM $MgCl_2$, 1 mM DTT, 0.03% BSA.

n. Reaction buffer for dehydrogenases

o. Reaction buffer for glutamate dehydrogenase (GDH)-based reactions consists of 100 mM KH_2PO_4 (pH 7.2), 10 mM NH_4Cl, 5 mM $MgCl_2$, and 0.15 mM NADH. NH_4Cl was removed from the buffer for the measurement of intracellular α-ketoglutarate.

Instruments

a. Cell culture incubator (Thermo Electron Corporation, MA, USA)

b. Inverted microscope (Carl Zeiss AG, Baden-Württemberg, Germany)

c. Biosafety chamber

d. Millipore water purifying system (Merck Millipore, MA, USA)

e. Centrifuge

e. Jasco V-750 Spectrophotometer (Japan Spectroscopic Corporation, Tokyo, Japan)

f. Agilent 1100s High-performance liquid chromatography, (Agilent Technologies, CA, USA) and and chromatographic columns with various static phase material (Phenomenex, CA, USA)

g. Enspire multi-well plate reader (Perkin Elmer, MA, USA)

h. Confocal microscope

i. Cell sorter (Bio-Rad Laboratories, CA, USA)

k. Nanodrop spectrophotometer (Bio-Rad Laboratories, CA, USA)

l. RT-PCR (Bio-Rad Laboratories, CA, USA)

2.1.2 Cell culture

MCF7 breast cancer cells were cultured in Dulbecco's Modified Eagle Medium (DMEM, 22.5 mM glucose) supplemented with 10% fetal bovine serum (FBS), penicillin and 2 mM glutamine. HepG2 hepatic cancer cells were cultured in Dulbecco's Modified Eagle Medium (DMEM, 5.5 mM glucose) supplemented with 10% fetal bovine serum (FBS), penicillin and 2 mM glutamine. Cell morphology was monitored by an optical microscope. If not specially mentioned, the cells were exposed in 4 mM 4-nitrobenzoate for more than 4 days to deplete CoQ10 level**.**

2.2 Methods

2.2.1 Flow cytometric of glucose uptake by 2-NBDG tracer

Cells were seeded in 10 cm dishes and used at sub-confluence after 24 h preincubation. Harvest cells and 2-5×10^6 were used for flow cytometry analysis and adjust cell density at approximate 1× 10^6/mL. Cells were preincubated in DMEM (0.5%) with 100 μM fluorescent glucose tracer 2-NBDG for 10 min. For each measurement, roughly 30,000 cells were analyzed and data of side scattering, forward scattering, and all fluorescent channels were used to collect data by using Bio-Rad flow cytometer.

Data from each flow cytometric measurement was analyzed by FCS Express vision 6. Forward scatting and FL1 were used to form the 2D dot density plot. 2-NBDG fluorescent intensity of each measurement was analyzed. Abnormal events were gated out, and remaining events were used for statistical analysis and comparative study. Mean and SEM was used for statistical analysis and t-test was used for the significance of the difference.

2.2.2 Glucose consumption measured by glucose oxidase catalytic kinetics

MCF7 cells were seeded in 24 well plates, and it was placed at 37 ºC, 5% CO_2 for 24 h. Phenol red-free culture medium was used to replace the culture medium. After 4 h, 8 h, 12 h, and 24h incubation

in 37 ºC, 5% CO_2, the culture medium was collected in Eppendorf and stored in -20 ºC before enzymatic assay. In parallel, cells were detached by trypsinization and protein was measured by Lowry assay.

A rapid and robust analytical method was established based on glucose oxidase (GO)-horseradish peroxidase (HRP) coupled enzyme kinetics. To ensure the validity of quantification of substrate concentration, the linearity of glucose concentrations-initial reaction rates are required to be validated. Various concentrations of glucose were mixed with glucose-free culture medium. The quantity of the enzymes and conditions were optimized and linearity of glucose concentrations-reaction rates.

Reactions were composed of 50 µM Amplex Red reagent, 0.1 U/mL horseradish peroxidase (HRP), 10 mU/mL glucose oxidase, and 50 µL of cell culture supernatants diluted 100 times in 50 mM sodium phosphate buffer (pH 7.4). After 30 min incubation at room temperature resorufin, fluorescence emission was measured at 590 nm. Glucose concentrations were calculated according to the D-glucose standard curve and normalized against total cellular protein content measured in cell lysates with Lowry assay.

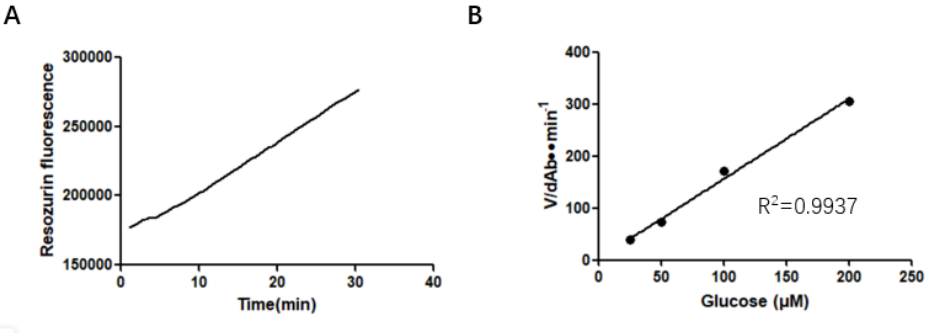

Figure 2.2.1 Fluorometric measurement of extracellular glucose concentration

(A) Kinetics of glucose oxidase (GO)-horseradish peroxidase (HRP)

(B) Linear regression of glucose concentrations vs. reaction rates ($R^2 > 0.99$)

2.2.3 GLUT2 (*SLC2A2*) gene expression

Detach the cells with trypsin, 3-5×10^6 cells were used for each sample. 0.3-0.6 mL Lysis Buffer with 2-mercaptoethanol to the sample. Cell pellets were vortexed until they were lysed and homogenized. 70% ethanol was added 1:1 to cell homogenate. Vortex to mix thoroughly and to disperse any visible precipitate to that may form after adding ethanol. Transfer up to 700 µL of the sample to the spin cartridge (with the collection tube). Centrifuge at 12,000×g for 15 s at room temperature. Discard the flow through and reinsert the spin cartridge into the same collection tube. Repeat the centrifugation until the entire sample has been processed. Then 700 µL washing buffer I was to spin cartridge and the centrifuge again at 12,000×g for 15 s at room temperature. Discard the flow-through and the collection tube. Place the spin cartridge back into a new collection tube. 500 µL washing buffer II and ethanol was added to the cartridge. Centrifuge at 12,000×g 15 s at room temperature and discard the flow through. Repeat the second washing. Centrifuge the spin cartridge at 12,000×g for 1-2 min to dry the membrane with bound RNA. Discard the collection tube and insert the spin the spin cartridge into a recovery tube. 30 µL RNase-free water was added to the spin cartridge of the spin cartridge and incubate at room temperature for 1 min to allow RNA to dissolve.

Centrifuge the spin cartridge for 2 min at 12,000×g at room temperature to elute the RNA from the

membrane into the recovery tube. Store the purified RNA on ice for immediate use and measurement the concentration of RNA by Nanodrop at a wavelength of 260 nm.

1μg RNA and primers were mixed, adjust volume to11.4 μL by using RNase-free H_2O. The mixtures were incubated at 28 ºC for 10 min. Besides, 4 μL Buffer， 0.5 μL RNase inhibitor, 2 μL Deoxynucleotide, 1μL DTT and 1.1 μL transcriptase were added and incubated at 48 ºC for 1 h. Afterward, incubated mixture at 85 ºC for 5 min.

Samples were analyzed by RT-PCR, the actin gene was used as the reference gene. Temperature program was set as 50°C 2 min, 1 cycle; 95°C 10 min, 1 cycle; 95 °C, 15 s -> 60 °C 30 s -> 72 °C 30 s, 40 cycles; 72°C 10 min, 1 cycle. Amplification curve was recorded and C_T was used for calculation of relative gene expression of GLUT2.

2.2.4 Immunostaining of GLUT1 and GLUT3

The immunofluorescence staining was optimized for analysis of GLUT1 and GLUT3. MCF7 cancer cells with and without 4NB were cultured on coverslips in 6-well plate. Cells were fixed for 10 min in 3% paraformaldehyde. Subsequently, coverslips were washed 3 times for 5 min in phosphate-buffered saline (PBS, 137 mmol/L sodium chloride, 3 mmol/L potassium chloride, 8 mmol/L sodium phosphate dibasic, 3 mmol/L potassium phosphate monobasic). GLUT1 and GLUT3 antibody (rabbit IgG, Abcam) was applied to the coverslips at a dilution of 1: 200 in 5% normal goat serum (NGS, Invitrogen) for 2 h at room temperature. The antibody used binds the cytosolic C terminal of GLUTs, as such the GLUT1 and GLUT3 visualized in this study represents both surface membrane-bound. Following primary antibody incubation, coverslips were washed 3 times for 5 min in PBS. Secondary antibodies were applied to cells for 30 min at room temperature at a dilution of 1:200 in PBS. After secondary antibody incubation, cells were washed 3 times for 5 min in PBS and coverslips were mounted with 20 μL mowiol; 6 g glycerol (Sigma Aldrich), 2.4 g mowiol 4-88 (Sigma Aldrich) and 0.026 g 1,4-diazobicyclo-[2,2,2]-octane (DABCO) (Sigma Aldrich) dissolved in 18 mL 0.2 mol/L Tris-buffer (pH 8.5). Fluorescence emission was detected using the green channel of the confocal microscope.

2.2.5 Quantification of extracellular lactate by HPLC-UV

MCF7 cells with 4 mM 4NB treatment and without 4NB treatment were plated in 16-well microplate and incubated for 24 h to allow cells to be stabilized. Replace culture medium with the 1.2 mL fresh complete culture medium with 4 mM 4NB and without 4NB. An aliquot of 30 μL culture medium was withdrawn at the time interval of 30 min, 60 min, 90 min, 120 min, 150 min, 180 min. 10 μM oligomycin was added in culture medium immediately. Samples were stored at -20 ºC until HPLC-UV analysis. Culture medium was mixed with HPLC mobile phase at the ratio of 1:1. Samples were centrifuged at 14,000×g for 5 min at 4 ºC. 20 μL of supernatant was injected into the HPLC system and analyzed. All experiments were carried out for triplicates.

A Phenomenex Zorbax Phenyl-SB HPLC column (250 mm, 4.6 mm, 5 μm) was used to analyze extracellular lactate. 100 mM phosphate buffer (PH 2.1) was used as mobile phase and isocratic elution was used at the flow rate of 1 mL/min. 30 min for a single analysis. And UV wavelength was set at 210 nm to measure lactate. Chromatographs were recorded and the peak area was obtained to calculate the concentration of lactate. A series of standard solutions of lactate were prepared and analyzed. Then the calibration curve was plotted for quantification.

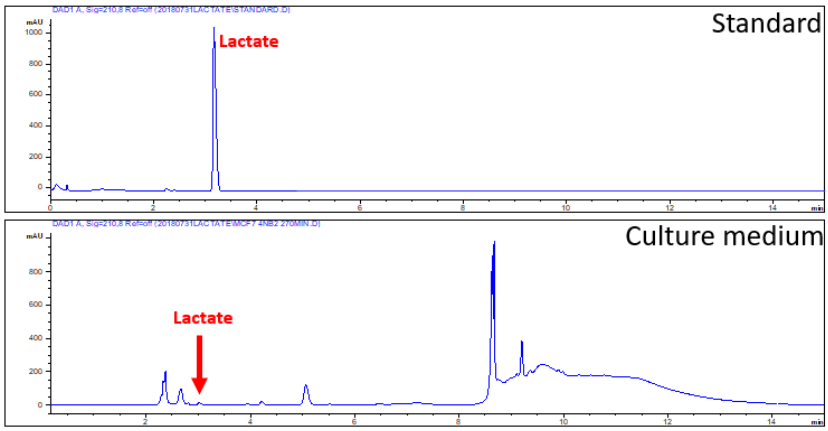

Figure 2.2.3 Representative chromatographs of lactate determination by HPLC-UV. A. chromatograph of standard lactate; B, chromatograph of lactate in the culture medium. The detection wavelength was 210 nm.

2.2.6 Pyruvate kinase (PK)

Reactions were performed in 1000 µL of 1X Buffer (100 mM KCl, 50 mM Tris 7.5, 5 mM $MgCl_2$, 1 mM DTT, 0.03% BSA, 180 µM NADH) at 37 ºC, 0.5 mM ATP and 4 units of lactate dehydrogenase (LDH). 980 µL reaction buffer was added into a quartz cuvette, and 10 µL of cell lysate was premixed with reaction buffer at 37 ºC for 3 minutes. And then various concentrations of phosphoenolpyruvate (PEP) was added to initiate the reaction. Enzymatic kinetics were obtained by the determination of NADH decrease continuously at a wavelength of 340 nm (Extinction absorption coefficient ε_{340nm}=6,220 $M^{-1}cm^{-1}$) for 3 min. And initial reaction rates were obtained from enzymatic kinetics. Michaelis-Menten plot and Lineweaver-Burk plot to analyze the Vmax and Km of pyruvate kinase (PK) in MCF7 cells with and without 4NB treatment.

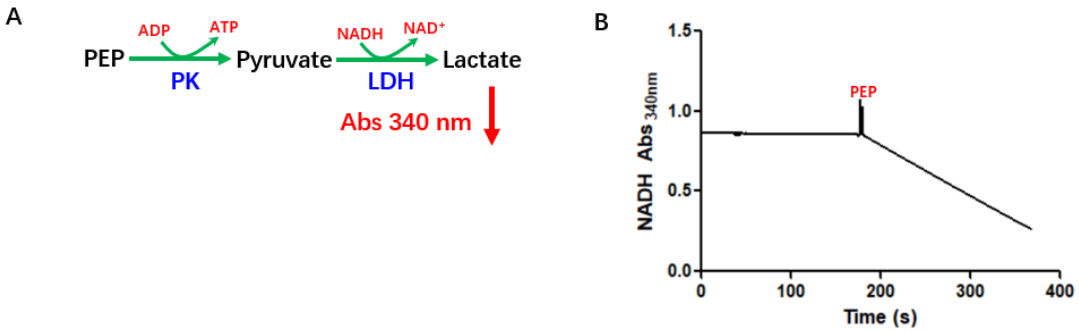

Figure 2.2.4 Colorimetric measurement of the kinetics of pyruvate kinase (PK)

(A) Schematic illustration of colorimetric measurement of pyruvate kinase activity

(B) Pyruvate kinase was coupled with lactate dehydrogenase (LDH, 4 units/mL) and kinetics of pyruvate kinase (PK) was measured by following the decrease of NADH absorbance after addition of phosphoenolpyruvate (PEP) at a wavelength of 340 nm.

2.2.7 Activity of $NAD(P)^+$ dependent dehydrogenases

A rapid and sensitive fluorometric method was established to determine the activity of $NAD(P)^+$ dependent dehydrogenases. A variety of dehydrogenases such as lactate dehydrogenase (LDH), pyruvate dehydrogenase complex (PDC), NAD^+-dependent isocitrate dehydrogenase (IDH3), $NADP^+$-dependent isocitrate dehydrogenase (IDH1/2), and α-ketoglutarate dehydrogenase complex (KGDC), malate dehydrogenase (MDH), malic enzyme (ME) and glutamate dehydrogenase (GDH)

use $NAD(P)^+$ as cofactor. Thus, the enzymes kinetics could be measured by following the formation of NADH or NADPH using fluorometric assay. In addition, glutaminase was investigated by coupling with glutamate dehydrogenase (2 units/mL). The principle of coupled-enzyme kinetic was presented in Figure 2.2.1.B. In a coupled enzyme kinetics, the initial reaction rate is not proportional to the first substrate because the second enzyme requires the building up of the second substrate (As shown in Figure 2.2.1). On top of that, if the second enzyme is the rate-limiting step of the reaction, the substrate of interest would not be proportional to the reaction rate. Thus, the Vmax of the following enzymes is required to be larger than the Vmax of first enzymes.

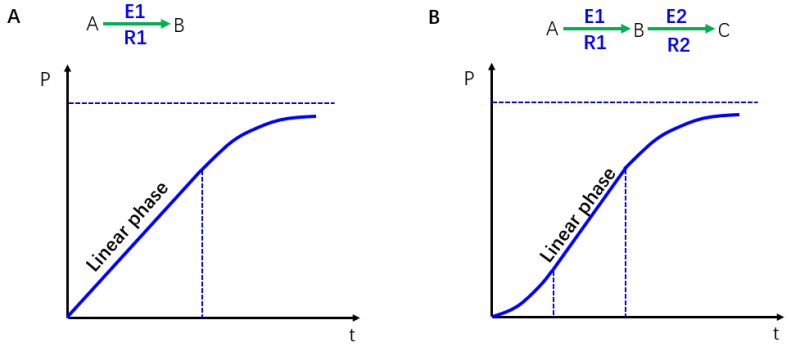

Figure 2.2.1 Kinetics of single-enzyme reaction and coupled-enzyme reaction.

Moreover, according to the following equation:

$$Vmax = Kcat * [E]t$$

In this equation, Vmax refers to maximal velocity, Kcat is a constant that refers to the turnover number, and [E]t refers to the quantity of enzyme. By that, the deregulation of enzymes, either Kcat or [E]t, would manifest a change of Vmax. Therefore, Vmax of dehydrogenases was obtained by measurement of enzyme kinetics. The cell lysate was prepared as described above.

This assay was adapted from a previously reported method[270]. Reaction buffer consists of 1 mM $MgCl_2$, 0.1 mM $CaCl_2$, 0.05 mM EDTA, 0.2% Triton X-100, 0.3 mM ThDP, rotenone 10 μM, 3 mM NAD^+, 0.75 mM resazurin. The assays were carried out in 50 mM Tris (pH 7.6) at 37 °C for 30 min. The specific substrate lactate, pyruvate, isocitrate, α-ketoglutarate, glutamine, glutamate and malate at a final concentration of 20 mM were added to initiate the specified reaction. When it comes to pyruvate dehydrogenase complex (PDC) and α-ketoglutarate dehydrogenase complex (KGDC), 1 mM CoA was additionally added in reaction buffer since pyruvate dehydrogenase complex) (PDC) and α-ketoglutarate dehydrogenase complex (KGDC) use CoA as substrate. Enzyme kinetics was recorded by detection of resorufin fluorescence emission at a wavelength of 590 nm. And Vmax of enzymes was analyzed by fitting first-order linearity ($R^2 > 0.99$).

2.2.8 Statistical analyses

All statistical analyses were performed using GraphPad Prism 5.0. Statistical significance was assessed using t-tests or ANOVA as indicated in figure legends. All error bars represent the standard deviation (SD) or standard error of the mean (SEM) as indicated in figure legends. And when the $p<0.001$, statistical significance was indicated by ***; When the significance was $p<0.01$, it was indicated by**; When $p<0.05$, it was indicated by *; When $p > 0.05$, it was indicated by NS.

2.3 Results

2.3.1 Glucose uptake

Driven by defective respiratory chain and hypoxia, glycolysis was speculated to be accelerated to compensate for ATP production. A fluorescent glucose tracer was employed to measure glucose

uptake (As shown in Figure 2.3.1). The results have shown that glucose uptake was enhanced in cells treated with 4NB. In addition, glucose oxidase-based enzymatic assay was used to measure extracellular glucose over time. Therefore, glucose consumption could be estimated.

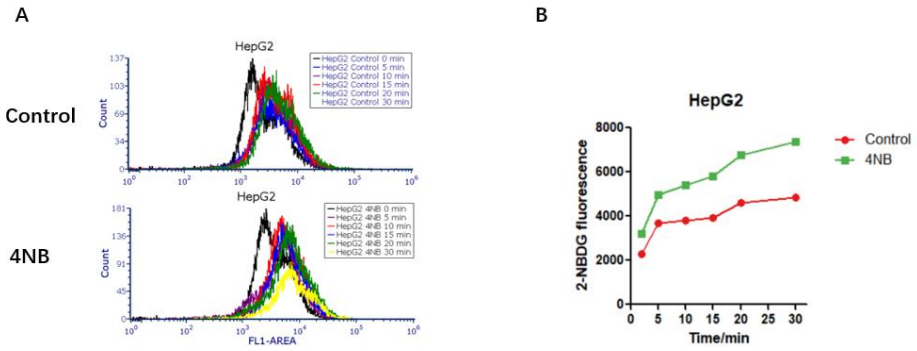

Figure 2.3.1 Measurement of glucose uptake by flow cytometry with fluorescent tracer 2-NBDG.

(A) Comparison of histograms from flow analysis showing the enhanced glucose uptake by 4NB in MCF7 cells. Cell population was expressed in a histogram, the number of the events on the Y-axis (cell count) and fluorescence intensity on the X-axis (FL1-area).

(B) The time course of glucose uptake by using 2-NBDG (100 μM) (Data were presented as Mean ±SEM).

2.3.2 Glucose consumption

To verify that glycolysis was accelerated in 4NB treated cells, glucose consumption was determined by using glucose oxidase (GO)/horseradish peroxidase (HPO) coupled reaction. The results have shown that glucose consumption of 4NB treated cells was significantly increased. The increase of glucose consumption confirmed that glucose flux into the 4NB treated cell was elevated in comparison to the controls. These results were consistent with the glucose uptake data traced by fluorescent analog 2-NBDG.

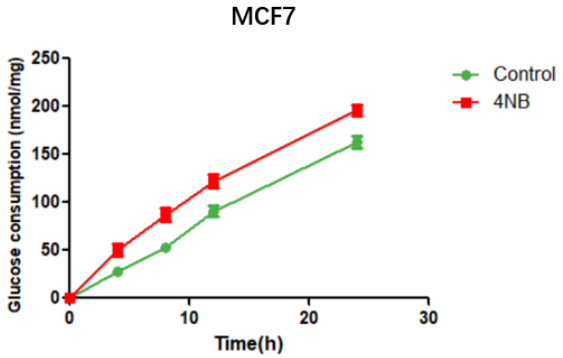

Figure 2.3.2 Glucose consumption measured by glucose oxidase (GO) catalyzed enzymatic assay. Extracellular glucose concentrations in culture medium were measured by using glucose oxidase (GO)-horseradish peroxidase (HRP) coupled reaction at indicated time points.

2.3.3 GLUT2 (*SLC2A2*) gene expression

We have demonstrated that glucose uptake was increased in MCF7 cells treated with 4NB. Furthermore, we investigated that gene expression of GLUT2 (*SLC2A2*) which is widely overexpressed in tumors. However, we found that there was no significant change in GLUT2

(*SLC2A2*) gene expression level although 4NB treatment increased glucose uptake in MCF7 cells.

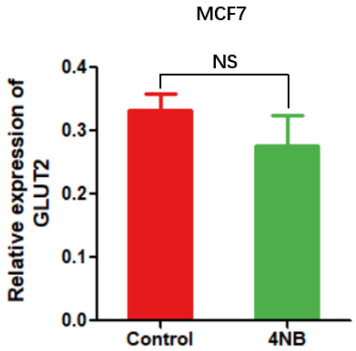

Figure 2.3.3 Relative expression of GLUT2 gene (*SLCA2*) in MCF7 with and without 4NB treatment.

2.3.3 Expression of GLUT1 and GLUT3

Glucose transporters (GLUTs) are usually overexpressed in cancer cells. To know how glycolysis responded to defective respiratory chain, we measured GLUT1 and GLUT3 expression in MCF7 cells. We found that the GLUT1 expression elevated significantly in 4NB treated MCF7 cells. It suggested that MCF7 cells with defective respiratory chain can promote the expression of GLUT1. Similarly, GLUT3 expression in 4NB treated MCF7 cells was slightly increased in comparison to the controls. Although GLUT1 and GLUT3 are not all of the glucose transporters in the MCF7 cell line, GLUT1 and GLUT3 largely contribute to glucose uptake given the fact that GLUT1 and GLUT3 have very high affinity to glucose. The overexpression of GLUT1 and GLUT3 indicated that MCF7 cell with compromised oxidative phosphorylation (OXPHOS) might switch to glycolysis for ATP production due to the metabolic stresses.

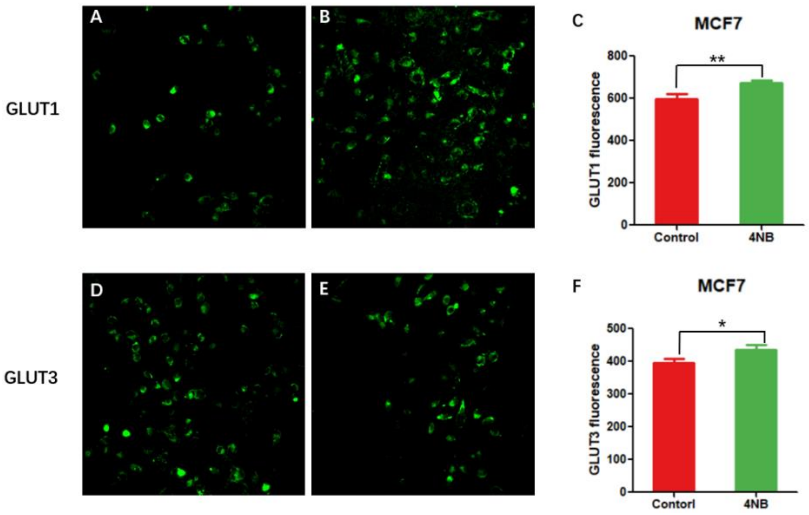

Figure 2.3.4 GLUT1 expression and GLUT3 in MCF7 cells measured by confocal microscopy with immunostaining.

(A) Representative images GLUT1 expression in MCF7 cells without 4NB treatment (B) Representative images GLUT1 expression in MCF7 cells with 4NB treatment (C) Fluorescence intensity analysis was carried out by ImageJ. (Mean ± SEM)

(D) Representative images GLUT3 expression in MCF7 cells without 4NB treatment. (E) Representative images GLUT3 expression in MCF7 cells with 4NB treatment (F) GLUT3 fluorescence intensity was quantified by ImageJ. (Mean ± SEM)

The statistical analysis was carried out by the t-student test. And when the $p<0.001$, significance was indicated by ***; when the significance was $p<0.01$, it was indicated by**; When the significance $p<0.05$, it was indicated by *; when there is no significant difference, it was indicated by NS.

2.3.4 Lactate secretion

Lactate is usually used as a maker of glycolysis because glycolytic flux partly contributes to lactate production. And lactate production largely contributes to the regeneration of cytosolic NAD^+ (As shown in Figure 2.3.5.A). In our study, extracellular lactate was determined by HPLC-UV. We obtained basal lactate secretion (nmol/mg)-time (min) curves from 0 to 180 min. After the measurement of basal lactate secretion rate, 10 μM oligomycin was added to block the ATP production by inhibition of ATP synthase. We obtained the maximum lactate secretion rate (As shown in Figure 2.3.5.B). We found that lactate secretion rate increased in response to ATP synthase inhibition. Furthermore, the linearity of curves was analyzed by utilizing first-order regression (R^2 >0.99). Therefore, we found that basal lactate secretion rate was 1.46±0.11 nmol/h/mg in the control and 1.03±0.09 nmol/h/mg in 4NB treated cell respectively. When cells were subjected to oligomycin (10 μM) inhibition, we found that basal lactate secretion rate is 3.78±0.29 nmol/h/mg in control, and 2.28±0.21 nmol/h/mg in 4NB treated cell. Lactate secretion rate rapidly enhanced after the addition of oligomycin due to the ATP synthase inhibition. And the increase of lactate secretion rate in response to oligomycin was lower in 4NB treated cells (As shown in Figure 2.3.5.C). The results confirmed that the oxidative phosphorylation was compromised in 4NB treated cells. Besides, the basal lactate secretion account for approximately 40% in control, while it accounts for approximately 45% in 4NB treated cells after addition of oligomycin. The results indicated a reduced glycolytic reserve in 4NB treated cells. It suggested that 4NB treated cells would be susceptible to glycolytic inhibition due to this bioenergetic alteration (As shown in Figure 2.3.5.D).

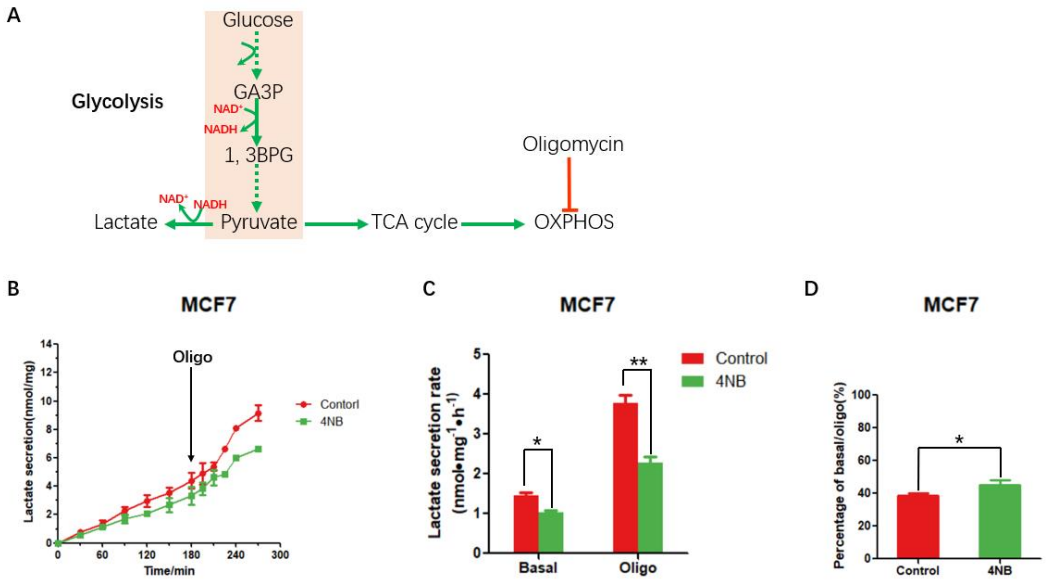

Figure 2.3.5 Lactate secretion in MCF7 cells over time measured by HPLC-UV

(A). Schematic representation of the relationship between glycolysis and lactate secretion.

(B). Basal lactate secretion (nmol/mg)-time (min) curve of MCF7 cell. ATP synthase was inhibited by the addition of oligomycin (at a final concentration of 10 μM) at 180 min. (Mean±SD, n=3)

(C). Basal lactate secretion rate of MCF7 cells and lactate secretion rate after addition of 10 μM

oligomycin treatment. (Mean±SD, n=3).

(D). Glycolytic reserve in cancer cells in the absence of 4NB and in the presence of 4NB. (Mean± SD, n=3)

The statistical analysis was performed by using t-student. And when the $p<0.001$, significance was indicated by ***; when the significance was $p<0.01$, it was indicated by**; When the significance $p<0.05$, it was indicated by *; when there is no significant difference, it was indicated by NS.

2.3.5 Characterization of pyruvate kinase (PK)

Pyruvate kinase (PK) is an enzyme that catalyzes the last step of glycolysis. And it is one of the major regulatory sites of glycolysis. In this study, the pyruvate kinase (PK) kinetics was measured by coupling with lactate dehydrogenase (LDH) (As shown in Figure 2.3.6.A). Moreover, enzyme velocities at various concentrations of phosphoenolpyruvate (PEP) were measured by a spectrophotometer. And the enzyme kinetics parameters were analyzed by Michalis-Menten plot and Lineweaver-Burk plot. Michalis-Menten plot and Lineweaver-Burk plot have shown that the Vmax of pyruvate kinase (PK) was unaffected in cancer cells in the presence of 4NB (As shown in Figure 2.3.6.B and Figure 2.3.6.C). However, Km of pyruvate kinase (PK) was reduced by 4NB treatment. The decrease of Km indicated that pyruvate kinase might be allosterically activated since it has a higher affinity to phosphoenolpyruvate (PEP) in cells treated with 4 mM 4NB. Whereas, the expression of pyruvate kinase (PK) was not promoted in cells treated with since Vmax was not altered by 4NB treatment.

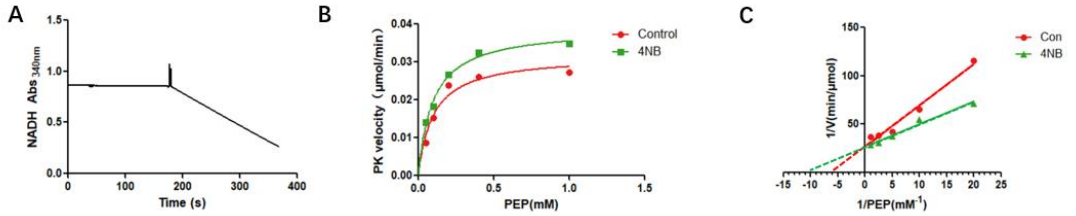

Figure 2.3.6 Characterization of pyruvate kinase (PK) in MCF7 cells with and without 4NB treatment.

A. Kinetics of pyruvate kinase (PK) in MCF7 cell lysate was measured by spectrophotometry. The pyruvate kinase (PK) was coupled with lactate dehydrogenase (LDH, 4 units/mL). And kinetics was followed by the decrease of NADH absorbance at a wavelength of 340 nm.

B. Michalis-Menten plot ($R^2>0.99$) of enzyme velocities measured for pyruvate kinase (PK) at various concentrations of phosphoenolpyruvate (PEP) in cells with or without 4NB treatment.

C. Lineweaver-Burk plot ($R^2>0.99$) of enzyme velocity measured for pyruvate kinase (PK) at various concentrations of phosphoenolpyruvate (PEP) in cells with or without 4NB treatment.

The statistical analysis was performed by the t-student test. And when the $p<0.001$, significance was indicated by ***; when the significance was $p<0.01$, it was indicated by**; When the significance $p<0.05$, it was indicated by *; when there is no significant difference, it was indicated by NS.

2.3.6 Activity of dehydrogenases

2.3.6.1 Activity of Lactate dehydrogenase (LDH) and pyruvate dehydrogenase complex (PDC)

We determined the activity of lactate dehydrogenase (LDH) and pyruvate dehydrogenase complex (PDC). We found that the activity of LDH was upregulated. However, the activity of pyruvate dehydrogenase was unaffected in cancer cells were treated with 4NB (As shown in Figure 2.3.7). It is worthwhile to point out PDC activity is tightly regulated by pyruvate dehydrogenase kinase (PDK) and some allosteric effectors such as NAD^+/NADH. Pyruvate can enter into mitochondria through

mitochondrial pyruvate carrier (MPC). Mitochondrial pyruvate can be converted to Acetyl-CoA by pyruvate dehydrogenase complex (PDC) and subsequently support the TCA cycle**.** However, this metabolic pathway is not favorable since compromised oxidative phosphorylation (OXPHOS) and elevated NADH level. Therefore, pyruvate flux might be redirected towards another pathway in 4NB treated cells instead of the conversion through lactate dehydrogenase (LDH). It is speculated that pyruvate might be shifted to amino acids formation such as alanine or aspartate. Because this conversion confers an advantage to glutaminolysis as well.

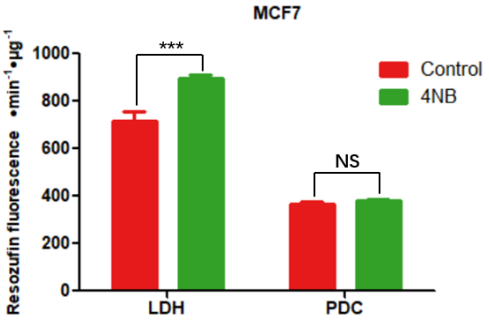

Figure 2.3.7 Activity of lactate dehydrogenase (LDH) and pyruvate dehydrogenase complex (PDC) in MCF7 cells with and without 4NB treatment(Mean±SD, n=3)

The statistical analysis was carried out by using t-student. And when the $p<0.001$, significance was indicated by ***; when the significance was $p<0.01$, it was indicated by**; When the significance $p<0.05$, it was indicated by *; when there is no significant difference, it was indicated by NS.

2.3.6.2 Activity of glutaminase (GLS) and glutamate dehydrogenase (GDH)

Anaplerotic replenishment from glutaminolysis is two steps conversion typically catalyzed by glutaminase (GLS) and glutamate dehydrogenase (GDH). In our study, we have demonstrated that glutaminase (GLS) activity was increased drastically in 4NB treated cells. The upregulated activity of glutaminase (GLS) indicated that the glutaminolysis was deregulated in 4NB treated cells. Although glutamate dehydrogenase (GDH) was unaffected, the conversion of glutamate to α-ketoglutarate (α-KG) through glutamate dehydrogenase (GDH) in 4NB treated cells was unfavored due to the elevated level of NADH. However, the conversion of glutamate to α-ketoglutarate (α-KG) can be alternatively catalyzed by aspartate-glutamate transaminase (AST) and alanine-glutamate transaminase (ALT). They can convert glutamate to α-ketoglutarate (α-KG) by using oxaloacetate (OAA) or pyruvate as substrate respectively.

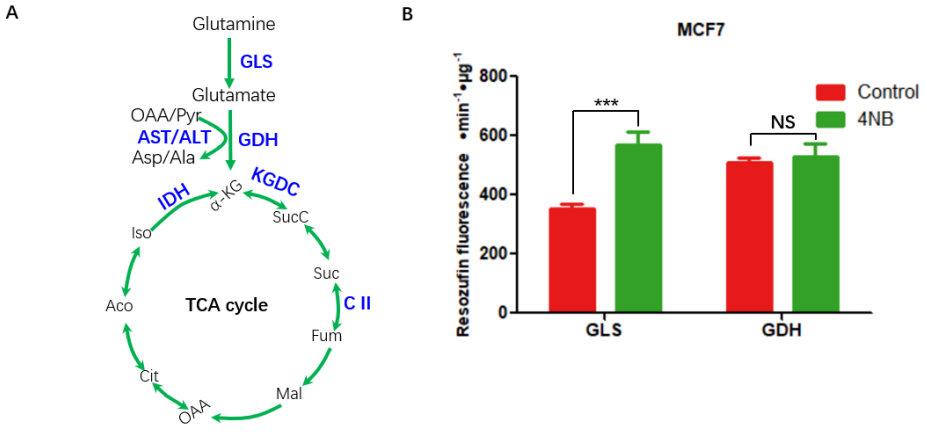

Figure 2.3.8 Activity of glutaminase (GLS) and glutamate dehydrogenase (GDH) in MCF7 cells with and without 4NB treatment.

Enzyme activities were measured by NAD^+-dependent enzymatic reactions. Enzymatic kinetics excitation wavelength at 550 nm and fluorescent emission of resorufin at 590 nm was measured by multi-well plate reader continuously.

(A) Schematic representation of the anaplerotic replenishment from glutaminolysis and the involvement of isocitrate dehydrogenase (IDH) and complex II in metabolic fate of α-ketoglutarate (α-KG).

(B) The activity of glutaminase (GLS) and glutamate dehydrogenase (GDH) in MCF7 cells with and without 4NB treatment. (Mean±SD, n=3)

The statistical analysis was performed by the t-student test. And when the $p<0.001$, significance was indicated by ***; when the significance was $p<0.01$, it was indicated by**; When the significance $p<0.05$, it was indicated by *; when there is no significant difference, it was indicated by NS.

2.3.7.3 Activity of $NADP^+$-dependent isocitrate dehydrogenase 1/2 (IDH) and $NADP^+$ dependent malic enzyme (ME)

Many studies have shown that $NADP^+$-dependent isocitrate dehydrogenase 1/2 (IDH1/2) plays a significant in oxidative homeostasis and *de novo* lipogenesis. The reductive carboxylation catalyzed by IDH1/2 contributes to the generation of citrate. And citrate is the primary precursor of *de novo* lipogenesis. In our study, we have demonstrated that both $NADP^+$-dependent isocitrate dehydrogenase 1/2 (IDH) was upregulated. The upregulation of IDH suggested that the reversible interconversion of isocitrate to α-ketoglutarate was favorable in 4NB treated cells. In addition, the complex II (succinate: ubiquinone oxidoreductase) was impaired in 4NB treated cells. The impaired complex suggested that the metabolic fate of α-ketoglutarate switched to reductive carboxylation in response to impaired complex II by 4NB treatment.

$NADP^+$-dependent malic enzymes, which is an enzyme that catalyzes the conversion of malate to pyruvate by using $NADP^+$ as a cofactor. Therefore, malic enzyme (ME) plays a very critical role in NADPH generation, as well as in glutaminolysis. The upregulation of malic enzyme (ME) might be driven by the higher demand of NADPH for antioxidative defense and deregulated glutaminolysis. However, it is needed to be demonstrated further by metabolic flux analysis.

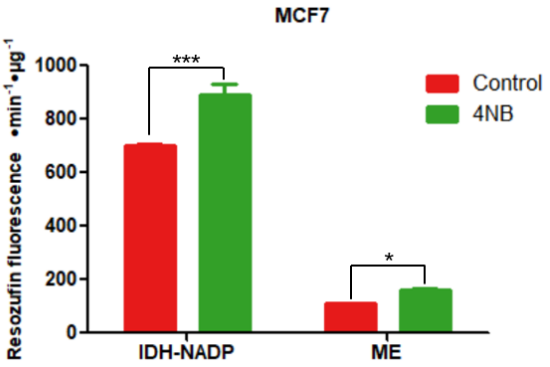

Figure 2.3.9 Activity of isocitrate dehydrogenase 1/2 (IDH1/2) and malic enzyme (ME) in MCF7 cells with and without 4NB treatment.

Enzyme activities were measured by $NADP^+$-dependent enzymatic reactions and excitation wavelength at 550 nm and fluorescent emission of resorufin at 590 nm was measured by multi-well plate reader continuously.

The statistical analysis was carried out by using t-student. And when the $p<0.001$, significance was

indicated by ***; when the significance was p<0.01, it was indicated by**; When the significance p<0.05, it was indicated by *; when there is no significant difference, it was indicated by NS. (Mean ±SD, n=3)

2.3.7.4 Activity of isocitrate dehydrogenase 3 (IDH3), α-ketoglutarate dehydrogenase (KGDC) and malate dehydrogenase (MDH)

Isocitrate dehydrogenase 3 (IDH3) is an isoform of IDH that utilizes NAD^+ as the cofactor. It catalyzes the reversible conversion of isocitrate to α-ketoglutarate (α-KG). And it has been proven that IDH3 was slightly upregulated in 4NB treated MCF7 cells.

Besides, α-ketoglutarate dehydrogenase complex (KGDH) is the enzyme that converts α-ketoglutarate(α-KG) to succinyl-CoA. Some studies have shown that the activity of KGDH could be inactivated ROS formation. However, in our study, the activity of KGDH was unaffected in 4NB treated cells although 4NB treated cells showed oxidative stress.

Malate dehydrogenase (MDH) catalyzes the reversible conversion of malate to oxaloacetate. It plays a significant role in malate shuttle. In 4NB treated cells, it is found that the activity of malate was unaffected. However, we can estimate that the conversion of malate to oxaloacetate was reduced in 4NB treated cells due to decreased activity of complex II and elevated level of NADH.

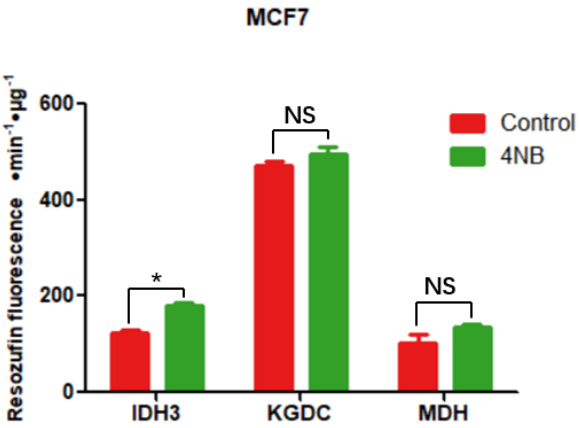

Figure 2.3.10 Activity of isocitrate dehydrogenase 3 (IDH3), α-ketoglutarate dehydrogenase complex (KGDC) and malate dehydrogenase (MDH) in MCF7 cells with and without 4NB treatment. Enzyme activities were measured by NAD^+-dependent enzymatic reactions and excitation wavelength at 550 nm and fluorescent emission of resorufin at 590 nm was measured by multi-well plate reader continuously. (Mean±SD, n=3)

The statistical analysis was carried out by using the t-student test. And when the p<0.001, significance was indicated by ***; when the significance was p<0.01, it was indicated by**; When the significance p<0.05, it was indicated by *; when there is no significant difference, it was indicated by NS.

2.4 Discussion

In a cancer cell, metabolic pathways are highly flexible to meet its bioenergetic, biosynthetic and redox requirements. In our study, deficient oxidative phosphorylation (OXPHOS) resulted from CoQ10 depletion by 4NB treatment have been demonstrated above. In addition, cancer cells with CoQ10 deficiency induced by 4NB exhibited fragmented mitochondria, elevated ROS, deregulated bioenergetics, as well as the hypoxic state. Many studies have demonstrated defective oxidative phosphorylation is very common metabolic hallmark of cancer cell and it has been implicated in

aerobic glycolysis. Because oxidative phosphorylation (OXPHOS) and glycolysis are predominant ATP producing pathways in cells, cancer cells compensate for ATP production from glycolysis when oxidative phosphorylation rate is decreased. Therefore, metabolic reprogramming occurs in cells with 4NB treatment in response to CoQ10 deficiency.

First of all, we found that 4NB treatment would have a profound impact on glycolysis. We found that glucose uptake enhanced in 4NB treated cells, as demonstrated by flow cytometric analysis with fluorescent glucose tracer (2-NBDG). Furthermore, we found that 4NB treatment increased glucose consumption regardless of lower GLUT2 gene expression. Moreover, we found 4NB treatment increased membrane exposure of glucose transporters, in particular, elevated expression of GLUT1 and GLUT3. Altogether, glycolysis was upregulated in cancer cells treated with 4NB.

Furthermore, we investigated the activity of pyruvate kinase (PK) which catalyzes vital important rate-limiting step of glycolysis. It has shown that the pyruvate kinase (PK) was activated since Km of pyruvate kinase (PK) for phosphoenolpyruvate (PEP) was decreased. It revealed that phosphoenolpyruvate (PEP) flux through pyruvate kinase (PK) might be increased. However, we found that lactate secretion rate in 4NB treated cells was slightly decreased regardless of unregulated glycolysis. Moreover, we measured the pyruvate dehydrogenase complex (PDC) activity in our study; its activity was unaffected by 4NB treatment. While pyruvate dehydrogenase complex (PDC) could be inactivated by numerous allosteric effectors such as AMP and NADH. We estimated that PDC kinetics was not favorable in 4NB treated cells due to elevated NADH level. We speculated that pyruvate flux might be redirected to other metabolic pathways. Importantly, pyruvate can also be converted alanine catalyzed by alanine transaminase (ALT) or aspartate transaminase (AST), concomitantly converts glutamate to α-ketoglutarate (α-KG) (As shown in **Figure 2.4.1)**. Notably, this proposed metabolic rearrangement also facilitates the loading of α-ketoglutarate (α-KG) into TCA intermediates pool from glutamine, particularly when glutamate dehydrogenase (GDH) is inactivated. Moreover, a recent study has proven that the conversion of pyruvate to alanine was upregulated in response to impairment of oxidative phosphorylation (OXPHOS)[151]. However, this metabolic reprogramming remains to be proven in this study.

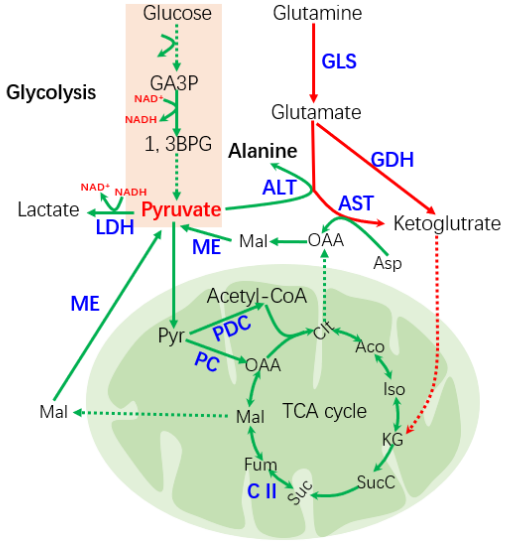

Figure 2.4.1 Schematic illustration of pyruvate metabolic fates in MCF7 cells.

GA3P, glyceraldehyde-3-phosphate; 1,3-BPG, 1,3-biphosphoglycerate; Pry, pyruvate; Cit, citrate; Aco, Aconitate; Iso, isocitrate; KG, ketoglutarate; SucC, succinyl-CoA; Suc, succinate; Fum,

fumarate; Mal, malate; OAA, oxaloacetate; Asp, aspartate; LDH, lactate dehydrogenase; ALT, alanine transaminase; PC, pyruvate carboxylase; PDC, pyruvate dehydrogenase complex; AST, aspartate transaminase; ME, malic enzyme;

Glutaminolysis begins with two-steps conversion to α-ketoglutarate (α-KG), typically through glutaminase (GLS) and glutamate dehydrogenase (GDH). We measured the activity of glutaminase (GLS) and glutamate dehydrogenase (GDH). Glutaminase (GLS) was increased in 4NB treated cells, indicating glutaminolysis might be deregulated by 4NB treatment. However, glutamine dehydrogenase (GDH) activity was unaffected by 4NB treatment. Considering that the elevated level NADH would inactivate glutamate dehydrogenase (GDH), conversion of glutamate to α-ketoglutarate (α-KG) would be more dependent on alanine transaminase (ALT) and aspartate transaminase (AST) in 4NB treated cancer cells (As shown in Figure 2.4.1).

Besides, α-ketoglutarate (α-KG) is at branchpoint of multiple metabolic pathways. Recently, Ramon C. Sun and his coworkers have reported that reduced α-ketoglutarate dehydrogenase complex (KGDH) activity by hypoxic regulation has shifted α-ketoglutarate (α-KG) metabolism from oxidation to reductive carboxylation[270]. Although the α-ketoglutarate dehydrogenase complex (KGDH) was unaffected by 4NB treatment, the downstream complex II (ubiquinone: succinate oxidoreductase) dehydrogenase was diminished. Besides, isocitrate dehydrogenase 1/2 (IDH1/2) which is responsible for carboxylation of α-ketoglutarate was significantly upregulated. As a result, we can infer that α-ketoglutarate (α-ketoglutarate) was possibly shifted from oxidation to reductive carboxylation, subsequently supply citrate for *de novo* lipogenesis.

As we found that CoQ10 deficiency induced by 4NB treatment resulted in elevated ROS, $NADP^+$ dependent dehydrogenases might be upregulated to counter excessive ROS production. We measured malic enzyme (ME) activity and isocitrate dehydrogenase (IDH1/2) which are primary NADPH generating enzymes. The results have shown that both malic enzyme (ME) and isocitrate dehydrogenase (IDH1/2) were upregulated in 4NB treated cells.

Chapter 3 Effect of antiproliferative agents on cancer cells with metabolic alterations

3.1 Materials and cell culture

3.1.1 Materials

a. Stock solution of 4-nitrobenzoic acid (4NB) 200mM. 4-nitrobenzoate was dissolved in PBS, adjust PH to 7.4 by using KOH. It was stored at -20 ºC before using.

b. RNAase, propidium iodide (PI, 50 μg/mL), ethanol

d. The stock solution of galactose was prepared at a concentration of 500 mM. It is sterilized by filtration, and aliquots were made and stored at -20 ºC. The stock solution of 2-deoxyglucose (2DG) was prepared at a concentration of 1M 2-deoxyglucose in DMEM.

e. Stock solution of 3-(4,5-dimethylthiazol-2-yl)-2,5-diphenyltetrazolium bromide (MTT) was prepared at a concentration of 15mM in PBS (7.4). It is sterilized by filtration, and aliquots were made and stored at -20 ºC.

f. TBH was stored at 4-8 ºC; it was dissolved in DMEM freshly.

g. The stock solution of doxorubicin was prepared at a concentration of 1.75 mM. Powder of doxorubicin was dissolved in DMSO and stored at 4-8 ºC. The stock solution of cisplatin was prepared at a concentration of 0.25 mM. Powder of cisplatin was dissolved in DMSO and stored at 4-8 ºC.

Instruments

a. Enspire multi-well plate reader (PerkinElmer, MA, USA)

b. Bio-Rad Se3 Cell sorter (Bio-Rad, CA, USA)

3.1.2 Cell culture

MCF7 breast cancer cells were cultured in Dulbecco's Modified Eagle Medium (DMEM, High glucose) supplemented with 10% fetal bovine serum (FBS), penicillin and 2 mM glutamine. HepG2 hepatic cancer cells were cultured in Dulbecco's Modified Eagle Medium (DMEM, Low glucose) supplemented with 10% fetal bovine serum (FBS), penicillin and 2 mM glutamine. Cell morphology was monitored by an optical microscope. If not specially mentioned, the cells were exposed in 4 mM 4-nitrobenzoate for more than 4 days to deplete Coenzyme Q10**.**

3.2 Methods

3.2.1 Inhibitory effect of 4NB on proliferation

Bright yellow MTT powder was dissolved in PBS buffer. 12 mM MTT stock solution was prepared and sterilized by filtration. The MTT was stored in -20 ºC freezer before using. A concentration of 300 μM working solution was made by diluting 40-folds in medium without FBS. Culture medium was removed and 200 μL working solution was added to each well to stain the cells and then cells were incubated for 2 h. The formazan product was dissolved in 150 μL DMSO, and all DMSO was recovered into a new 96-well microplate. 96-well microplate was read by Enspire Multimode Plate Reader (PerkinElmer), and the optical density (OD value) of was recorded each well at the wavelength of 570 nM.

$0.5\text{-}1\times10^4$ MCF7 cells or HepG2 cells with various treatments were plated in 96-well microplate for each well. The concentration of 0 mM, 2 mM, 4 mM, 6 mM, and 8 mM 4NB were prepared by diluting stock solution in the respective complete culture medium. And old culture medium was removed, and culture medium with various concentrations of 4NB was added to 96-well microplate. Cell viability was measured after 24 h, 48 h, 72 h, and 96 h respectively by MTT assay described as above.

3.2.2 Cell cycle analysis

Cells were harvested in the appropriate manner and they were washed by PBS. Cells were fixed in cold 70% ethanol. Ethanol was added dropwise to the pellet while vortexing. The vortexing should ensure the fixation of all cells and minimize clumping. Cells were placed at 4°C for 30 min, followed by 2 times washing in PBS. Cells suspension was spin at 850 g in a centrifuge and be careful to avoid cell loss when discarding the supernatant especially after spinning out of ethanol. Treat the cells with ribonuclease. Add 50 μl of a 100 μg/ml sock of RNase. The addition of RNase will ensure only DNA, not RNA, is stained. Afterward, 200 μl PI Propidium iodide (PI, from 50 μg/ml stock solution) was added. And then flow cytometry was carried by determining PI fluorescence emission at a wavelength of 605 nm. And the cell cycle was analyzed by fitting Gaussian curves.

3.2.3 Effect of glucose deprivation on cancer cells

$0.5\text{-}1\times10^4$ MCF7 cells or HepG2 cells with various treatments were plated in each well of 96-well

microplate. After 24 h incubation, the culture medium was replaced by fresh DMEM with and without 5.5 mM galactose. Viability was measured at 24 h, 48 h, and 72h after glucose deprivation by MTT assay. An MTT assay was carried out by using 10 mM hexokinase (HK) inhibitor 2-deoxyglucose (2-DG) as well. Viability was measured at 24 h, 48 h, and 72h after addition of 2-DG by MTT assay. 500 mM stock solution of galactose was prepared by dissolving galactose in deionized water and store at -20 ºC before use. In addition, 500 mM stock solution of 2-deoxy-D-glucose (2-DG) in FBS-free culture medium and it was stored at 4-8 ºC.

3.2.4 Effect of glutamine deprivation on cancer cell proliferation

$0.5\text{-}1\times10^4$ MCF7 cells or HepG2 cells with 4NB treatment and without 4NB treatment were plated in 96-well microplate for each well. After 24 h incubation, complete culture medium (10% FBS) was replaced by glutamine-free DMEM and 10% (v/v) of dialyzed FBS. Cell viability was measured after 24 h, 48 h, and 72 h respectively by MTT assay described as above.

3.2.5 ROS induction by glucose deprivation and glutamine deprivation

Glucose deprivation was performed by using 5.5 mM galactose and glutamine deprivation was performed by using glutamine-free culture medium and dialyzed FBS as described above. Culture medium with 5 μM H2DCFDA was used to stain cells after 48 h of glucose deprivation and glutamine deprivation. After 30 min incubation at 37 ºC, cells were washed three times using PBS buffer (pH 7.4). The fluorescence of H2DCFDA was measured by multi-well plate reader Enspire (Perkin Elmer, MA, USA). The excitation wavelength was 490 nm, and fluorescence emission was detected at a wavelength of 520 nm.

3.2.6 Effect of TBH on cancer cell proliferation

$0.5\text{-}1\times10^4$ MCF7 cells or HepG2 cells with 4NB treatment and without 4NB treatment were plated in 96-well microplate for each well. After 24 h incubation at 37 ºC, 5% CO_2, complete culture medium (10% FBS) was replaced culture medium with 100 μM tert-Butyl hydroperoxide (TBH). Cell viability was measured after 2 h, 4 h, and 8 h respectively by MTT assay described as above.

3.2.7 Effect of doxorubicin and cisplatin on cancer cell proliferation

$0.5\text{-}1\times10^5$ MCF7 cells or HepG2 cells with various treatments were plated in 96-well microplate for each well. Place 96-well microplate in a cell incubator for 24 h to allow cells to be stabilized. Cells were treated as described below. The stock solution of doxorubicin was prepared by dissolving the powder in DMSO and it is stored at 4-8 ºC. And working solutions were prepared freshly before use. 0 μM, 0.15 μM, 0.3 μM, 0.6 μM, 1.5 μM and 3 μM working solutions were prepared by diluting stocking solution in a complete culture medium, and DMSO was adjusted to the same concentration. Afterward, the culture medium in 96-well microplate was replaced by complete culture medium in the presence of varying concentrations of doxorubicin. Cells were exposed to doxorubicin for 72 h. After treatment, the survival rate was quantified by MTT assay as mentioned above. The stock solution of cisplatin was prepared by dissolving the powder in 0.9% NaCl and it is stored at 4-8 ºC. Working solutions were prepared freshly before use. 0 μM, 0.5 μM, 1 μM, 2 μM, 5 μM and 10 μM working solutions were prepared by diluting stocking solution in a complete culture medium, and DMSO was adjusted to the same concentration, every experiment was done for triplicates. Then the dose-survival rate curves were plotted, and IC50 was estimated by fitting the Hill equation.

3.2.8 Effect of trifluoromethyl benzyl-α-ketoglutarate (Tα-KG) cancer cell proliferation

$0.5\text{-}1\times10^5$ MCF7 cells or HepG2 cells with and without 4NB treatment were plated in 96-well microplate. Place 96-well microplate in a cell incubator for 24 h to allow cells to be stabilized. Cells

were treated as described below. A series of culture medium in the presence of various concentrations of trifluoromethyl benzyl-α-ketoglutarate (Tα-KG) were used to treat cells. And cell viabilities after 48 h treatment was measured by MTT as described above. Ethanol was adjusted to the same concentration, and every experiment was done for triplicates. Then the dose-survival rate curves were plotted, and IC50 was estimated by fitting the Hill equation.

3.2.9 Statistical analyses

All statistical analyses were performed using GraphPad Prism 5.0. Statistical significance was assessed using t-tests or ANOVA as indicated in figure legends. All error bars represent the standard deviation (SD) or standard error of the mean (SEM) as indicated in figure legends. And when the $p<0.001$, statistical significance was indicated by ***; When the significance was $p<0.01$, it was indicated by**; When $p<0.05$, it was indicated by *; When $p > 0.05$, it was indicated by NS.

3.3 Results

3.3.1 The antiproliferative effect of 4NB

Notably, 4NB treatment suppressed cancer cell proliferation in a concentration-dependent manner. Besides, MCF7 cancer cells in the presence of 4 mM 4-nitrobenzoate (4NB) were less proliferative and at relatively quiescent state, implying 4NB treated cells have switched to relatively slower cell division and anabolism due to relatively reduced energy generation.

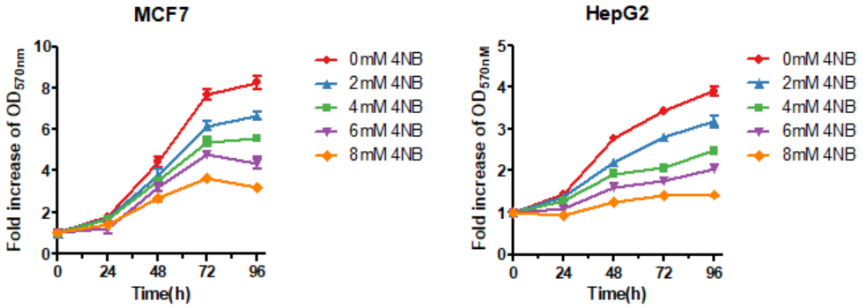

Figure 3.3.1 The inhibitory effect of 4NB on cancer cell proliferation. Various concentrations of 4NB were used to treat MCF7 cancer cells and HepG2 cancer cells. Cell viability was measured by MTT assay at indicated time points. (Mean±SD, n=3)

3.3.2 Cell cycle analysis

Furthermore, cell cycle has been demonstrated in MCF7 cells, 4NB treatment suppressed S-phase entry of in MCF7 cells, with only 30% cells in S phase after five days of culture in the presence of 4 mM 4 nitrobenzoate (4NB). The transition of quiescent G0-G1 stage to a dividing S stage suggested cells were partly arrested. In MCF7, we observed that approximately 48% of cells from G1 entered S phase after 4 days incubation without 4NB. Therefore, cell cycle progression was delayed in 4NB treated cells.

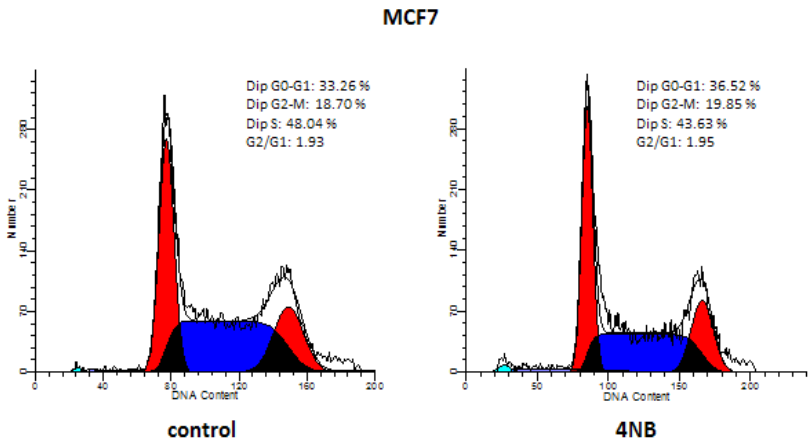

Figure 3.3.2 Cell cycle analysis by flow cytometry. Cellular DNA content of MCF7 cells and 4NB treated MCF cells were analyzed by propidium iodide staining (40 mg/mL). PI fluorescence was subject to flow cytometric analysis at an emission wavelength of 605 nm so that it can be measured by FL2. Distribution of G0/G1 (red), G2/M (red) and S phases (blue) were analyzed by the algorithm to fit Gaussian curves. A histogram reprensented the cell cycle, DNA content is on X-axis and the cell number is on the Y-axis.

3.3.3 Effect of glucose deprivation on cancer cell proliferation

Cancer cells with defective OXPHOS are usually more sensitive to glycolytic inhibition due to more bioenergetic dependency on glycolysis and metabolic rigidity. In our study, we studied cancer cell survival to the energetic depletion by inhibiting glucose utilization. As one crucial source of cellular energy metabolism, cells would be subjected to energy shortage when they are deprived of glucose. We noted that the cells with compromised OXPHOS were relatively more sensitive to glucose deprivation by using galactose.

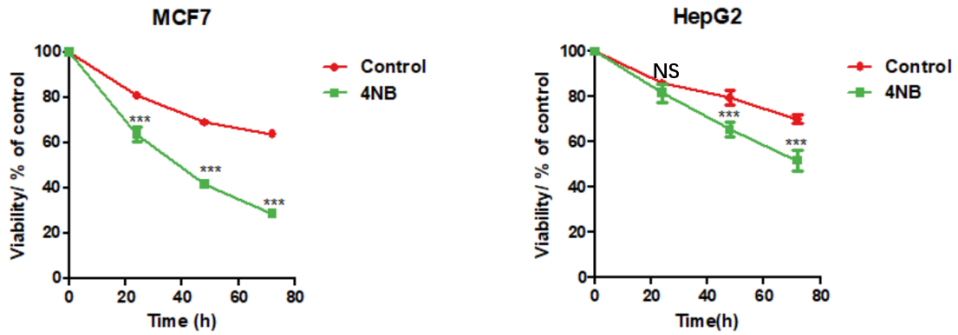

Figure 3.3.4 Effect of galactose on the viability of MCF7 cells and HepG2 cells with 4NB treatment and without 4NB treatment. Galactose (5.5 mM) were used to replace glucose in high glucose DMEM and low glucose DMEM respectively. Cell viability was measured by MTT at 24 h, 48 h, and 72 h after glucose deprivation (Mean±SD, n=3)

The statistical comparison was carried out by ANOVA analysis. And when the $p<0.001$, significance was indicated by ***; when the significance was $p<0.01$, it was indicated by**; When the significance $p<0.05$, it was indicated by *;

To ensure the strict validity of this finding, we took another measure to confirm the susceptibility to glycolytic inhibition by using 10 mM 2-deoxy-D-glucose(2-DG). However, 2-deoxy-D-glucose (2-DG) which is reportedly a glucose analog used to inhibit hexokinase (HK) did not agree with that of glucose deprivation by galactose. Cancer cells with reduced OXPHOS were more resistant to 2-

DG treatment.

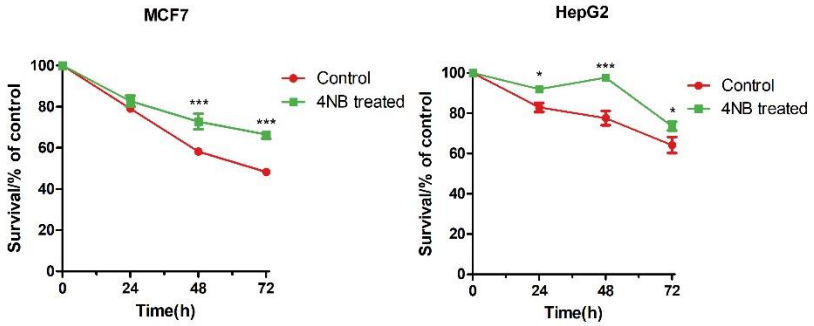

Figure 3.3.3 Effect of 2-deoxyglucose (10 mM) on the viability of MCF7 cells and HepG2 cells with 4NB treatment and without 4NB treatment. 2-deoxyglucose (10 mM) was used to inhibit hexokinase (HK) in both MCF7 cells and HepG2 cells. Cell viabilities were measured by MTT at 24 h, 48 h, and 72 h after glucose deprivation. (Mean±SD, n=3)

The statistical comparison was carried out by ANOVA analysis. And when the $p<0.001$, significance was indicated by ***; when the significance was $p<0.01$, it was indicated by**; When the significance $p<0.05$, it was indicated by *; when there is no significant difference, it was indicated by NS.

3.3.4 Effect of glutamine deprivation on cancer cell proliferation

Targeting glutamine mentalism has been widely regarded as an anti-cancer strategy due to cancer cells addict to glutamine for growth. Therefore, many glutamine metabolism inhibitors are under development. In our study, glutamine-free DMEM and dialyzed FBS were used to culture the cells. In response to glutamine deprivation, the survival rate of 4NB treated cells is enhanced in comparison to that of the control. Additionally, the enzymatic assay has shown glutaminase (GLS) was downregulated in 4NB treated cells. Although some studies have shown that glutamine oxidation was increased[20]. And reductive pathway of glutamine metabolism was presumably promoted by HIF-1α when mitochondrial metabolism was impaired[16, 21, 22].

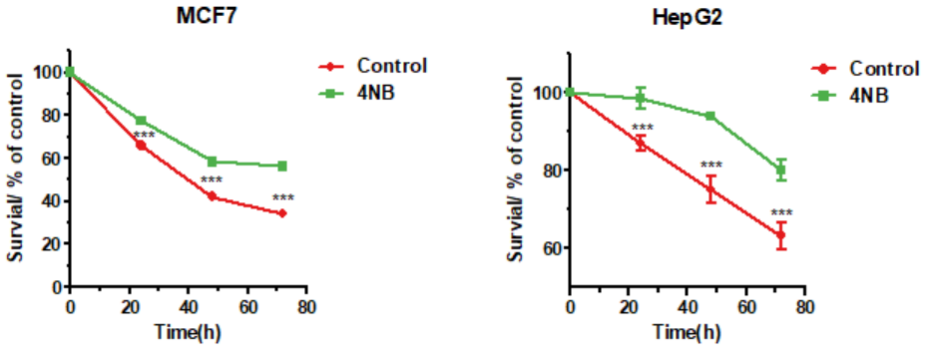

Figure 3.3.5 Effect of glutamine deprivation on the viability of MCF7 cells and HepG2 cells with 4NB treatment and without 4NB treatment. Glutamine-free DMEM and dialyzed FBS were used to culture MCF7 cells and HepG2 cells. Cell viabilities were measured by MTT at 24 h, 48 h, and 72 h after glutamine deprivation. The statistical comparison was carried out by t-student analysis. And when the $p<0.001$, significance was indicated by ***; when the significance was $p<0.01$, it was indicated by**; When the significance $p<0.05$, it was indicated by *; (Mean±SD, n=3)

3.2.5 ROS induction by glucose deprivation and glutamine deprivation

We assessed the ROS induction by glucose deprivation and glutamine deprivation. We found that

both glucose deprivation and glutamine deprivation can induce ROS production in MCF7 cells. When cells were deprived of glucose, ROS in control and 4NB treated cells increased by approximately 1.3 folds and 1.9 folds respectively. It suggested that ROS production in response to glucose deprivation may contribute to cell death. And, cells with 4NB treatment. Moreover, when cells were deprived of glutamine, ROS in control and 4NB treated cell increased approximately 3.3-folds and 1.5 folds respectively. The differential ROS production in control and 4NB treated might be associated with the different contribution of glucose to NADPH production in cancer cells with or without 4NB treatment.

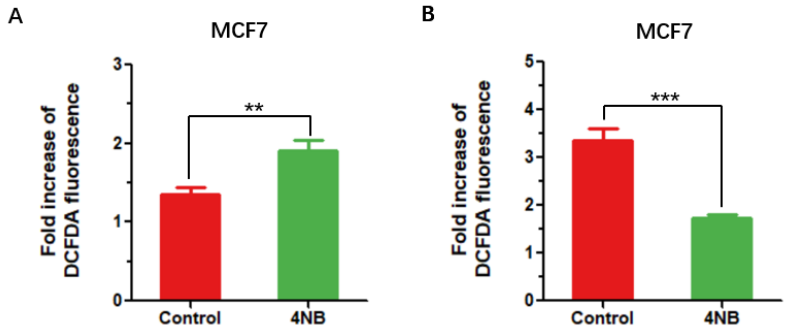

Figure 3.3.6 The ROS induction by glucose deprivation and glutamine deprivation was assessed by 5 µM H2DCFDA. (A) The fold increase of ROS induction by glucose deprivation. (B) The fold increase of ROS induction by glutamine deprivation. (Mean±SD, n=3)

The statistical comparison was carried out by t-student analysis. And when the $p<0.001$, significance was indicated by ***; when the significance was $p<0.01$, it was indicated by**; When the significance $p<0.05$, it was indicated by *; when there is no significant difference, it was indicated by NS.

3.3.6 Effect of TBH on cancer cell proliferation

A potent oxidant tertbutyl hydroperoxide was used to evaluate the cancer cell survival to free radicals. Both MCF7 cells and HepG2 cancer cells died off in the presence of 100 µM tertbutyl hydroperoxide due to the excessive ROS induction. By contrast to the control, the survival rates at indicated time points were reduced considerably in 4NB treated cells. The results suggested that 4NB treatment sensitized cancer cells to oxidative stress induced by TBH. The results were consistent with the data aforementioned because of enhanced oxidative stress due to CoQ10 depletion in 4NB treated cells.

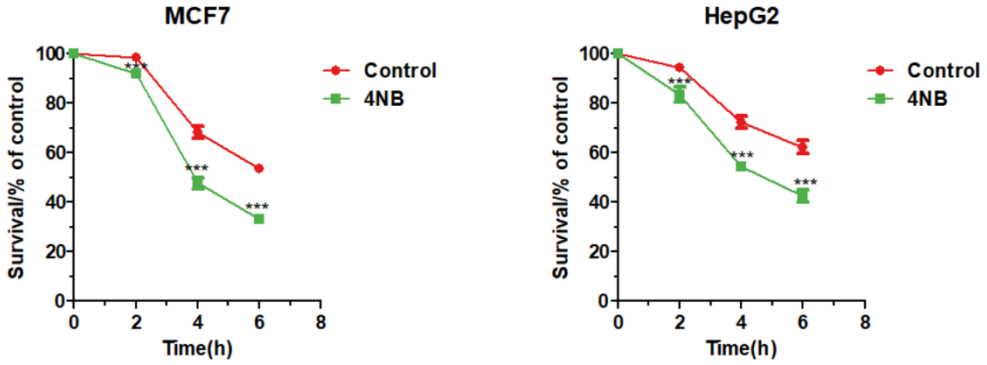

Figure 3.3.7 Effect of TBH (100µM) on the viability of MCF7 and HepG2 cell with 4NB treatment and without 4NB treatment. (Mean±SD, n=3)

The statistical comparison was carried out by t-student analysis. And when the $p<0.001$, significance

was indicated by ***; when the significance was p<0.01, it was indicated by**; When the significance p<0.05, it was indicated by *; when there is no significant difference, it was indicated by NS.

3.3.7 The effect of cisplatin and doxorubicin on cancer proliferation

Cell cycle non-specific antineoplastic agent doxorubicin and cisplatin were used to inhibit the proliferation of MCF7 cells and HepG2 cells. The results have shown that cells without 4NB treatment were more sensitive to doxorubicin in comparison to cells with 4NB treatment. On MCF7 cells, the IC50 of doxorubicin to cells without 4NB treatment and 4NB treated cells were 0.196 μM and 1. 275 μM respectively. On HepG2 cells, the IC50 of doxorubicin to the control and 4NB treated cell was 1.112 μM and 4.128 μM respectively. It indicated that 4NB treated cell was more resistant to doxorubicin. While a crosslink agent cisplatin was also used to test the resistance of the cancer cells. As shown in results, cells with 4NB treatment were more responsive to cisplatin.

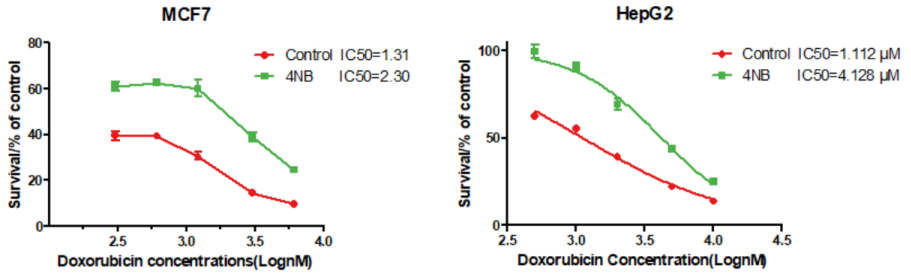

Figure 3.3.8 Dose-response relationship of cytotoxic agent doxorubicin on the viability of MCF7 cells and HepG2 cells with 4NB treatment and without 4NB treatment. V MCF7 and HepG2 cells were exposed to various concentrations of doxorubicin as indicated. Cell viabilities were measured by MTT after 72 h exposure to doxorubicin. (Mean±SD, n=3)

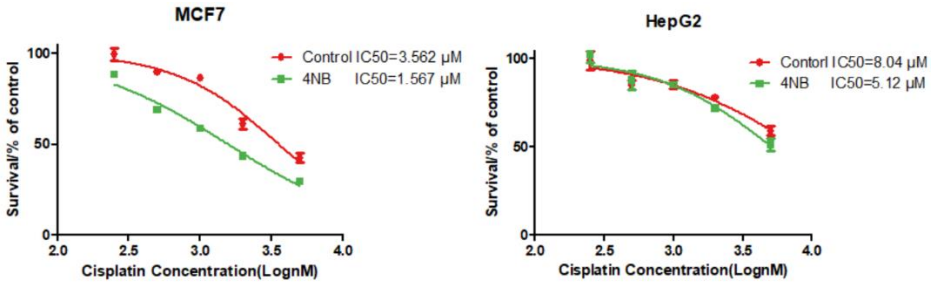

Figure 3.3.9 Effect of cisplatin on the viability of MCF7 and HepG2 cell with 4NB treatment and without 4NB treatment. MCF7 and HepG2 cells were exposed to various concentrations of cisplatin as indicated. Cell viabilities were measured by MTT after 48 h exposure to cisplatin. And IC50 was obtained by fitting Hill equation. (Mean±SD, n=3)

3.3.8 Effect of trifluoromethyl benzyl-α-ketoglutarate (Tα-KG) on cancer proliferation

The results obtained with the fluorescent Iridium derivatives suggested that 4NB treated cells were under hypoxic conditions (see section 1.3.7). Moreover, it is well documented that α-ketoglutarate can increase the degradation of HIF-1α by reactivating prolyl domain hydrogenases (PDHs). In our study, we evaluated the effect of cell-permeable α-ketoglutarate (TαKG) cancer cells treated and untreated with 4NB. We found that TαKG was harmful to both cell lines tested. In fact, the IC50 for TαKG was decreased in both cell lines (Fig.3.3.9). However, cancer cells treated with 4NB were more sensitive to TαKG, indicating 4NB treated cells were more dependent on hypoxia-inducible

factor 1α (HIF-1α).

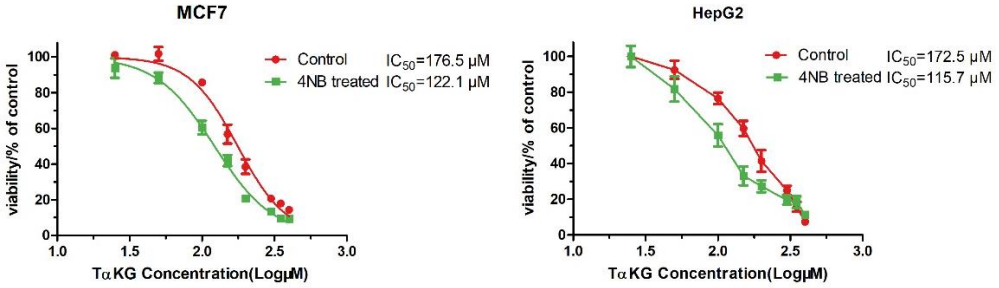

Figure 3.3.10 The Effect of TαKG on the viability of MCF7 and HepG2 cells with and without 4NB treatment. The viability of MCF7 and HepG2 cells were measured by MTT assay in the presence of various concentrations of TαKG as indicated. The IC50 was estimated by fitting Hill-equation($R^2 > 0.99$). (Mean±SD, n=3).

3.4 Discussion

Depletion of bioenergetics, through either inhibition of oxidative phosphorylation (OXPHOS) or inhibition of glycolysis, has been proposed as an anti-cancer strategy since cancer cells mostly have higher energetic demand than normal cells. However, it is challenging to strongly inhibit cancer growth since cancer cells display variable oxidative phosphorylation, concomitantly with variable glycolysis. By that, cancer cells can counter energetic stress since cancer cells can switch to glycolysis for energy production and decelerated anabolic pathways. This metabolic flexibility confers cancer cells survival from inhibition of oxidative phosphorylation (OXPHOS) or inhibition of glycolysis. Considering that cancer cells can survive from transient and mild energetic stress. Notably, 4-nitrobenzoate (4NB) inhibits cancer cell growth in a dose-dependent manner, and it delayed cell cycle progression. However, this might not be a good anti-cancer strategy since no evidence has shown that cancer cells overly dependent on CoQ10. Despite that, those results have demonstrated that inhibition of oxidative phosphorylation (OXPHOS) induced by CoQ10 depletion can inhibit cancer growth to some extent.

Inhibition of glycolysis has been proposed to be a potential anti-cancer strategy. Particularly in tumors with aerobic glycolysis (Warburg effect), cancer cells overly depend on glycolysis for energy production and biosynthetic intermediates. Small molecule inhibitors such as 2-deoxyglucose (2-DG), 3-bromopyruvate (3-BP)[96], pentavalent arsenic compounds have been reported to inhibit glycolysis and repress cancer proliferation. In our study, the hexokinase (HK) inhibitor 2-DG was used to inhibit glycolysis. However, cancer cells with compromised OXPHOS were less susceptible to 2-DG treatment.

Although galactose is a pyranose could be converted to glucose-6-phosphate (G6P) through three steps conversion and subsequently undertake glycolysis, it is commonly used to inhibit glucose utilization by replacing glucose in vitro cell culture due to its slow conversion[271, 272]. Cancer cells with impaired respiratory chain were more sensitive to this glycolytic inhibition, indicating inhibition of OXPHOS rate sensitizes cancer cells to glycolytic inhibition.

Recently, many studies have suggested that targeting glutaminolysis appears to be a potential anti-cancer strategy. However, the results have revealed that 4NB treated cell is more resistant to glutamine deprivation as opposed to the control.

Glucose deprivation and glutamine deprivation have been usually implicated in bioenergetic depletion and biosynthesis inhibition since both glucose and glutamine participate in energy

metabolism and biomass biosynthesis. We investigated how glucose deprivation and glutamine deprivation affect ROS production. The results have that both glucose deprivation and glutamine deprivation give rise to ROS production. Notably, cancer cells have different responses glucose deprivation, and glutamine deprivation might be partly due to different ROS induction.

Mitochondrial respiratory chain is the primary site of ROS production. Many studies have shown that interference of complex I, complex III as well as CoQ10 can alter ROS production. In our study, we have found that CoQ10 depletion can induce oxidative stress. Based on that, we investigated the effect of potent prooxidant tertbutyl hydroperoxide (TBH) on cell death. We observed that CoQ10 depletion sensitized cancer cells to prooxidant tertbutyl hydroperoxide (TBH) due to increased oxidative stress.

We noted that both MCF7 cells and HepG2 cells treated with 4NB were more resistant to doxorubicin. Resistance to chemotherapy could be associated with hypoxia and glycolysis addiction. Many studies have shown that hypoxia confers chemotherapy resistance. Moreover, increased glycolysis also elicits therapeutic resistance. Apart from that, the inhibition of the intrinsic apoptotic pathway was speculated to account for the resistance as mitochondrial abnormalities existed when CoQ10 was depleted. Many studies have shown dysfunctional mitochondria leads to resistance, while the reasons remain unclear. Deregulation of the intrinsic apoptosis pathway of dysfunctional mitochondria is likely to account for this resistance. The underlying mechanisms need to be elucidated by investigation of BCL2 anti-apoptotic proteins.

Intriguingly, targeting to HIFs as an anti-cancer strategy is also under development. In our study, an activator of prolyl domain hydrogenases (PDHs) was used to promote the degradation of HIF-1α. And it was found cells with overexpressed HIF-1α were more sensitive to TαKG. It suggested that inhibition of HIF-1α could be an effective anti-cancer strategy. Many studies have shown that HIF-1α can upregulate expression of LDH and downregulate expression of PDH though PDK, leading to switching from mitochondrial respiration to glycolysis.

References

[1] Chan, T. S., Teng, S., Wilson, J. X., Galati, G., Khan, S., O'Brien, P. J., 2002. Coenzyme Q cytoprotective mechanisms for mitochondrial complex I cytopathies involves NAD(P)H: quinone oxidoreductase 1(NQO1). Free radical research. 36(4):421-427.

[2] Ross, D., Siegel, D., 2017. Functions of NQO1 in Cellular Protection and CoQ(10) Metabolism and its Potential Role as a Redox Sensitive Molecular Switch. Front Physiol. 8:595.

[3] Littarru, G. P., Tiano, L., 2007. Bioenergetic and antioxidant properties of coenzyme Q10: recent developments. Molecular biotechnology. 37(1):31-37.

[4] Littlefield, N., Beckstrand, R. L., Luthy, K. E., 2014. Statins' effect on plasma levels of Coenzyme Q10 and improvement in myopathy with supplementation. Journal of the American Association of Nurse Practitioners. 26(2):85-90.

[5] Apostolopoulou, M., Corsini, A., Roden, M., 2015. The role of mitochondria in statin-induced myopathy. European journal of clinical investigation. 45(7):745-754.

[6] Taylor, B. A., Lorson, L., White, C. M., Thompson, P. D., 2015. A randomized trial of coenzyme Q10 in patients with confirmed statin myopathy. Atherosclerosis. 238(2):329-335.

[7] Vrablik, M., Zlatohlavek, L., Stulc, T., Adamkova, V., Prusikova, M., Schwarzova, L., et al., 2014. Statin-associated myopathy: from genetic predisposition to clinical management. Physiological research. 63 Suppl 3:S327-334.

[8] Ayer, A., Macdonald, P., Stocker, R., 2015. CoQ(1)(0) Function and Role in Heart Failure and

Ischemic Heart Disease. Annual review of nutrition. 35:175-213.
[9] Zahedi, H., Eghtesadi, S., Seifirad, S., Rezaee, N., Shidfar, F., Heydari, I., et al., 2014. Effects of CoQ10 Supplementation on Lipid Profiles and Glycemic Control in Patients with Type 2 Diabetes: a randomized, double blind, placebo-controlled trial. Journal of diabetes and metabolic disorders. 13:81.
[10] Suksomboon, N., Poolsup, N., Juanak, N., 2015. Effects of coenzyme Q10 supplementation on metabolic profile in diabetes: a systematic review and meta-analysis. Journal of clinical pharmacy and therapeutics. 40(4):413-418.
[11] Amin, M. M., Asaad, G. F., Abdel Salam, R. M., El-Abhar, H. S., Arbid, M. S., 2014. Novel CoQ10 antidiabetic mechanisms underlie its positive effect: modulation of insulin and adiponectine receptors, Tyrosine kinase, PI3K, glucose transporters, sRAGE and visfatin in insulin resistant/diabetic rats. PloS one. 9(2):e89169.
[12] Yamagishi, K., Ikeda, A., Moriyama, Y., Chei, C. L., Noda, H., Umesawa, M., et al., 2014. Serum coenzyme Q10 and risk of disabling dementia: the Circulatory Risk in Communities Study (CIRCS). Atherosclerosis. 237(2):400-403.
[13] Yang, X., Zhang, Y., Xu, H., Luo, X., Yu, J., Liu, J., et al., 2016. Neuroprotection of Coenzyme Q10 in Neurodegenerative Diseases. Current topics in medicinal chemistry. 16(8):858-866.
[14] Ajith, T. A., Padmajanair, G., 2015. Mitochondrial Pharmaceutics: A New Therapeutic Strategy to Ameliorate Oxidative Stress in Alzheimer's Disease. Current aging science. 8(3):235-240.
[15] Li, Z., Wang, P., Yu, Z., Cong, Y., Sun, H., Zhang, J., et al., 2015. The effect of creatine and coenzyme q10 combination therapy on mild cognitive impairment in Parkinson's disease. European neurology. 73(3-4):205-211.
[16] Hickey, M. A., Zhu, C., Medvedeva, V., Franich, N. R., Levine, M. S., Chesselet, M. F., 2012. Evidence for behavioral benefits of early dietary supplementation with CoEnzymeQ10 in a slowly progressing mouse model of Huntington's disease. Molecular and cellular neurosciences. 49(2):149-157.
[17] Siemieniuk, E., Skrzydlewska, E., 2005. [Coenzyme Q10: its biosynthesis and biological significance in animal organisms and in humans]. Postepy higieny i medycyny doswiadczalnej (Online). 59:150-159.
[18] Tran, U. C., Clarke, C. F., 2007. Endogenous Synthesis of Coenzyme Q in Eukaryotes. Mitochondrion. 7(Suppl):S62-S71.
[19] Quinzii, C. M., Lopez, L. C., Von-Moltke, J., Naini, A., Krishna, S., Schuelke, M., et al., 2008. Respiratory chain dysfunction and oxidative stress correlate with severity of primary CoQ10 deficiency. FASEB journal : official publication of the Federation of American Societies for Experimental Biology. 22(6):1874-1885.
[20] Quinzii, C. M., Hirano, M., 2011. Primary and secondary CoQ(10) deficiencies in humans. BioFactors (Oxford, England). 37(5):361-365.
[21] Quinzii, C. M., Tadesse, S., Naini, A., Hirano, M., 2012. Effects of inhibiting CoQ10 biosynthesis with 4-nitrobenzoate in human fibroblasts. PloS one. 7(2):e30606.
[22] Pierrel, F., 2017. Impact of Chemical Analogs of 4-Hydroxybenzoic Acid on Coenzyme Q Biosynthesis: From Inhibition to Bypass of Coenzyme Q Deficiency. Front Physiol. 8:7.
[23] Bergamini, C., Moruzzi, N., Sblendido, A., Lenaz, G., Fato, R., 2012. A Water Soluble CoQ(10) Formulation Improves Intracellular Distribution and Promotes Mitochondrial Respiration in Cultured Cells. PloS one. 7(3):e33712.

[24] Banach, M., Serban, C., Ursoniu, S., Rysz, J., Muntner, P., Toth, P. P., et al., 2015. Statin therapy and plasma coenzyme Q10 concentrations--A systematic review and meta-analysis of placebo-controlled trials. Pharmacological research. 99:329-336.
[25] Duberley, K. E., Heales, S. J., Abramov, A. Y., Chalasani, A., Land, J. M., Rahman, S., et al., 2014. Effect of Coenzyme Q10 supplementation on mitochondrial electron transport chain activity and mitochondrial oxidative stress in Coenzyme Q10 deficient human neuronal cells. Int J Biochem Cell Biol. 50:60-63.
[26] Fragaki, K., Chaussenot, A., Benoist, J. F., Ait-El-Mkadem, S., Bannwarth, S., Rouzier, C., et al., 2016. Coenzyme Q10 defects may be associated with a deficiency of Q10-independent mitochondrial respiratory chain complexes. Biological research. 49:4.
[27] Kikusato, M., Nakamura, K., Mikami, Y., Mujahid, A., Toyomizu, M., 2016. The suppressive effect of dietary coenzyme Q10 on mitochondrial reactive oxygen species production and oxidative stress in chickens exposed to heat stress. Animal science journal = Nihon chikusan Gakkaiho. 87(10):1244-1251.
[28] Bhagavan, H. N., Chopra, R. K., 2006. Coenzyme Q10: absorption, tissue uptake, metabolism and pharmacokinetics. Free radical research. 40(5):445-453.
[29] Shackelford, D. B., 2013. Unravelling the connection between metabolism and tumorigenesis through studies of the liver kinase B1 tumour suppressor. Journal of Carcinogenesis. 12:16.
[30] DeBerardinis, R. J., Chandel, N. S., 2016. Fundamentals of cancer metabolism. Sci Adv. 2(5):e1600200.
[31] Pavlova, Natalya N., Thompson, Craig B., 2016. The Emerging Hallmarks of Cancer Metabolism. Cell Metabolism. 23(1):27-47.
[32] Vander Heiden, M. G., 2011. Targeting cancer metabolism: a therapeutic window opens. Nature reviews Drug discovery. 10(9):671-684.
[33] Antoniewicz, M. R., 2018. A guide to 13C metabolic flux analysis for the cancer biologist. Experimental & Molecular Medicine. 50(4):19.
[34] Jiang, L., Boufersaoui, A., Yang, C., Ko, B., Rakheja, D., Guevara, G., et al., 2017. Quantitative metabolic flux analysis reveals an unconventional pathway of fatty acid synthesis in cancer cells deficient for the mitochondrial citrate transport protein. Metabolic engineering. 43(Pt B):198-207.
[35] Wuest, M., Hamann, I., Bouvet, V., Glubrecht, D., Marshall, A., Trayner, B., et al., 2018. Molecular Imaging of GLUT1 and GLUT5 in Breast Cancer: A Multitracer Positron Emission Tomography Imaging Study in Mice. Molecular pharmacology. 93(2):79-89.
[36] Zamora-Leon, S. P., Golde, D. W., Concha, II, Rivas, C. I., Delgado-Lopez, F., Baselga, J., et al., 1996. Expression of the fructose transporter GLUT5 in human breast cancer. Proc Natl Acad Sci U S A. 93(5):1847-1852.
[37] Karim, S., Adams, D. H., Lalor, P. F., 2012. Hepatic expression and cellular distribution of the glucose transporter family. World Journal of Gastroenterology : WJG. 18(46):6771-6781.
[38] Barron, C. C., Bilan, P. J., Tsakiridis, T., Tsiani, E., 2016. Facilitative glucose transporters: Implications for cancer detection, prognosis and treatment. Metabolism: clinical and experimental. 65(2):124-139.
[39] Yamamoto, N., Ueda, M., Sato, T., Kawasaki, K., Sawada, K., Kawabata, K., et al., 2011. Measurement of glucose uptake in cultured cells. Current protocols in pharmacology. Chapter 12:Unit 12.14.11-22.
[40] Zhou, X. J., Fadda, G. Z., Perna, A. F., Massry, S. G., 1991. Phosphate depletion impairs insulin

secretion by pancreatic islets. Kidney international. 39(1):120-128.
[41] Zou, C., Wang, Y., Shen, Z., 2005. 2-NBDG as a fluorescent indicator for direct glucose uptake measurement. Journal of Biochemical and Biophysical Methods. 64(3):207-215.
[42] Liberti, M. V., Locasale, J. W., 2016. The Warburg Effect: How Does it Benefit Cancer Cells? Trends in Biochemical Sciences. 41(3):211-218.
[43] Patra, K. C., Wang, Q., Bhaskar, P. T., Miller, L., Wang, Z., Wheaton, W., et al., 2013. Hexokinase 2 is required for tumor initiation and maintenance and its systemic deletion is therapeutic in mouse models of cancer. Cancer cell. 24(2):213-228.
[44] Pastorino, J. G., Shulga, N., Hoek, J. B., 2002. Mitochondrial binding of hexokinase II inhibits Bax-induced cytochrome c release and apoptosis. The Journal of biological chemistry. 277(9):7610-7618.
[45] Houddane, A., Bultot, L., Novellasdemunt, L., Johanns, M., Gueuning, M.-A., Vertommen, D., et al., 2017. Role of Akt/PKB and PFKFB isoenzymes in the control of glycolysis, cell proliferation and protein synthesis in mitogen-stimulated thymocytes. Cellular Signalling. 34:23-37.
[46] Marsin, A. S., Bertrand, L., Rider, M. H., Deprez, J., Beauloye, C., Vincent, M. F., et al., 2000. Phosphorylation and activation of heart PFK-2 by AMPK has a role in the stimulation of glycolysis during ischaemia. Current biology : CB. 10(20):1247-1255.
[47] Ji, S., Zhang, B., Liu, J., Qin, Y., Liang, C., Shi, S., et al., 2016. ALDOA functions as an oncogene in the highly metastatic pancreatic cancer. Cancer Lett. 374(1):127-135.
[48] Chang, Y. C., Chan, Y. C., Chang, W. M., Lin, Y. F., Yang, C. J., Su, C. Y., et al., 2017. Feedback regulation of ALDOA activates the HIF-1alpha/MMP9 axis to promote lung cancer progression. Cancer Lett. 403:28-36.
[49] Huang, Z., Hua, Y., Tian, Y., Qin, C., Qian, J., Bao, M., et al., 2018. High expression of fructose-bisphosphate aldolase A induces progression of renal cell carcinoma. Oncology reports. 39(6):2996-3006.
[50] Chang, L., Ni, J., Beretov, J., Wasinger, V. C., Hao, J., Bucci, J., et al., 2017. Identification of protein biomarkers and signaling pathways associated with prostate cancer radioresistance using label-free LC-MS/MS proteomic approach. Scientific reports. 7:41834.
[51] Long, F., Cai, X., Luo, W., Chen, L., Li, K., 2014. Role of aldolase A in osteosarcoma progression and metastasis: in vitro and in vivo evidence. Oncology reports. 32(5):2031-2037.
[52] Kusakabe, T., Motoki, K., Hori, K., 1997. Mode of interactions of human aldolase isozymes with cytoskeletons. Arch Biochem Biophys. 344(1):184-193.
[53] Kawai, K., Uemura, M., Munakata, K., Takahashi, H., Haraguchi, N., Nishimura, J., et al., 2017. Fructose-bisphosphate aldolase A is a key regulator of hypoxic adaptation in colorectal cancer cells and involved in treatment resistance and poor prognosis. International journal of oncology. 50(2):525-534.
[54] Schindler, R., Weichselsdorfer, E., Wagner, O., Bereiter-Hahn, J., 2001. Aldolase-localization in cultured cells: cell-type and substrate-specific regulation of cytoskeletal associations. Biochemistry and cell biology = Biochimie et biologie cellulaire. 79(6):719-728.
[55] Meira, D. D., Marinho-Carvalho, M. M., Teixeira, C. A., Veiga, V. F., Da Poian, A. T., Holandino, C., et al., 2005. Clotrimazole decreases human breast cancer cells viability through alterations in cytoskeleton-associated glycolytic enzymes. Molecular Genetics and Metabolism. 84(4):354-362.
[56] Morita, M., Sato, T., Nomura, M., Sakamoto, Y., Inoue, Y., Tanaka, R., et al., 2018. PKM1 Confers Metabolic Advantages and Promotes Cell-Autonomous Tumor Cell Growth. Cancer Cell.

33(3):355-367.e357.
[57] Lunt, Sophia Y., Muralidhar, V., Hosios, Aaron M., Israelsen, William J., Gui, Dan Y., Newhouse, L., et al., 2015. Pyruvate Kinase Isoform Expression Alters Nucleotide Synthesis to Impact Cell Proliferation. Molecular Cell. 57(1):95-107.
[58] Allen, A. E., Locasale, J. W., 2018. Glucose Metabolism in Cancer: The Saga of Pyruvate Kinase Continues. Cancer Cell. 33(3):337-339.
[59] Cortes-Cros, M., Hemmerlin, C., Ferretti, S., Zhang, J., Gounarides, J. S., Yin, H., et al., 2013. M2 isoform of pyruvate kinase is dispensable for tumor maintenance and growth. Proc Natl Acad Sci U S A. 110(2):489-494.
[60] Dayton, T. L., Gocheva, V., Miller, K. M., Israelsen, W. J., Bhutkar, A., Clish, C. B., et al., 2016. Germline loss of PKM2 promotes metabolic distress and hepatocellular carcinoma. Genes & development. 30(9):1020-1033.
[61] Lau, A. N., Israelsen, W. J., Roper, J., Sinnamon, M. J., Georgeon, L., Dayton, T. L., et al., 2017. PKM2 is not required for colon cancer initiated by APC loss. Cancer & Metabolism. 5(1):10.
[62] Li, X., Deng, S., Liu, M., Jin, Y., Zhu, S., Deng, S., et al., 2018. The responsively decreased PKM2 facilitates the survival of pancreatic cancer cells in hypoglucose. Cell Death & Disease. 9(2):133.
[63] Israelsen, W. J., Dayton, T. L., Davidson, S. M., Fiske, B. P., Hosios, A. M., Bellinger, G., et al., 2013. PKM2 isoform-specific deletion reveals a differential requirement for pyruvate kinase in tumor cells. Cell. 155(2):397-409.
[64] Anastasiou, D., Yu, Y., Israelsen, W. J., Jiang, J.-K., Boxer, M. B., Hong, B. S., et al., 2012. Pyruvate kinase M2 activators promote tetramer formation and suppress tumorigenesis. Nature Chemical Biology. 8:839.
[65] Hitosugi, T., Kang, S., Vander Heiden, M. G., Chung, T. W., Elf, S., Lythgoe, K., et al., 2009. Tyrosine phosphorylation inhibits PKM2 to promote the Warburg effect and tumor growth. Sci Signal. 2(97):ra73.
[66] Chaiyawat, P., Chokchaichamnankit, D., Lirdprapamongkol, K., Srisomsap, C., Svasti, J., Champattanachai, V., 2015. Alteration of O-GlcNAcylation affects serine phosphorylation and regulates gene expression and activity of pyruvate kinase M2 in colorectal cancer cells. Oncology reports. 34(4):1933-1942.
[67] Wang, Y., Liu, J., Jin, X., Zhang, D., Li, D., Hao, F., et al., 2017. O-GlcNAcylation destabilizes the active tetrameric PKM2 to promote the Warburg effect. Proceedings of the National Academy of Sciences. 114(52):13732-13737.
[68] Yang, W., Xia, Y., Hawke, D., Li, X., Liang, J., Xing, D., et al., 2012. PKM2 Phosphorylates Histone H3 and Promotes Gene Transcription and Tumorigenesis. Cell. 150(4):685-696.
[69] Tennant, Daniel A., 2011. PK-M2 Makes Cells Sweeter on HIF1. Cell. 145(5):647-649.
[70] Luo, W., Hu, H., Chang, R., Zhong, J., Knabel, M., O'Meally, R., et al., 2011. Pyruvate Kinase M2 Is a PHD3-Stimulated Coactivator for Hypoxia-Inducible Factor 1. Cell. 145(5):732-744.
[71] Guzman, M. L., 2013. Cytokine Induced Nuclear Localization Of Pyruvate Kinase M2 In Acute Myeloid Leukemia. Blood. 122(21):5406.
[72] Semenza, G. L., 2008. Tumor metabolism: cancer cells give and take lactate. The Journal of Clinical Investigation. 118(12):3835-3837.
[73] Brizel, D. M., Schroeder, T., Scher, R. L., Walenta, S., Clough, R. W., Dewhirst, M. W., et al., 2001. Elevated tumor lactate concentrations predict for an increased risk of metastases in head-and-neck cancer. International Journal of Radiation Oncology • Biology • Physics. 51(2):349-353.

[74] Bonuccelli, G., Tsirigos, A., Whitaker-Menezes, D., Pavlides, S., Pestell, R. G., Chiavarina, B., et al., 2010. Ketones and lactate "fuel" tumor growth and metastasis. Cell Cycle. 9(17):3506-3514.
[75] Pinheiro, C., Longatto-Filho, A., Azevedo-Silva, J., Casal, M., Schmitt, F. C., Baltazar, F., 2012. Role of monocarboxylate transporters in human cancers: state of the art. Journal of bioenergetics and biomembranes. 44(1):127-139.
[76] Tsouko, E., Khan, A. S., White, M. A., Han, J. J., Shi, Y., Merchant, F. A., et al., 2014. Regulation of the pentose phosphate pathway by an androgen receptor–mTOR-mediated mechanism and its role in prostate cancer cell growth. Oncogenesis. 3(5):e103.
[77] Jiang, P., Du, W., Wu, M., 2014. Regulation of the pentose phosphate pathway in cancer. Protein & Cell. 5(8):592-602.
[78] Stanton, R. C., 2012. Glucose-6-phosphate dehydrogenase, NADPH, and cell survival. IUBMB life. 64(5):362-369.
[79] Xu, S.-N., Wang, T.-S., Li, X., Wang, Y.-P., 2016. SIRT2 activates G6PD to enhance NADPH production and promote leukaemia cell proliferation. Scientific reports. 6:32734.
[80] Islamian, J. P., Aghaee, F., Farajollahi, A., Baradaran, B., Fazel, M., 2015. Combined Treatment with 2-Deoxy-D-Glucose and Doxorubicin Enhances the in Vitro Efficiency of Breast Cancer Radiotherapy. Asian Pacific journal of cancer prevention : APJCP. 16(18):8431-8438.
[81] Siqueira, J. A., Hardoim, P., Ferreira, P. C. G., Nunes-Nesi, A., Hemerly, A. S., 2018. Unraveling Interfaces between Energy Metabolism and Cell Cycle in Plants. Trends in plant science. 23(8):731-747.
[82] Schieke, S. M., McCoy, J. P., Jr., Finkel, T., 2008. Coordination of mitochondrial bioenergetics with G1 phase cell cycle progression. Cell Cycle. 7(12):1782-1787.
[83] Kaplon, J., van Dam, L., Peeper, D., 2015. Two-way communication between the metabolic and cell cycle machineries: the molecular basis. Cell Cycle. 14(13):2022-2032.
[84] Liang, J., Shao, S. H., Xu, Z.-X., Hennessy, B., Ding, Z., Larrea, M., et al., 2007. The energy sensing LKB1–AMPK pathway regulates p27kip1 phosphorylation mediating the decision to enter autophagy or apoptosis. Nature Cell Biology. 9:218.
[85] Cooper, R., Sarioglu, S., Sokmen, S., Fuzun, M., Kupelioglu, A., Valentine, H., et al., 2003. Glucose transporter-1 (GLUT-1): a potential marker of prognosis in rectal carcinoma? Br J Cancer. 89(5):870-876.
[86] Zhao, Z.-X., Lu, L.-W., Qiu, J., Li, Q.-P., Xu, F., Liu, B.-J., et al., 2018. Glucose transporter-1 as an independent prognostic marker for cancer: a meta-analysis. Oncotarget. 9(2):2728-2738.
[87] Granchi, C., Fancelli, D., Minutolo, F., 2014. An update on therapeutic opportunities offered by cancer glycolytic metabolism. Bioorganic & Medicinal Chemistry Letters. 24(21):4915-4925.
[88] Wang, D., Chu, P. C., Yang, C. N., Yan, R., Chuang, Y. C., Kulp, S. K., et al., 2018. Retraction of "Development of a Novel Class of Glucose Transporter Inhibitors". Journal of medicinal chemistry. 61(11):5056.
[89] Granchi, C., Tuccinardi, T., Minutolo, F. Design, Synthesis, and Evaluation of GLUT Inhibitors. In: Lindkvist-Petersson, K, Hansen, JS, editors. Glucose Transport: Methods and Protocols. New York, NY: Springer New York; 2018. p. 93-108.
[90] Wang, Y. D., Li, S. J., Liao, J. X., 2013. Inhibition of glucose transporter 1 (GLUT1) chemosensitized head and neck cancer cells to cisplatin. Technology in cancer research & treatment. 12(6):525-535.
[91] Rastogi, S., Banerjee, S., Chellappan, S., Simon, G. R., 2007. Glut-1 antibodies induce growth

arrest and apoptosis in human cancer cell lines. Cancer Letters. 257(2):244-251.
[92] Chung, K. W., Chan, Y. W., Fung, K. P., 2004. Anti-proliferative effect of antisense oligonucleotides against glucose transporter 5 (Glut 5) on human breast cancer cells. Cancer Research. 64(7 Supplement):680.
[93] Yan, S.-X., Luo, X.-M., Zhou, S.-H., Bao, Y.-Y., Fan, J., Lu, Z.-J., et al., 2013. Effect of Antisense Oligodeoxynucleotides Glucose Transporter-1 on Enhancement of Radiosensitivity of Laryngeal Carcinoma. International Journal of Medical Sciences. 10(10):1375-1386.
[94] Stein, M., Lin, H., Jeyamohan, C., Dvorzhinski, D., Gounder, M., Bray, K., et al., 2010. Targeting tumor metabolism with 2-deoxyglucose in patients with castrate-resistant prostate cancer and advanced malignancies. The Prostate. 70(13):1388-1394.
[95] Ben Sahra, I., Laurent, K., Giuliano, S., Larbret, F., Ponzio, G., Gounon, P., et al., 2010. Targeting cancer cell metabolism: the combination of metformin and 2-deoxyglucose induces p53-dependent apoptosis in prostate cancer cells. Cancer Res. 70(6):2465-2475.
[96] Ho, N., Morrison, J., Silva, A., Coomber, Brenda L., 2016. The effect of 3-bromopyruvate on human colorectal cancer cells is dependent on glucose concentration but not hexokinase II expression. Bioscience Reports. 36(1):e00299.
[97] Porporato, P. E., Dhup, S., Dadhich, R. K., Copetti, T., Sonveaux, P., 2011. Anticancer targets in the glycolytic metabolism of tumors: a comprehensive review. Front Pharmacol. 2.
[98] Nath, K., Guo, L., Nancolas, B., Nelson, D. S., Shestov, A. A., Lee, S. C., et al., 2016. Mechanism of antineoplastic activity of lonidamine. Biochim Biophys Acta. 1866(2):151-162.
[99] Vander Heiden, M. G., Christofk, H. R., Schuman, E., Subtelny, A. O., Sharfi, H., Harlow, E. E., et al., 2010. Identification of small molecule inhibitors of pyruvate kinase M2. Biochemical pharmacology. 79(8):1118-1124.
[100] Li, L., Fath, M. A., Scarbrough, P. M., Watson, W. H., Spitz, D. R., 2015. Combined inhibition of glycolysis, the pentose cycle, and thioredoxin metabolism selectively increases cytotoxicity and oxidative stress in human breast and prostate cancer. Redox Biology. 4:127-135.
[101] Stanton, R. C., 2012. Glucose-6-Phosphate Dehydrogenase, NADPH, and Cell Survival. IUBMB life. 64(5):362-369.
[102] Dong, Y., Wang, M., 2017. Knockdown of TKTL1 additively complements cisplatin-induced cytotoxicity in nasopharyngeal carcinoma cells by regulating the levels of NADPH and ribose-5-phosphate. Biomedicine & Pharmacotherapy. 85:672-678.
[103] Kämmerer, U., Gires, O., Pfetzer, N., Wiegering, A., Klement, R. J., Otto, C., 2015. TKTL1 expression in human malign and benign cell lines. BMC Cancer. 15(1):2.
[104] Li, J., Zhu, S.-C., Li, S.-G., Zhao, Y., Xu, J.-R., Song, C.-Y., 2015. TKTL1 promotes cell proliferation and metastasis in esophageal squamous cell carcinoma. Biomedicine & Pharmacotherapy. 74:71-76.
[105] da Costa, I. A., Hennenlotter, J., Stühler, V., Kühs, U., Scharpf, M., Todenhöfer, T., et al., 2018. Transketolase like 1 (TKTL1) expression alterations in prostate cancer tumorigenesis. Urologic Oncology: Seminars and Original Investigations.
[106] Fantin, V. R., St-Pierre, J., Leder, P., 2006. Attenuation of LDH-A expression uncovers a link between glycolysis, mitochondrial physiology, and tumor maintenance. Cancer Cell. 9(6):425-434.
[107] Xie, H., Hanai, J.-i., Ren, J.-G., Kats, L., Burgess, K., Bhargava, P., et al., 2014. Targeting Lactate Dehydrogenase-A Inhibits Tumorigenesis and Tumor Progression in Mouse Models of Lung Cancer and Impacts Tumor-Initiating Cells. Cell Metabolism. 19(5):795-809.

[108] Zhou, M., Zhao, Y., Ding, Y., Liu, H., Liu, Z., Fodstad, O., et al., 2010. Warburg effect in chemosensitivity: Targeting lactate dehydrogenase-A re-sensitizes Taxol-resistant cancer cells to Taxol. Molecular cancer. 9(1):33.
[109] Lei, W., Kang, W., Nan, Y., Lei, Z., Zhongdong, L., Demin, L., et al., 2018. The downregulation of miR-200c promotes lactate dehydrogenase A expression and non-small cell lung cancer progression. Oncol Res.
[110] Saunier, E., Antonio, S., Regazzetti, A., Auzeil, N., Laprevote, O., Shay, J. W., et al., 2017. Resveratrol reverses the Warburg effect by targeting the pyruvate dehydrogenase complex in colon cancer cells. Scientific reports. 7(1):6945.
[111] Kankotia, S., Stacpoole, P. W., 2014. Dichloroacetate and cancer: new home for an orphan drug? Biochim Biophys Acta. 1846(2):617-629.
[112] Khan, A., Andrews, D., Blackburn, A. C., 2016. Long-term stabilization of stage 4 colon cancer using sodium dichloroacetate therapy. World Journal of Clinical Cases. 4(10):336-343.
[113] Sun, R. C., Fadia, M., Dahlstrom, J. E., Parish, C. R., Board, P. G., Blackburn, A. C., 2010. Reversal of the glycolytic phenotype by dichloroacetate inhibits metastatic breast cancer cell growth in vitro and in vivo. Breast Cancer Research and Treatment. 120(1):253-260.
[114] Xu, R. H., Pelicano, H., Zhou, Y., Carew, J. S., Feng, L., Bhalla, K. N., et al., 2005. Inhibition of glycolysis in cancer cells: a novel strategy to overcome drug resistance associated with mitochondrial respiratory defect and hypoxia. Cancer Res. 65(2):613-621.
[115] Fu, J., Jiang, H., Wu, C., Jiang, Y., Xiao, L., Tian, Y., 2016. Overcoming cetuximab resistance in Ewing's sarcoma by inhibiting lactate dehydrogenase-A. Molecular medicine reports. 14(1):995-1001.
[116] Zhao, Z., Han, F., Yang, S., Wu, J., Zhan, W., 2015. Oxamate-mediated inhibition of lactate dehydrogenase induces protective autophagy in gastric cancer cells: Involvement of the Akt–mTOR signaling pathway. Cancer Letters. 358(1):17-26.
[117] Daye, D., Wellen, K. E., 2012. Metabolic reprogramming in cancer: Unraveling the role of glutamine in tumorigenesis. Seminars in Cell & Developmental Biology. 23(4):362-369.
[118] Wise, D. R., DeBerardinis, R. J., Mancuso, A., Sayed, N., Zhang, X. Y., Pfeiffer, H. K., et al., 2008. Myc regulates a transcriptional program that stimulates mitochondrial glutaminolysis and leads to glutamine addiction. Proc Natl Acad Sci U S A. 105(48):18782-18787.
[119] Gao, P., Tchernyshyov, I., Chang, T. C., Lee, Y. S., Kita, K., Ochi, T., et al., 2009. c-Myc suppression of miR-23a/b enhances mitochondrial glutaminase expression and glutamine metabolism. Nature. 458(7239):762-765.
[120] Qie, S., Chu, C., Li, W., Wang, C., Sang, N., 2014. ErbB2 activation upregulates glutaminase 1 expression which promotes breast cancer cell proliferation. Journal of cellular biochemistry. 115(3):498-509.
[121] Bhutia, Y. D., Ganapathy, V., 2016. Glutamine transporters in mammalian cells and their functions in physiology and cancer. Biochim Biophys Acta. 1863(10):2531-2539.
[122] Yanagida, O., Kanai, Y., Chairoungdua, A., Kim, D. K., Segawa, H., Nii, T., et al., 2001. Human L-type amino acid transporter 1 (LAT1): characterization of function and expression in tumor cell lines. Biochimica et Biophysica Acta (BBA) - Biomembranes. 1514(2):291-302.
[123] Nicklin, P., Bergman, P., Zhang, B., Triantafellow, E., Wang, H., Nyfeler, B., et al., 2009. Bidirectional transport of amino acids regulates mTOR and autophagy. Cell. 136(3):521-534.
[124] Cohen, A., Hall, M. N., 2009. An Amino Acid Shuffle Activates mTORC1. Cell. 136(3):399-400.

[125] Jewell, J. L., Kim, Y. C., Russell, R. C., Yu, F.-X., Park, H. W., Plouffe, S. W., et al., 2015. Differential regulation of mTORC1 by leucine and glutamine. Science (New York, NY). 347(6218):194-198.
[126] Tan, H. W. S., Sim, A. Y. L., Long, Y. C., 2017. Glutamine metabolism regulates autophagy-dependent mTORC1 reactivation during amino acid starvation. Nature communications. 8(1):338.
[127] Lorin, S., Tol, M. J., Bauvy, C., Strijland, A., Poüs, C., Verhoeven, A. J., et al., 2013. Glutamate dehydrogenase contributes to leucine sensing in the regulation of autophagy. Autophagy. 9(6):850-860.
[128] Durán, Raúl V., Oppliger, W., Robitaille, Aaron M., Heiserich, L., Skendaj, R., Gottlieb, E., et al., 2012. Glutaminolysis Activates Rag-mTORC1 Signaling. Molecular Cell. 47(3):349-358.
[129] Duran, R. V., Hall, M. N., 2012. Glutaminolysis feeds mTORC1. Cell Cycle. 11(22):4107-4108.
[130] Durán, R. V., MacKenzie, E. D., Boulahbel, H., Frezza, C., Heiserich, L., Tardito, S., et al., 2012. HIF-independent role of prolyl hydroxylases in the cellular response to amino acids. Oncogene. 32:4549.
[131] Cormerais, Y., Massard, P. A., Vucetic, M., Giuliano, S., Tambutte, E., Durivault, J., et al., 2018. The glutamine transporter ASCT2 (SLC1A5) promotes tumor growth independently of the amino acid transporter LAT1 (SLC7A5). The Journal of biological chemistry. 293(8):2877-2887.
[132] Chen, Q., Kirk, K., Shurubor, Y. I., Zhao, D., Arreguin, A. J., Shahi, I., et al., 2018. Rewiring of Glutamine Metabolism Is a Bioenergetic Adaptation of Human Cells with Mitochondrial DNA Mutations. Cell Metabolism. 27(5):1007-1025.e1005.
[133] Birsoy, K., Wang, T., Chen, Walter W., Freinkman, E., Abu-Remaileh, M., Sabatini, David M., 2015. An Essential Role of the Mitochondrial Electron Transport Chain in Cell Proliferation Is to Enable Aspartate Synthesis. Cell. 162(3):540-551.
[134] Pike Winer, L. S., Wu, M., 2014. Rapid Analysis of Glycolytic and Oxidative Substrate Flux of Cancer Cells in a Microplate. PloS one. 9(10):e109916.
[135] Sun, R. C., Denko, N. C., 2014. Hypoxic regulation of glutamine metabolism through HIF1 and SIAH2 supports lipid synthesis that is necessary for tumor growth. Cell metabolism. 19(2):285-292.
[136] Fan, J., Kamphorst, J. J., Mathew, R., Chung, M. K., White, E., Shlomi, T., et al., 2013. Glutamine-driven oxidative phosphorylation is a major ATP source in transformed mammalian cells in both normoxia and hypoxia. Molecular systems biology. 9:712.
[137] Lee, J.-S., Kang, J. H., Lee, S.-H., Hong, D., Son, J., Hong, K. M., et al., 2016. Dual targeting of glutaminase 1 and thymidylate synthase elicits death synergistically in NSCLC. Cell Death &Amp; Disease. 7:e2511.
[138] Cassago, A., Ferreira, A. P. S., Ferreira, I. M., Fornezari, C., Gomes, E. R. M., Greene, K. S., et al., 2012. Mitochondrial localization and structure-based phosphate activation mechanism of Glutaminase C with implications for cancer metabolism. Proceedings of the National Academy of Sciences of the United States of America. 109(4):1092-1097.
[139] van den Heuvel, A. P. J., Jing, J., Wooster, R. F., Bachman, K. E., 2012. Analysis of glutamine dependency in non-small cell lung cancer: GLS1 splice variant GAC is essential for cancer cell growth. Cancer biology & therapy. 13(12):1185-1194.
[140] Cassago, A., Ferreira, A. P. S., Ferreira, I. M., Fornezari, C., Gomes, E. R. M., Greene, K. S., et al., 2012. Mitochondrial localization and structure-based phosphate activation mechanism of Glutaminase C with implications for cancer metabolism. Proceedings of the National Academy of Sciences. 109(4):1092-1097.

[141] Stalnecker, C. A., Ulrich, S. M., Li, Y., Ramachandran, S., McBrayer, M. K., DeBerardinis, R. J., et al., 2015. Mechanism by which a recently discovered allosteric inhibitor blocks glutamine metabolism in transformed cells. Proceedings of the National Academy of Sciences. 112(2):394-399.
[142] Pan, T., Gao, L., Wu, G., Shen, G., Xie, S., Wen, H., et al., 2015. Elevated expression of glutaminase confers glucose utilization via glutaminolysis in prostate cancer. Biochem Biophys Res Commun. 456(1):452-458.
[143] Hu, W., Zhang, C., Wu, R., Sun, Y., Levine, A., Feng, Z., 2010. Glutaminase 2, a novel p53 target gene regulating energy metabolism and antioxidant function. Proceedings of the National Academy of Sciences. 107(16):7455-7460.
[144] Xiang, L., Xie, G., Liu, C., Zhou, J., Chen, J., Yu, S., et al., 2013. Knock-down of glutaminase 2 expression decreases glutathione, NADH, and sensitizes cervical cancer to ionizing radiation. Biochimica et Biophysica Acta (BBA) - Molecular Cell Research. 1833(12):2996-3005.
[145] Suzuki, S., Tanaka, T., Poyurovsky, M. V., Nagano, H., Mayama, T., Ohkubo, S., et al., 2010. Phosphate-activated glutaminase (GLS2), a p53-inducible regulator of glutamine metabolism and reactive oxygen species. Proceedings of the National Academy of Sciences. 107(16):7461-7466.
[146] Liu, J., Zhang, C., Lin, M., Zhu, W., Liang, Y., Hong, X., et al., 2014. Glutaminase 2 negatively regulates the PI3K/AKT signaling and shows tumor suppression activity in human hepatocellular carcinoma. Oncotarget. 5(9):2635-2647.
[147] Li, M., Li, C., Allen, A., Stanley, C. A., Smith, T. J., 2012. The structure and allosteric regulation of mammalian glutamate dehydrogenase. Arch Biochem Biophys. 519(2):69-80.
[148] Haigis, M. C., Mostoslavsky, R., Haigis, K. M., Fahie, K., Christodoulou, D. C., Murphy, Andrew J., et al., 2006. SIRT4 Inhibits Glutamate Dehydrogenase and Opposes the Effects of Calorie Restriction in Pancreatic β Cells. Cell. 126(5):941-954.
[149] Miyo, M., Yamamoto, H., Konno, M., Colvin, H., Nishida, N., Koseki, J., et al., 2015. Tumour-suppressive function of SIRT4 in human colorectal cancer. British Journal Of Cancer. 113:492.
[150] Mullen, Andrew R., Hu, Z., Shi, X., Jiang, L., Boroughs, Lindsey K., Kovacs, Z., et al., 2014. Oxidation of Alpha-Ketoglutarate Is Required for Reductive Carboxylation in Cancer Cells with Mitochondrial Defects. Cell Reports. 7(5):1679-1690.
[151] Chen, Q., Kirk, K., Shurubor, Y. I., Zhao, D., Arreguin, A. J., Shahi, I., et al., 2018. Rewiring of Glutamine Metabolism Is a Bioenergetic Adaptation of Human Cells with Mitochondrial DNA Mutations. Cell Metab. 27(5):1007-1025.e1005.
[152] Jeong, S. M., Hwang, S., Park, K., Yang, S., Seong, R. H., 2016. Enhanced mitochondrial glutamine anaplerosis suppresses pancreatic cancer growth through autophagy inhibition. Scientific reports. 6:30767.
[153] Zheng, P.-P., van der Weiden, M., van der Spek, P. J., Vincent, A. J. P. E., Kros, J. M., 2012. Isocitrate dehydrogenase 1R132H mutation in microglia/macrophages in gliomas: indication of a significant role of microglia/macrophages in glial tumorigenesis. Cancer biology & therapy. 13(10):836-839.
[154] Metallo, C. M., Gameiro, P. A., Bell, E. L., Mattaini, K. R., Yang, J., Hiller, K., et al., 2011. Reductive glutamine metabolism by IDH1 mediates lipogenesis under hypoxia. Nature. 481(7381):380-384.
[155] Mullen, A. R., Wheaton, W. W., Jin, E. S., Chen, P.-H., Sullivan, L. B., Cheng, T., et al., 2011. Reductive carboxylation supports growth in tumour cells with defective mitochondria. Nature.

481:385.
[156] Alberghina, L., Gaglio, D., 2014. Redox control of glutamine utilization in cancer. Cell Death & Disease. 5(12):e1561.
[157] Ho, H.-Y., Lin, Y.-T., Lin, G., Wu, P.-R., Cheng, M.-L., 2017. Nicotinamide nucleotide transhydrogenase (NNT) deficiency dysregulates mitochondrial retrograde signaling and impedes proliferation. Redox Biology. 12:916-928.
[158] Wang, Q., Hardie, R. A., Hoy, A. J., van Geldermalsen, M., Gao, D., Fazli, L., et al., 2015. Targeting ASCT2-mediated glutamine uptake blocks prostate cancer growth and tumour development. The Journal of pathology. 236(3):278-289.
[159] Marshall, A. D., van Geldermalsen, M., Otte, N. J., Lum, T., Vellozzi, M., Thoeng, A., et al., 2017. ASCT2 regulates glutamine uptake and cell growth in endometrial carcinoma. Oncogenesis. 6(7):e367.
[160] Ye, J., Huang, Q., Xu, J., Huang, J., Wang, J., Zhong, W., et al., 2018. Targeting of glutamine transporter ASCT2 and glutamine synthetase suppresses gastric cancer cell growth. Journal of cancer research and clinical oncology. 144(5):821-833.
[161] van Geldermalsen, M., Wang, Q., Nagarajah, R., Marshall, A. D., Thoeng, A., Gao, D., et al., 2016. ASCT2/SLC1A5 controls glutamine uptake and tumour growth in triple-negative basal-like breast cancer. Oncogene. 35(24):3201-3208.
[162] Wise, D. R., Thompson, C. B., 2010. Glutamine Addiction: A New Therapeutic Target in Cancer. Trends in biochemical sciences. 35(8):427-433.
[163] Ohshima, Y., Kaira, K., Yamaguchi, A., Oriuchi, N., Tominaga, H., Nagamori, S., et al., 2016. Efficacy of system l amino acid transporter 1 inhibition as a therapeutic target in esophageal squamous cell carcinoma. Cancer Science. 107(10):1499-1505.
[164] Imai, H., Kaira, K., Oriuchi, N., Shimizu, K., Tominaga, H., Yanagitani, N., et al., 2010. Inhibition of L-type amino acid transporter 1 has antitumor activity in non-small cell lung cancer. Anticancer research. 30(12):4819-4828.
[165] Dixon, S. J., Patel, D. N., Welsch, M., Skouta, R., Lee, E. D., Hayano, M., et al., 2014. Pharmacological inhibition of cystine–glutamate exchange induces endoplasmic reticulum stress and ferroptosis. eLife. 3:e02523.
[166] Nagane, M., Kanai, E., Shibata, Y., Shimizu, T., Yoshioka, C., Maruo, T., et al., 2018. Sulfasalazine, an inhibitor of the cystine-glutamate antiporter, reduces DNA damage repair and enhances radiosensitivity in murine B16F10 melanoma. PloS one. 13(4):e0195151.
[167] Shin, C.-S., Mishra, P., Watrous, J. D., Carelli, V., D'Aurelio, M., Jain, M., et al., 2017. The glutamate/cystine xCT antiporter antagonizes glutamine metabolism and reduces nutrient flexibility. Nature communications. 8:15074.
[168] Sheikh, T. N., Patwardhan, P. P., Cremers, S., Schwartz, G. K., 2017. Targeted inhibition of glutaminase as a potential new approach for the treatment of NF1 associated soft tissue malignancies. Oncotarget. 8(55):94054-94068.
[169] Mackinnon, A., Bennett, M., Rodriguez, M., Parlati, F., 2014. Biomarkers of Response to the Glutaminase Inhibitor CB-839 in Multiple Myeloma Cells. Blood. 124(21):3429.
[170] Gross, M. I., Demo, S. D., Dennison, J. B., Chen, L., Chernov-Rogan, T., Goyal, B., et al., 2014. Antitumor activity of the glutaminase inhibitor CB-839 in triple-negative breast cancer. Mol Cancer Ther. 13(4):890-901.
[171] Huber, K. R., Rosenfeld, H., Roberts, J., 1988. Uptake of glutamine antimetabolites 6-diazo-

5-oxo-L-norleucine (DON) and acivicin in sensitive and resistant tumor cell lines. International journal of cancer. 41(5):752-755.
[172] Jin, L., Alesi, G. N., Kang, S., 2016. Glutaminolysis as a target for cancer therapy. Oncogene. 35(28):3619-3625.
[173] Villar, V. H., Nguyen, T. L., Delcroix, V., Terés, S., Bouchecareilh, M., Salin, B., et al., 2017. mTORC1 inhibition in cancer cells protects from glutaminolysis-mediated apoptosis during nutrient limitation. Nature communications. 8:14124.
[174] Cervantes-Madrid, D., Duenas-Gonzalez, A., 2015. Antitumor effects of a drug combination targeting glycolysis, glutaminolysis and de novo synthesis of fatty acids. Oncology reports. 34(3):1533-1542.
[175] Lampa, M., Arlt, H., He, T., Ospina, B., Reeves, J., Zhang, B., et al., 2017. Glutaminase is essential for the growth of triple-negative breast cancer cells with a deregulated glutamine metabolism pathway and its suppression synergizes with mTOR inhibition. PloS one. 12(9):e0185092.
[176] Lyons, S. D., Sant, M. E., Christopherson, R. I., 1990. Cytotoxic mechanisms of glutamine antagonists in mouse L1210 leukemia. The Journal of biological chemistry. 265(19):11377-11381.
[177] Bennett, L. L., Schabel, F. M., Skipper, H. E., 1956. Studies on the mode of action of azaserine. Archives of Biochemistry and Biophysics. 64(2):423-436.
[178] Moore, E. C., LePage, G. A., 1957. In Vivo Sensitivity of Normal and Neoplastic Mouse Tissues to Azaserine. Cancer Research. 17(8):804.
[179] Chittur, S. V., Klem, T. J., Shafer, C. M., Davisson, V. J., 2001. Mechanism for Acivicin Inactivation of Triad Glutamine Amidotransferases. Biochemistry. 40(4):876-887.
[180] van Geldermalsen, M., Wang, Q., Nagarajah, R., Marshall, A. D., Thoeng, A., Gao, D., et al., 2015. ASCT2/SLC1A5 controls glutamine uptake and tumour growth in triple-negative basal-like breast cancer. Oncogene. 35:3201.
[181] Foster, A. C., Rangel-Diaz, N., Staubli, U., Yang, J.-Y., Penjwini, M., Viswanath, V., et al., 2017. Phenylglycine analogs are inhibitors of the neutral amino acid transporters ASCT1 and ASCT2 and enhance NMDA receptor-mediated LTP in rat visual cortex slices. Neuropharmacology. 126:70-83.
[182] Marshall, A. D., van Geldermalsen, M., Otte, N. J., Lum, T., Vellozzi, M., Thoeng, A., et al., 2017. ASCT2 regulates glutamine uptake and cell growth in endometrial carcinoma. Oncogenesis. 6:e367.
[183] Grewer, C., Grabsch, E., 2004. New inhibitors for the neutral amino acid transporter ASCT2 reveal its Na+-dependent anion leak. The Journal of physiology. 557(Pt 3):747-759.
[184] Todorova, V. K., Kaufmann, Y., Luo, S., Klimberg, V. S., 2011. Tamoxifen and raloxifene suppress the proliferation of estrogen receptor-negative cells through inhibition of glutamine uptake. Cancer chemotherapy and pharmacology. 67(2):285-291.
[185] Giuliani, N., Chiu, M., Bolzoni, M., Accardi, F., Bianchi, M. G., Toscani, D., et al., 2017. The potential of inhibiting glutamine uptake as a therapeutic target for multiple myeloma. Expert opinion on therapeutic targets. 21(3):231-234.
[186] Lin, L., Yee, S. W., Kim, R. B., Giacomini, K. M., 2015. SLC Transporters as Therapeutic Targets: Emerging Opportunities. Nature reviews Drug discovery. 14(8):543-560.
[187] Lewerenz, J., Hewett, S. J., Huang, Y., Lambros, M., Gout, P. W., Kalivas, P. W., et al., 2013. The

to Novel Therapeutic Opportunities. Antioxidants & redox signaling. 18(5):522-555.
[188] Kinoshita, H., Okabe, H., Beppu, T., Chikamoto, A., Hayashi, H., Imai, K., et al., 2013. Cystine/glutamic acid transporter is a novel marker for predicting poor survival in patients with hepatocellular carcinoma. Oncology reports. 29(2):685-689.
[189] Xie, L., Song, X., Yu, J., Guo, W., Wei, L., Liu, Y., et al., 2011. Solute carrier protein family may involve in radiation-induced radioresistance of non-small cell lung cancer. Journal of cancer research and clinical oncology. 137(12):1739-1747.
[190] Hasegawa, M., Takahashi, H., Rajabi, H., Alam, M., Suzuki, Y., Yin, L., et al., 2016. Functional interactions of the cystine/glutamate antiporter, CD44v and MUC1-C oncoprotein in triple-negative breast cancer cells. Oncotarget. 7(11):11756-11769.
[191] Sato, M., Kusumi, R., Hamashima, S., Kobayashi, S., Sasaki, S., Komiyama, Y., et al., 2018. The ferroptosis inducer erastin irreversibly inhibits system x(c)− and synergizes with cisplatin to increase cisplatin's cytotoxicity in cancer cells. Scientific reports. 8:968.
[192] Dahlmanns, M., Yakubov, E., Chen, D., Sehm, T., Rauh, M., Savaskan, N., et al., 2017. Chemotherapeutic xCT inhibitors sorafenib and erastin unraveled with the synaptic optogenetic function analysis tool. Cell Death Discovery. 3:17030.
[193] Xiang, Y., Stine, Z. E., Xia, J., Lu, Y., O'Connor, R. S., Altman, B. J., et al., 2015. Targeted inhibition of tumor-specific glutaminase diminishes cell-autonomous tumorigenesis. J Clin Invest. 125(6):2293-2306.
[194] Elgogary, A., Xu, Q., Poore, B., Alt, J., Zimmermann, S. C., Zhao, L., et al., 2016. Combination therapy with BPTES nanoparticles and metformin targets the metabolic heterogeneity of pancreatic cancer. Proc Natl Acad Sci U S A. 113(36):E5328-5336.
[195] Nagana Gowda, G. A., Barding, G. A., Jr., Dai, J., Gu, H., Margineantu, D. H., Hockenbery, D. M., et al., 2018. A Metabolomics Study of BPTES Altered Metabolism in Human Breast Cancer Cell Lines. Frontiers in molecular biosciences. 5:49.
[196] Xiang, Y., Stine, Z. E., Xia, J., Lu, Y., O'Connor, R. S., Altman, B. J., et al., 2015. Targeted inhibition of tumor-specific glutaminase diminishes cell-autonomous tumorigenesis. The Journal of Clinical Investigation. 125(6):2293-2306.
[197] Huang, Q., Stalnecker, C., Zhang, C., McDermott, L. A., Iyer, P., O'Neill, J., et al., 2018. Characterization of the interactions of potent allosteric inhibitors with glutaminase C, a key enzyme in cancer cell glutamine metabolism. The Journal of biological chemistry. 293(10):3535-3545.
[198] Gross, M. I., Demo, S. D., Dennison, J. B., Chen, L., Chernov-Rogan, T., Goyal, B., et al., 2014. Antitumor Activity of the Glutaminase Inhibitor CB-839 in Triple-Negative Breast Cancer. Molecular Cancer Therapeutics.
[199] Yuan, L., Sheng, X., Clark, L. H., Zhang, L., Guo, H., Jones, H. M., et al., 2016. Glutaminase inhibitor compound 968 inhibits cell proliferation and sensitizes paclitaxel in ovarian cancer. American Journal of Translational Research. 8(10):4265-4277.
[200] Wang, J.-B., Erickson, J. W., Fuji, R., Ramachandran, S., Gao, P., Dinavahi, R., et al., 2010. Targeting mitochondrial glutaminase activity inhibits oncogenic transformation. Cancer cell. 18(3):207-219.
[201] Chen, L., Cui, H., 2015. Targeting Glutamine Induces Apoptosis: A Cancer Therapy Approach. International journal of molecular sciences. 16(9):22830-22855.
[202] Yang, C., Sudderth, J., Dang, T., Bachoo, R. G., McDonald, J. G., DeBerardinis, R. J., 2009.

Glioblastoma Cells Require Glutamate Dehydrogenase to Survive Impairments of Glucose Metabolism or Akt Signaling. Cancer Research. 69(20):7986.
[203] Li, C., Li, M., Chen, P., Narayan, S., Matschinsky, F. M., Bennett, M. J., et al., 2011. Green tea polyphenols control dysregulated glutamate dehydrogenase in transgenic mice by hijacking the ADP activation site. The Journal of biological chemistry. 286(39):34164-34174.
[204] Lorin, S., Tol, M. J., Bauvy, C., Strijland, A., Pous, C., Verhoeven, A. J., et al., 2013. Glutamate dehydrogenase contributes to leucine sensing in the regulation of autophagy. Autophagy. 9(6):850-860.
[205] Zhang, J., Wang, G., Mao, Q., Li, S., Xiong, W., Lin, Y., et al., 2016. Glutamate dehydrogenase (GDH) regulates bioenergetics and redox homeostasis in human glioma. Oncotarget. Advance publications:1-12.
[206] Jin, L., Li, D., Alesi, Gina N., Fan, J., Kang, H.-B., Lu, Z., et al., 2015. Glutamate Dehydrogenase 1 Signals through Antioxidant Glutathione Peroxidase 1 to Regulate Redox Homeostasis and Tumor Growth. Cancer Cell. 27(2):257-270.
[207] Korangath, P., Teo, W. W., Sadik, H., Han, L., Mori, N., Huijts, C. M., et al., 2015. Targeting Glutamine Metabolism in Breast Cancer with Aminooxyacetate. Clinical cancer research : an official journal of the American Association for Cancer Research. 21(14):3263-3273.
[208] Kauppinen, R. A., Sihra, T. S., Nicholls, D. G., 1987. Aminooxyacetic acid inhibits the malate-aspartate shuttle in isolated nerve terminals and prevents the mitochondria from utilizing glycolytic substrates. Biochimica et Biophysica Acta (BBA) - Molecular Cell Research. 930(2):173-178.
[209] Wang, C., Chen, H., Zhang, M., Zhang, J., Wei, X., Ying, W., 2016. Malate-aspartate shuttle inhibitor aminooxyacetic acid leads to decreased intracellular ATP levels and altered cell cycle of C6 glioma cells by inhibiting glycolysis. Cancer Letters. 378(1):1-7.
[210] Greenhouse, W. V. V., Lehninger, A. L., 1976. Occurrence of the Malate-Aspartate Shuttle in Various Tumor Types. Cancer Research. 36(4):1392.
[211] Korangath, P., Teo, W. W., Sadik, H., Han, L., Mori, N., Huijts, C. M., et al., 2015. Targeting Glutamine Metabolism in Breast Cancer with Aminooxyacetate. Clinical cancer research : an official journal of the American Association for Cancer Research. 21(14):3263-3273.
[212] Kunji, E. R. S., Robinson, A. J., 2010. Coupling of proton and substrate translocation in the transport cycle of mitochondrial carriers. Current Opinion in Structural Biology. 20(4):440-447.
[213] Yu, W., Dittenhafer-Reed, K. E., Denu, J. M., 2012. SIRT3 protein deacetylates isocitrate dehydrogenase 2 (IDH2) and regulates mitochondrial redox status. The Journal of biological chemistry. 287(17):14078-14086.
[214] Vatrinet, R., Leone, G., De Luise, M., Girolimetti, G., Vidone, M., Gasparre, G., et al., 2017. The α-ketoglutarate dehydrogenase complex in cancer metabolic plasticity. Cancer & Metabolism. 5(1):3.
[215] McLain, A. L., Szweda, P. A., Szweda, L. I., 2011. α-Ketoglutarate dehydrogenase: A mitochondrial redox sensor. Free radical research. 45(1):29-36.
[216] Tretter, L., Adam-Vizi, V., 2005. Alpha-ketoglutarate dehydrogenase: a target and generator of oxidative stress. Philosophical Transactions of the Royal Society B: Biological Sciences. 360(1464):2335.
[217] Ilic, N., Birsoy, K., Aguirre, A. J., Kory, N., Pacold, M. E., Singh, S., et al., 2017. PIK3CA mutant tumors depend on oxoglutarate dehydrogenase. Proceedings of the National Academy of Sciences.

[218] Christen, S., Lorendeau, D., Schmieder, R., Broekaert, D., Metzger, K., Veys, K., et al., 2016. Breast Cancer-Derived Lung Metastases Show Increased Pyruvate Carboxylase-Dependent Anaplerosis. Cell Reports. 17(3):837-848.
[219] Sellers, K., Fox, M. P., Bousamra, M., II, Slone, S. P., Higashi, R. M., Miller, D. M., et al., 2015. Pyruvate carboxylase is critical for non–small-cell lung cancer proliferation. The Journal of Clinical Investigation. 125(2):687-698.
[220] Cheng, T., Sudderth, J., Yang, C., Mullen, A. R., Jin, E. S., Matés, J. M., et al., 2011. Pyruvate carboxylase is required for glutamine-independent growth of tumor cells. Proceedings of the National Academy of Sciences.
[221] Phannasil, P., Thuwajit, C., Warnnissorn, M., Wallace, J. C., MacDonald, M. J., Jitrapakdee, S., 2015. Pyruvate Carboxylase Is Up-Regulated in Breast Cancer and Essential to Support Growth and Invasion of MDA-MB-231 Cells. PloS one. 10(6):e0129848.
[222] Zaidi, N., Lupien, L., Kuemmerle, N. B., Kinlaw, W. B., Swinnen, J. V., Smans, K., 2013. Lipogenesis and lipolysis: the pathways exploited by the cancer cells to acquire fatty acids. Progress in lipid research. 52(4):585-589.
[223] Hlouschek, J., Hansel, C., Jendrossek, V., Matschke, J., 2018. The Mitochondrial Citrate Carrier (SLC25A1) Sustains Redox Homeostasis and Mitochondrial Metabolism Supporting Radioresistance of Cancer Cells With Tolerance to Cycling Severe Hypoxia. Frontiers in oncology. 8:170.
[224] Fernandez, H. R., Gadre, S. M., Tan, M., Graham, G. T., Mosaoa, R., Ongkeko, M. S., et al., 2018. The mitochondrial citrate carrier, SLC25A1, drives stemness and therapy resistance in non-small cell lung cancer. Cell death and differentiation. 25(7):1239-1258.
[225] Wellen, K. E., Hatzivassiliou, G., Sachdeva, U. M., Bui, T. V., Cross, J. R., Thompson, C. B., 2009. ATP-citrate lyase links cellular metabolism to histone acetylation. Science (New York, NY). 324(5930):1076-1080.
[226] Icard, P., Poulain, L., Lincet, H., 2012. Understanding the central role of citrate in the metabolism of cancer cells. Biochim Biophys Acta. 1825(1):111-116.
[227] Lin, R., Tao, R., Gao, X., Li, T., Zhou, X., Guan, K.-L., et al., 2013. Acetylation Stabilizes ATP-Citrate Lyase to Promote Lipid Biosynthesis and Tumor Growth. Molecular Cell. 51(4):506-518.
[228] Marino, G., Pietrocola, F., Eisenberg, T., Kong, Y., Malik, S. A., Andryushkova, A., et al., 2014. Regulation of autophagy by cytosolic acetyl-coenzyme A. Mol Cell. 53(5):710-725.
[229] Luo, J., Hong, Y., Lu, Y., Qiu, S., Chaganty, B. K., Zhang, L., et al., 2017. Acetyl-CoA carboxylase rewires cancer metabolism to allow cancer cells to survive inhibition of the Warburg effect by cetuximab. Cancer Lett. 384:39-49.
[230] Guaragnella, N., Giannattasio, S., Moro, L., 2014. Mitochondrial dysfunction in cancer chemoresistance. Biochemical pharmacology. 92(1):62-72.
[231] Ma, L., Wang, R., Duan, H., Nan, Y., Wang, Q., Jin, F., 2015. Mitochondrial dysfunction rather than mtDNA sequence mutation is responsible for the multi-drug resistance of small cell lung cancer. Oncology reports. 34(6):3238-3246.
[232] Urban, D. J., Martinez, N. J., Davis, M. I., Brimacombe, K. R., Cheff, D. M., Lee, T. D., et al., 2017. Assessing inhibitors of mutant isocitrate dehydrogenase using a suite of pre-clinical discovery assays. Scientific reports. 7:12758.
[233] Dang, L., Yen, K., Attar, E. C., 2016. IDH mutations in cancer and progress toward development of targeted therapeutics. Annals of oncology : official journal of the European Society

for Medical Oncology. 27(4):599-608.
[234] King, A., Selak, M. A., Gottlieb, E., 2006. Succinate dehydrogenase and fumarate hydratase: linking mitochondrial dysfunction and cancer. Oncogene. 25(34):4675-4682.
[235] Tretter, L., Patocs, A., Chinopoulos, C., 2016. Succinate, an intermediate in metabolism, signal transduction, ROS, hypoxia, and tumorigenesis. Biochimica et Biophysica Acta (BBA) - Bioenergetics. 1857(8):1086-1101.
[236] Duran, R. V., MacKenzie, E. D., Boulahbel, H., Frezza, C., Heiserich, L., Tardito, S., et al., 2013. HIF-independent role of prolyl hydroxylases in the cellular response to amino acids. Oncogene. 32(38):4549-4556.
[237] Carew, J. S., Huang, P., 2002. Mitochondrial defects in cancer. Molecular cancer. 1:9.
[238] Boland, M. L., Chourasia, A. H., Macleod, K. F., 2013. Mitochondrial dysfunction in cancer. Frontiers in oncology. 3:292.
[239] Wheaton, W. W., Weinberg, S. E., Hamanaka, R. B., Soberanes, S., Sullivan, L. B., Anso, E., et al., 2014. Metformin inhibits mitochondrial complex I of cancer cells to reduce tumorigenesis. eLife. 3:e02242.
[240] Cameron, A. R., Logie, L., Patel, K., Erhardt, S., Bacon, S., Middleton, P., et al., 2018. Metformin selectively targets redox control of complex I energy transduction. Redox Biology. 14:187-197.
[241] Zi, F., Zi, H., Li, Y., He, J., Shi, Q., Cai, Z., 2018. Metformin and cancer: An existing drug for cancer prevention and therapy. Oncology letters. 15(1):683-690.
[242] Li, X., Li, T., Liu, Z., Gou, S., Wang, C., 2017. The effect of metformin on survival of patients with pancreatic cancer: a meta-analysis. Scientific reports. 7(1):5825.
[243] Andrzejewski, S., Gravel, S.-P., Pollak, M., St-Pierre, J., 2014. Metformin directly acts on mitochondria to alter cellular bioenergetics. Cancer & Metabolism. 2:12-12.
[244] Hodeib, M., Ogrodzinski, M. P., Vergnes, L., Reue, K., Karlan, B. Y., Lunt, S. Y., et al., 2018. Metformin induces distinct bioenergetic and metabolic profiles in sensitive versus resistant high grade serous ovarian cancer and normal fallopian tube secretory epithelial cells. Oncotarget. 9(3):4044-4060.
[245] Mohamed Suhaimi, N. A., Phyo, W. M., Yap, H. Y., Choy, S. H. Y., Wei, X., Choudhury, Y., et al., 2017. Metformin Inhibits Cellular Proliferation and Bioenergetics in Colorectal Cancer Patient-Derived Xenografts. Mol Cancer Ther. 16(9):2035-2044.
[246] Ben Sahra, I., Laurent, K., Giuliano, S., Larbret, F., Ponzio, G., Gounon, P., et al., 2010. Targeting Cancer Cell Metabolism: The Combination of Metformin and 2-Deoxyglucose Induces p53-Dependent Apoptosis in Prostate Cancer Cells. Cancer Research. 70(6):2465-2475.
[247] Ben Sahra, I., Tanti, J. F., Bost, F., 2010. The combination of metformin and 2-deoxyglucose inhibits autophagy and induces AMPK-dependent apoptosis in prostate cancer cells. Autophagy. 6(5):670-671.
[248] Bizjak, M., Malavašič, P., Dolinar, K., Pohar, J., Pirkmajer, S., Pavlin, M., 2017. Combined treatment with Metformin and 2-deoxy glucose induces detachment of viable MDA-MB-231 breast cancer cells in vitro. Scientific reports. 7:1761.
[249] Cheong, J. H., Park, E. S., Liang, J., Dennison, J. B., Tsavachidou, D., Nguyen-Charles, C., et al., 2011. Dual inhibition of tumor energy pathway by 2-deoxyglucose and metformin is effective against a broad spectrum of preclinical cancer models. Mol Cancer Ther. 10(12):2350-2362.
[250] Kim, E. H., Lee, J. H., Oh, Y., Koh, I., Shim, J. K., Park, J., et al., 2017. Inhibition of glioblastoma tumorspheres by combined treatment with 2-deoxyglucose and metformin. Neuro-oncology.

19(2):197-207.
[251] Pollak, M., 2013. Targeting Oxidative Phosphorylation: Why, When, and How. Cancer Cell. 23(3):263-264.
[252] Poolsri, W. A., Phokrai, P., Suwankulanan, S., Phakdeeto, N., Phunsomboon, P., Pekthong, D., et al., 2018. Combination of Mitochondrial and Plasma Membrane Citrate Transporter Inhibitors Inhibits De Novo Lipogenesis Pathway and Triggers Apoptosis in Hepatocellular Carcinoma Cells. BioMed research international. 2018:3683026.
[253] Gnoni, G. V., Priore, P., Geelen, M. J., Siculella, L., 2009. The mitochondrial citrate carrier: metabolic role and regulation of its activity and expression. IUBMB life. 61(10):987-994.
[254] Vacanti, Nathaniel M., Divakaruni, Ajit S., Green, Courtney R., Parker, Seth J., Henry, Robert R., Ciaraldi, Theodore P., et al., 2014. Regulation of Substrate Utilization by the Mitochondrial Pyruvate Carrier. Molecular Cell. 56(3):425-435.
[255] Yang, C., Ko, B., Hensley, Christopher T., Jiang, L., Wasti, Ajla T., Kim, J., et al., 2014. Glutamine Oxidation Maintains the TCA Cycle and Cell Survival during Impaired Mitochondrial Pyruvate Transport. Molecular Cell. 56(3):414-424.
[256] Qu, Q., Zeng, F., Liu, X., Wang, Q. J., Deng, F., 2016. Fatty acid oxidation and carnitine palmitoyltransferase I: emerging therapeutic targets in cancer. Cell Death &Amp; Disease. 7:e2226.
[257] Pike, L. S., Smift, A. L., Croteau, N. J., Ferrick, D. A., Wu, M., 2011. Inhibition of fatty acid oxidation by etomoxir impairs NADPH production and increases reactive oxygen species resulting in ATP depletion and cell death in human glioblastoma cells. Biochimica et Biophysica Acta (BBA) - Bioenergetics. 1807(6):726-734.
[258] Fujii, T., Khawaja, M. R., DiNardo, C. D., Atkins, J. T., Janku, F., 2016. Targeting isocitrate dehydrogenase (IDH) in cancer. Discovery medicine. 21(117):373-380.
[259] Upadhyay, V. A., Brunner, A. M., Fathi, A. T., 2017. Isocitrate dehydrogenase (IDH) inhibition as treatment of myeloid malignancies: Progress and future directions. Pharmacology & therapeutics. 177:123-128.
[260] Mondesir, J., Willekens, C., Touat, M., de Botton, S., 2016. IDH1 and IDH2 mutations as novel therapeutic targets: current perspectives. Journal of Blood Medicine. 7:171-180.
[261] Murphy, M. P., 2009. How mitochondria produce reactive oxygen species. The Biochemical journal. 417(1):1-13.
[262] Fan, J., Ye, J., Kamphorst, J. J., Shlomi, T., Thompson, C. B., Rabinowitz, J. D., 2014. Quantitative flux analysis reveals folate-dependent NADPH production. Nature. 510:298.
[263] Lewis, C. A., Parker, S. J., Fiske, B. P., McCloskey, D., Gui, D. Y., Green, C. R., et al., 2014. Tracing compartmentalized NADPH metabolism in the cytosol and mitochondria of mammalian cells. Molecular cell. 55(2):253-263.
[264] Hofmann, D., Wirtz, A., Santiago-Schübel, B., Disko, U., Pohl, M., 2010. Structure elucidation of the thermal degradation products of the nucleotide cofactors NADH and NADPH by nano-ESI-FTICR-MS and HPLC-MS. Analytical and Bioanalytical Chemistry. 398(7):2803-2811.
[265] Prior, S., Kim, A., Yoshihara, T., Tobita, S., Takeuchi, T., Higuchi, M., 2014. Mitochondrial respiratory function induces endogenous hypoxia. PLoS One. 9(2).
[266] Wheaton, W. W., Weinberg, S. E., Hamanaka, R. B., Soberanes, S., Sullivan, L. B., Anso, E., et al., 2014. Metformin inhibits mitochondrial complex I of cancer cells to reduce tumorigenesis. eLife. 3:e02242.
[267] Andrzejewski, S., Gravel, S. P., Pollak, M., St-Pierre, J., 2014. Metformin directly acts on

mitochondria to alter cellular bioenergetics. Cancer Metab. 2:12.
[268] Pelicano, H., Xu, R. H., Du, M., Feng, L., Sasaki, R., Carew, J. S., et al., 2006. Mitochondrial respiration defects in cancer cells cause activation of Akt survival pathway through a redox-mediated mechanism. The Journal of cell biology. 175(6):913-923.
[269] Iommarini, L., Kurelac, I., Capristo, M., Calvaruso, M. A., Giorgio, V., Bergamini, C., et al., 2014. Different mtDNA mutations modify tumor progression in dependence of the degree of respiratory complex I impairment. Hum Mol Genet. 23(6):1453-1466.
[270] Sun, R. C., Denko, N. C., 2014. Hypoxic regulation of glutamine metabolism through HIF1 and SIAH2 supports lipid synthesis that is necessary for tumor growth. Cell Metab. 19(2):285-292.
[271] Kase, E. T., Nikolic, N., Bakke, S. S., Bogen, K. K., Aas, V., Thoresen, G. H., et al., 2013. Remodeling of oxidative energy metabolism by galactose improves glucose handling and metabolic switching in human skeletal muscle cells. PloS one. 8(4):e59972.
[272] Aguer, C., Gambarotta, D., Mailloux, R. J., Moffat, C., Dent, R., McPherson, R., et al., 2011. Galactose enhances oxidative metabolism and reveals mitochondrial dysfunction in human primary muscle cells. PloS one. 6(12):e28536.